Walking energetics, optimization and control

by

Jessica C. Selinger

M.Sc., Queen's University, 2009
B.Sc. (Hons.), Queen's University, 2007

Thesis Submitted in Partial Fulfillment of the
Requirements for the Degree of
Doctor of Philosophy

in the
Department of Biomedical Physiology and Kinesiology
Faculty of Science

SIMON FRASER UNIVERSITY

Fall 2015

Approval

Name: **Jessica C. Selinger**

Degree: **Doctor of Philosophy**

Title: ***Walking energetics, optimization and control***

Examining Committee: **Chair:** Dr. Miriam Rosin
Professor

Dr. J. Maxwell Donelan
Senior Supervisor
Associate Professor

Dr. James M. Wakeling
Supervisor
Professor

Dr. Dawn C. Mackey
Internal Examiner
Assistant Professor
Department of Biomedical Physiology and Kinesiology

Timothy J. Carroll
External Examiner
Associate Professor
School of Human Movement Sciences and Nutrition
University of Queensland

Date Defended/Approved: December 9, 2015

Ethics Statement

The author, whose name appears on the title page of this work, has obtained, for the research described in this work, either:

a. human research ethics approval from the Simon Fraser University Office of Research Ethics,

or

b. advance approval of the animal care protocol from the University Animal Care Committee of Simon Fraser University;

or has conducted the research

c. as a co-investigator, collaborator or research assistant in a research project approved in advance,

or

d. as a member of a course approved in advance for minimal risk human research, by the Office of Research Ethics.

A copy of the approval letter has been filed at the Theses Office of the University Library at the time of submission of this thesis or project.

The original application for approval and letter of approval are filed with the relevant offices. Inquiries may be directed to those authorities.

Simon Fraser University Library
Burnaby, British Columbia, Canada

update Spring 2010

Abstract

To walk in the real world, we continually alter our gait to cope with changing terrains, goals, and constraints on the body. This is a nontrivial feat—individual muscle activities must be adjusted to produce a desired gait and that desired gait must be selected from a myriad of possible coordination patterns. How this is accomplished is poorly understood. One principle that could guide the control of legged locomotion is an optimization process that seeks to meet some objective. The main goal of my thesis is to investigate the role of optimization, and in particular energy optimization, in the control of human gait. To do so, I undertook four distinct studies. In the first study, I developed a control system for a lower limb exoskeleton that leverages the body's internal control by tapping directly into the user's muscle activity. The myoelectric controller accurately identifies the user's desired motion, automatically gradates the actuation of an exoskeleton, and is adaptable to varying gaits and terrains. In my second study, I sought to understand how entire coordination patterns, rather than individual muscle activities, may be optimized. I hypothesized that humans continuously optimize their gait to minimize energy expenditure. To test this, I used exoskeletons to alter the energetic consequences of various gaits. I made abnormal ways of walking energetically optimal and found that when given broad experience with the novel energetic landscapes subjects discovered the optimal gaits and opted to walk at them, even when the energetic benefits were small. In a third study, I found that the nervous system can be primed to initiate this optimization when perturbed toward low cost gaits, or can spontaneously initiate optimization when natural gait variability is high enough to elucidate a clear energetic gradient. Once optimization is initiated, I found evidence that the nervous system employs a 'local search' strategy to gradually descend energetic gradients and converge on novel optima. Given that energetic cost plays a central role in continuously shaping movement, in my fourth and final study I developed a technique to estimate instantaneous muscle energy use during non-steady state walking. This technique now makes it possible to measure a physiological signal that likely plays a central role in the control and optimization of human movement.

Keywords: energetics; optimization; exoskeletons; control; gait

Acknowledgements

First and foremost I'd like to thank my family, and in particular my parents. It is only because of your love, encouragement, and support that any of this has been possible. You have seen me through all the ups and downs of graduate work, despite my moving to the other side of the country. I have missed you, but have always had the comfort of knowing you are here for me. There is little else to say other than that I am truly blessed to have all of you.

I owe so many thanks to my senior supervisor Dr. Max Donelan. Max, it has been an honour to work with you over the years. Your passion, creativity and optimism are inspiring and something I will always strive for. Thank you for helping me become the scientist I am today. You have taught me to see and seek out the questions that are most interesting and scientifically important to my work. You have spent countless hours helping me, pushing me, to better communicate my findings and express my ideas. For this and so much more, thank you.

I'd also like to thank Dr. James Wakeling, a member of my supervisory committee. James, thank you for all your feedback along the way. You have been so generous with your time and expertise. It has been a pleasure working with you.

To all my lab mates, I could not have asked for a more incredible group of people to work with over the years. I want to thank all of you for the conversations and laughter, both inside the lab and out.

To Kyle, you have been my best friend and partner through this adventure and so many others. It's been wonderful to share in each other's struggles and successes over the years. Thank you for all of your love and support, and for always reminding me of what's truly important.

I'd also like to thank my funding sources including the Vanier Canada Graduate Scholarship, the National Sciences and Engineering Research Council of Canada, the Michael Smith Foreign Study Supplement, the UNESCO-L'Oreal for Women in Science

Program, and Simon Fraser University. This work would not have been possible without their financial support and I am grateful for all the opportunities it has created.

A final thanks to all the volunteers that participated in my experiments—for their time, which they gave generously, and their energy, which they gave sparingly.

Table of Contents

List of Tables

List of Figures

Glossary

Adaptation	The process of modifying or adjusting a well-learned movement or motor skill to meet new demands. Adapted from (*1*).
Biomechanical energy harvesters	Devices that derive or scavenge energy from the mechanical movement of biological sources or systems. In the context of this thesis, a knee mounted biomechanical energy harvesting exoskeleton is used to harvest energy from the natural motion of human walking.
Energetic cost	An umbrella term used throughout this thesis to refer to the amount of metabolic energy consumed, or ATP used, as a result of a given motor task. It is used interchangeably with terms such as metabolic cost, metabolic power, energy expenditure, and energy consumption.
Exoskeletons	Wearable mechanical devices, which are anthropometric in form and are designed to work in concert with the user's movements. They are typically designed to rehabilitate or restore the mobility of those with impairments or enhance the mobility of able-bodied individuals. In this thesis, exoskeletons are used for more atypical purposes: for biomechanical energy harvesting and to perturb and study the control of human gait.
Objective function	A quantitative definition of the motor task performance. Can also be referred to as a 'cost function'. For example, the underlying objective function for reaching is often proposed to be a weighted sum of accuracy and effort. Any given reach whether fast or slow, straight or curved trajectory, will produce a given level of accuracy and effort, and can therefore be defined by the objective function.
Optimization	The selection of the optimum, be that a maximum or minimum, of some objective function. In the context of motor control, it is the process of dynamically adapting a movement or motor skill in order to maximize task performance, with task performance being defined by the objective function. Optimization allows one to optimally adapt to novel contexts, but is likely slow due to sensing delays, averaging over multiple movements and iterative convergence. Adapted from (*2*) and (*3*).
Prediction	The recall of a previously learned, or pre-programed, motor pattern embedded within the neural circuitry. Prediction is rapid, but requires prior experience with a given movement, context and environment in order to adapt optimally. Adapted from (*2*) and (*3*).

Published Studies

Research contained in this thesis has been published in the following peer-reviewed journals:

Chapter 2	Selinger J.C. and Donelan J.M. (in press). Myoelectric control for adaptable biomechanical energy harvesting. IEEE Transactions on Neural Systems and Rehabilitation Engineering.
Chapter 3	Selinger J.C., O'Connor S. M, Wong, J. D., Donelan J.M. (2015). Humans Can Continuously Optimize Energetic Cost during Walking. Current Biology 25: 2452–2456.
Chapter 5	Selinger J.C. and Donelan J.M. (2014). Estimating instantaneous energetic cost during non-steady state gait. Journal of Applied Physiology 117(11): 1406-1415.

Chapter 1.

Introduction

When walking in the real world, people continually adapt their gait to accommodate changing terrains, tasks, and even constraints on the body. For example, when we encounter a steep hill or carry a heavy load we must change how we walk. Although we appear to do this with relative ease, the underlying control is strikingly complex. To coordinate the movement of our limbs, we adjust the time-varying activation of tens of thousands of motor units. In turn, by altering muscle contraction patterns we can choose between different gaits, such as walking, running or even skipping, and we can adjust countless gait parameters, such as speed, step frequency, and limb symmetry. Given the seemingly limitless degrees of freedom we are afforded during walking, our elegant control of gait is both impressive and non-trivial. Yet, how this is accomplished is poorly understood.

Over decades, many theories of motor control have been proposed (*4*). In the late 19th century Sherrington and colleagues proposed that voluntary movements result predominately from feedforward reflex pathways in response to stimuli presented to the extremities (*5*). By the early 20th century, Bernstein had aptly articulated the degrees of freedom problem, highlighting that there existed many redundant ways to accomplish a motor task (*6*). His work was among the first to highlight the complexity of controlling movement and shifted theories of motor control away from more simplistic feedforward control to more complex closed-loop feedback control. As a solution to the problem of redundancy he proposed that the central nervous system could functionally restrict particular degrees of freedom, always controlling certain aspects of movement in unison. This idea is closely related to the more modern theory of muscle synergies, where fixed sets of relative muscle activations are used to produce more complex movements (*7*-*9*). By only using a limited number of synergies, the redundancy problem of motor control

could be greatly reduced. However, some recent experiments have failed to find empirical support for the existence of synergies and some have questioned the need for, or usefulness of, the nervous system so greatly limiting it's flexibly (*8*, *10*, *11*). Other have put forth the minimal intervention principle of motor control, which instead proposes that the nervous system only controls degrees of freedom related to the performance of a given motor task, leaving all others free to vary (*11*, *12*). A closely related and potentially unifying theory of motor control, is optimal control (*13-15*). Optimal control proposes that movements are selected in order to maximize task performance, with task performance being defined by some objective function. Although still debated, optimal control models have successfully explained complex and varied biological movement. Of course, the definition of the underlying objective function for a particular movement in an important consideration. While many different reaching objectives, including accuracy, effort and smoothness, have been proposed, modeled and subject to careful experimental testing, relatively less is understood regarding the optimal control of walking.

In this thesis I will investigate the role of optimization, and in particular energy optimization, in the control of human gait. In the next three sections of this introduction, I will provide a brief introductory background review of three emerging research areas relevant to this investigation. First, I will discuss current literature focused on understanding how humans adapt their gait to meet new demands. Second, I will present a framework proposing that energy optimization is the underlying objective function driving these gait adaptations. And, third, I will discuss how exoskeleton technology will not only benefit from an unified understanding of locomotor control, but can also be used as a powerful tool to explore fundamental questions about why we move the way we do. These three sections are not intended as an exhaustive review, but instead to introduce general theory, concepts and technology that will reoccur throughout the thesis.

1.1. Adaptation during walking

Motor adaptation is defined as the process of modifying or adjusting a well-learned movement or motor skill to meet new demands (*1*). Although walking is the

motor skill of interest throughout this thesis, it is important to note that much of current day motor adaptation theory originated from upper limb reaching experiments. These experiments can be broadly categorized into two distinct classes of perturbations. One class tests the adaptability of the visuo-motor map by perturbing visual feedback, either using prism glasses or by altering the representation of limb position in a virtual reality environment (*4*, *16-20*). The other class involves applying mechanical perturbations to movement, either by altering the inertial properties of a limb using weights or by applying a force field using a robotic manipulandum (*4*, *18*, *21*, *22*). These experiments all reveal common features of adaptation, including initial deviations from intended movement, adaptation of over the course of a number of movements, and aftereffects when the perturbation is removed. As an example, let us consider the force-field adaptation experiments carried out by Shadmehr and Mussa-Ivaldi in the 1990s (*21*), as it is perhaps one of the most influential adaptation works. In brief, subjects in these experiments are required to reach to a target while a manipulandum applies novel forces to the arm. Subjects initially show large kinematic deviations from straight line reaching, but gradually take into account the novel limb dynamics by adjusting their muscle activity to once again achieve normal straight-line limb trajectories. When the force-field is then removed, subjects present with what is referred to as an aftereffect—they show deviations in hand trajectory that are mirror images of that which they initially displayed. These aftereffects, as well as subjects' ability to extrapolate their learning to closely related tasks, suggest that an internal representation of the force field is composed by the nervous system and then used to predict and compensate for the effects of the external environment. This powerful paradigm greatly influenced the field of motor adaptation is still used extensively today to study motor control.

More recently, this paradigm has been applied to the lower limb, providing growing evidence that similar internal representations are used in the control of gait. For example, Lam et al. (2006) used a lower limb exoskeleton to apply velocity dependent resistance to knee and hip motion during walking and found evidence of predictive control strategies (*23*). During pre-swing, knee flexor activity gradually increased in the presence of resistance and persisted when the resistance was removed, which is consistent with adaptation. However, during swing other muscles such as the knee extensor and ankle flexor muscle activity increased immediately in the presence of

resistance and did not persist when the resistance was removed. Similarly, Blanchette and Bouyer (2009), using an elastic band to produce a position dependent force field, found that knee flexor activity displayed adaptation during pre-swing (near toe–off), yet not throughout the remainder of swing (*24*). Taken together, these results suggest that control of lower limb locomotion is adaptable to force-field exposure yet may be both muscle and timing specific. Others have focused on understanding how locomotor adaptation generalizes across tasks or limbs in order to gain insight into neuronal circuitry. For example, Choi and Bastian (2007) used a split-belt treadmill to adapt the limbs to different speeds and directions (forward and backward walking) (*25*). While these conditions initially produce asymmetrical gaits over time the nervous system adapts toward symmetry. By testing if adaptation transferred across limbs and directions, they found evidence of separate functional networks for controlling each limb, as well as forward and backward walking. This same group has also found that cerebral stroke patients are able to adapt to split belt walking (*26*), while patients with cerebellar damage lack the ability to make the necessary predictive adjustments (*27*). These findings support the hypothesis that cerebellum plays a prominent role in locomotor adaptation and learning. While the discussed work has begun to quantify the patterns, timescales, and neural circuitry associated with locomotor adaptation, the underlying physiological goal that drives adaptation during gait is unclear.

Traditionally, minimization of kinematic trajectory error is presented as the primary objective function, or goal, driving upper limb adaptation (*21*, *28*-*32*). Deviations from a straight-line reaching path are defined as errors and thought to be the signal that the nervous system seeks to minimize. However, this objective is likely less important during gait adaptation, where precision is not as paramount. The examples of gait adaptation discussed previously demonstrated that force-field paradigms can result in adaptation of muscle activity (*25*-*27*), and split belt paradigms results in adaptations toward symmetry (*23*, *24*), yet it is not clear why. A unifying objective through which to understand the control of legged locomotion has remained elusive. One likely candidate—energy minimization—is discussed in the subsequent section and is a focus of this thesis.

1.2. Energy optimization during walking

Energy minimization may provide a central framework to understand the mechanisms underlying locomotion adaptation. It has long been established that people move in ways that minimize energy expenditure. For example, they tend to walk at a speed that minimizes the metabolic energy cost per unit distance traveled (*33-36*). And at a given speed, people consistently select the appropriate step frequency, step length and step width that keeps cost minimized (*34*, *37-39*). But the processes by which people discover their optimal patterns are not clear. One possibility is that our optimal gait patterns are established over evolutionary timescales, through changes to body shape, muscle action, and the hardwiring of neural circuitry (*40-43*). Another possibility is that energy optimization may additionally occur over the course of a lifetime, as years of experience could allow people to learn the optimal way to move in familiar situations and allow training to tune physiology to be more economical (*44*). An alternative hypothesis, addressed within this thesis, is that energy expenditure is continuously optimized, in real-time, to drive gait adaptation.

Although direct evidence of real-time energetic cost optimization has remained elusive, recent findings have tantalizingly suggested that this may be the case. Our group has demonstrated that following perturbations, people can rapidly predict their energetically optimal gait (*2*, *45*). While this finding is consistent with optimal patterns being hard-wired or well-learned by the body, there was also evidence of a slower fine-tuning process, consistent with adaptation and occurring on a timescale similar to changes in energy expenditure (*46*). Other groups have also recently begun to consider the role of energetic cost during classic adaptation paradigms. For example, Finely et al (2013) has shown that reductions in energetic cost track motor adaptation in split belt walking paradigms, indicating that the tendency toward symmetry may be the consequence of a desire to reduce cost (*47*). Even those performing classic reaching paradigms have begun to explore if adaptations, traditionally thought to minimize kinematic error, could also be cost driven. Here the results are mixed, with Kistemaker et al (2010) showing that people did not adapt toward paths expected to be energetically optimal (*48*). However, Huang et al (2012), who directly measured metabolic cost, found that energy use was lower after adaptation than before during reaching (*49*). In either

case, it is perhaps logical that minimization of energy expenditure be a more important term in the objective function underlying walking than reaching.

It does appear that the nervous system is equipped to sense energy expenditure in real-time. A number of candidate physiological sensors can directly sense energy use, potentially providing the signal that guides adaptation. For example, chemoreceptors located in the medulla oblongata and the carotid and aortic bodies are sensitive to changes in the concentration of oxygen and carbon dioxide in the blood, which is associated with metabolic rate (*50*-*52*). These sensors could provide a measure of energy expenditure reflective of total body energy use, and analogous to that which is measured experimentally using indirect calorimetry. It is also possible that metabolic cost is directly sensed by peripheral muscle receptors, such as group IV muscle afferents, sensitive to the local by-products of muscle metabolism (*53*-*55*). Indeed these sensors have previously been shown to play a role in the exercise pressor reflex that increases heart rate and ventilation upon onset of exercise. These sensors also offer the advantage of providing more localized information about energy use, which may aid in the search for optimal coordination patterns.

Optimizing gait using these direct sensors of energy use is necessarily slow. Circulating blood gas concentrations can take tens of seconds to fully reflect new energetic demands (*46*, *56*). Although muscle afferents sensitive to local metabolites are faster, they have still been found to require seconds to produce a physiological response (*54*, *57*-*59*). These sensing delays are compounded by the fact that optimization itself is likely time consuming. To accurately assess, and perhaps trust, a new steady-state energy expenditure it may be necessary to average over multiple gait cycles. Moreover, a single new measurement is likely insufficient for optimization. Instead, the body may need to iteratively adjust and explore different gaits in order to gradually converge on energetic optima. This slow convergence is consistent with adaptation to a novel context, but may be impractical in real world walking where tasks and terrains change frequently.

To overcome this limitation, the body may instead, or in addition, rely on indirect information that it has learned is related to energetic cost. For example, vision could

provide immediate information about a soon to be encountered hill and the body may be able to predict, based on past experience, the energetically optimal gait for this new terrain. This is a kin to forming and storing an internal representation of a task in classic adaptation and learning paradigms. Of course, to use these indirect sources of information about energy expenditure, prior experience with a given gait or terrain is necessary. This renders rapid indirect sensing ineffectual when encountering novel contexts.

Our lab has proposed that the control of walking is governed by both the optimization and prediction of metabolic cost (*2*, *3*, *45*, *60*). Indirect prediction can be used to rapidly improve gait economy when contexts are changed, while direct optimization can be used to fine-tune this selection over time. Moreover, when faced with novel contexts and prediction is inadequate, we have hypothesized that optimization will play a primary role and can inform, or update, the body's internal prediction. Although locomotor adaptations consistent with both of these processes have been identified in both walking and running (*2*, *3*, *45*), direct evidence of energetic cost optimization has remained elusive. A primary goal of my thesis is determine the role of energy optimization in the control of human gait. To do so, I leverage an emerging technology, lower limb exoskeletons, which can be used to both augment and understand movement. In the subsequent section, I briefly discuss the advance of exoskeleton technology, the importance of using physiology to inform exoskeleton design, and the potential of exoskeletons as a tool to explore fundamental questions about the control of human gait.

1.3. Use of exoskeletons to augment and understand walking

Augmenting locomotion has the potential to redefine how and where one can move. Whether a recovering stroke patient or a dismounted infantry soldier, a technology that can augment natural movement could both broaden the tasks that are feasible and expand the terrain that is accessible. Robotic exoskeletons, which were once restricted to the pages of science fiction, are designed to do just that. These wearable mechanical devices, which are anthropometric in form and are designed to

work in concert with the user's movements, have become a part of our reality. While lower limb exoskeleton prototypes were designed as early as the 1960's, the past decade has seen a revival and booming interest in the field (*61*, *62*). Recent advances in both robotic hardware and software have pushed back technological boundaries, allowing for the development of more sophisticated, light weight, and intelligent designs. There are currently groups all over the world developing lower limb exoskeletons and orthoses for the purposes of assisting and enhancing human locomotion (*61*-*68*). Specific applications include providing robot-mediated physical therapy in a clinical setting, assisting those with mobility impairments during everyday activities, and enhancing the locomotor capabilities of military personal in complex terrain. The first commercially available lower limb exoskeletons are now on the market and this rapidly evolving technology shows few signs of slowing down.

Despite this progress, limited data are available on the physiological response of the human user when donning an exoskeleton. Many wearable exoskeletons are assessed on their ability to produce motion that is kinematically equivalent to natural walking (*61*, *62*, *69*). While there is value in these metrics, it does not allow one to assess if walking is in fact made easier for the user. Perhaps so few assess physiological metrics, such as metabolic cost or muscle activity, because it is inherently very difficult to design an exoskeleton that can seamlessly coordinate with the human neuromuscular system and show physiological improvements. In fact, only in the last two years have three groups been able to show reductions in energetic cost below the level of walking without an exoskeleton (*70*-*72*). While this is certainly in part do to the difficulty of designing and controlling these devices, it may also be because few consider how the human user adapts to the novel technology. These devices by definition alter the relationship between motor commands, produced movements, and resulting sensory feedback, yet few have examined the motor adaptation or learning process associated with donning an exoskeleton (*73*). Very practical considerations remain unclear, such as how and over what timescale a user adapts to an exoskeleton, or how this adaptation can be best facilitated. To effectively augment human movement, we must consider the interaction between human and machine.

While physiology has the potential advance the design of exoskeletons, exoskeletons also have the potential to advance our understanding of physiology. They can serve as tool with which we can learn about the mechanics, energetics, and neural control of gait. For example, Sawicki and Ferris (2008) have used a powered ankle exoskeleton to quantify the efficiency of the ankle joint and show that elastic energy storage and return contributes a significant amount of ankle joint positive power during push off (*74*). The same group have also tested different exoskeleton control schemes, including myoelectric control and kinematic control, and found that controllers designed to mimic the human sensorimotor loop produced more rapid adaptation than those that do not (*75*). This indicates that exoskeleton controllers could be used as a tool to test hypothesises about unknown aspects of motor control. The potential of exoskeleton technology, to study the fundamental principles that underlie the physiology of legged locomotion, has yet to be fully realized.

1.4. Aims

The overall goal of this thesis is to investigate the role of optimization in the control of human gait. In my first study, I will use optimization techniques to design an exoskeleton controller that is integrated into the user's sensorimotor loop. My aim is to develop a myoelectric control system for a lower limb exoskeleton and test it's adaptability to various locomotor tasks. In my second and third study, I will use the lower limb exoskeletons to disrupt the natural sensorimotor loop, allowing me to explore fundamental aspects of locomotor control. Specifically, my aim in the second study is to test the hypothesis that humans continuously optimize their gait, in real-time, to minimize energy expenditure. My aim in the third study is to test multiple competing hypotheses about how the nervous system initiates this optimization and the process used to converge on novel optima. In my fourth and final study, my aim is to develop a technique to estimate instantaneous muscle energy use during non-steady state gait. This technique will not only allow researchers to explore fundamental questions about the role of energetic cost in locomotor adaptation and learning, but can also be used to optimize exoskeleton design and control.

Readers should note that the second and third studies of this thesis, found in Chapters 3 and 4, have been formatted such at the detailed Experimental Procedures are presented after the Results and Discussion sections. I have chosen to do so because I think it improves the clarity of the work and allows the reader to more fluently link the findings and implications to the proposed hypotheses in the Introduction. Aspects of the experimental design critical to understanding the results are reported throughout the Results section. The first and fourth studies of this thesis, found in Chapters 2 and 5, are methods driven and have therefore been presented in a more traditional format.

Chapter 2.

Myoelectric control for adaptable biomechanical energy harvesting

2.1. Abstract

We have designed and tested a myoelectric controller that automatically adapts energy harvesting from the motion of leg joints to match the power available in different walking conditions. To assist muscles in performing negative mechanical work, the controller engages power generation only when estimated joint mechanical power is negative. When engaged, the controller scales its resistive torque in proportion to estimated joint torque, thereby automatically scaling electrical power generation in proportion to the available mechanical power. To produce real-time estimates of joint torque and mechanical power, the controller leverages a simple model that predicts these variables from measured muscle activity and joint angular velocity. We first tested the model using available literature data for a range of walking speeds and found that estimates of knee joint torque and power well match the corresponding literature profiles (torque R^2: 0.73-0.92; power R^2: 0.60-0.94). We then used human subject experiments to test the performance of the entire controller. Over a range of steady state walking speeds and inclines, as well as a number of non-steady walking conditions, the myoelectric controller accurately identified when the knee generated negative mechanical power, and automatically adjusted the magnitude of electrical power generation.

2.2. Introduction

This decade has seen rapid progress in the development of powered exoskeletons designed to augment the function of human joints (*61*, *62*, *69*). Within this larger field of wearable robotics, our focus has been on developing devices to capture mechanical energy normally wasted during walking and convert it to electricity (*76*, *77*). Although these biomechanical energy harvesters are exoskeletons, we have not designed them to provide additional torque whenever the user needs it. Instead, our design goal is to generate useful amounts of electrical energy without substantial increases in user effort. To do so, we control the timing and magnitude of power generation such that it assists muscles in performing negative mechanical work (*76*, *77*). Although the intended use is different from most powered exoskeletons, the control goal is similar—to apply torque with the ideal timing and magnitude.

A central challenge of effective exoskeleton design is a controller that automatically adapts its action to match the requirements of different phases of the gait cycle and different walking conditions. For example, it may be desirable for a powered exoskeleton to assist trailing leg push-off work during walking (*72*, *78-81*). The timing and magnitude of helpful push-off work will likely depend on both walking speed and slope (*78*, *82*, *83*). Energy harvesting from leg joint motion faces similar challenges—the negative joint work available for harvesting, as well as the magnitude of torque required to do so effectively, depend on the phase of the walking cycle (*84*, *85*). For example, the knee joint generates negative mechanical work with large extension torques at slow flexion speeds at the beginning of stance, and with small flexor torques at high extension speeds at the end of swing (*86*, *87*). An ideal energy harvester controller would adapt its resistive torque to match that available from the knee at each phase of the walking cycle (*85*, *88*). Furthermore, as walking speed changes, the appropriate level of torque for each phase also changes. And at different walking slopes, some phases of the walking cycle may stop producing negative work whereas others might start (*89*, *90*). More generally, a typical walking bout in the real world does not occur at a steady-state speed or slope. Instead, it involves speeding up and slowing down while walking over variable terrain and negotiating disturbances such as stepping over obstacles. An ideal

exoskeleton controller would adapt its action to optimize its performance under these variable conditions.

To effectively adapt the action of an exoskeleton, a controller needs to measure or estimate the required joint torque. One logical method is to measure the electrical activity of the muscles that are typically responsible for the joint torque. These electromyography (EMG) signals, which can be non-invasively measured from the surface of the skin, indicate the excitation of the underlying muscle and give indirect insight into its force (*91*-*93*). Conveniently, EMG also provides advance insight into user intent as the measured activity often precedes measurable acceleration or deceleration of the limb by approximately 20-100 ms (*94*, *95*). As a consequence of these benefits, EMG has been used extensively to control upper limb prosthetics (*96*-*98*) and is beginning to be employed in the control of lower limb prosthetics (*99*, *100*). Ferris and colleagues are among the first to develop myoelectric controllers for lower limb exoskeletons (*67*, *101*). In their ankle-foot orthoses, the air pressures of two artificial pneumatic muscles—a plantar flexor and a dorsi flexor—are regulated in proportion to the activity of the soleus and tibialis anterior muscles. Naïve users are able to quickly adapt to walking with the novel device by adjusting muscle activity to take advantage of the exoskeleton assistance (*67*). The Hybrid Assistive Leg (HAL-5) exoskeleton developed by the University of Tsukuba, Japan also uses myoelectric signals as inputs into their controller. But, rather than simply make actuator activity proportional to a single muscle's EMG, this controller uses the measured activity to first estimate joint torque, which is in turn used to control the exoskeleton torque (*65*). Although most lower limb exoskeletons rely on other methods to control their action (*69*), the success of the few existing devices that employ myoelectric control, as well as the promise of tapping into the user's own intentions, highlight the potential of myoelectric controllers.

Our purpose in this study was to design a myoelectric controller that would automatically adapt energy harvesting to match the mechanical power available in different walking conditions, and then test its performance. As detailed in the next section of this paper, our controller uses real-time estimates of joint torque and mechanical power to determine the timing and magnitude of electrical power generation. The following section describes our model for estimating joint torque and mechanical

power from measured muscle activity and joint angular velocity. It includes a relatively simple procedure for identifying the unknown model gains and delays, and then tests the model performance against literature data collected at a range of walking speeds. In the final section, we combine our candidate controller and our model for estimating joint torque and power to control energy harvesting exoskeletons worn by a human subject. We test its ability to automatically adapt the timing and magnitude of electrical power generation across a range of steady-state walking speeds and slopes, as well as a number of non-steady walking conditions.

2.3. Controller Design

Our controller relies on real-time estimates of knee joint torque (τ_j) and knee joint angular velocity (ω_j), the product of which produces an estimate of knee joint power (P_j) (Figure 2.1a). We designed our controller to engage power generation only when estimated knee joint power is negative. When engaged, the resistive torque that the exoskeleton applies to the body (τ_a) is made proportional to knee joint torque by a constant K:

$$\tau_a = \begin{cases} K \cdot \tau_j & \text{if } P_j < 0, \\ 0 & \text{otherwise} \end{cases} \tag{2.1}$$

Since the total torque acting about the knee joint (τ_t) is the sum of the torque provided by the body (τ_j) and the exoskeleton (τ_a), the fraction of total torque contributed by the exoskeleton can be expressed as:

$$\frac{\tau_a}{\tau_t} = \frac{K}{K+1} \tag{2.2}$$

If $K = 1$, the exoskeleton and joint each contribute half of the total torque. If K is reduced to 0.5, the torque fraction applied by the exoskeleton would drop to 1/3 with the remainder contributed by the body. This relationship, between the torque applied by the body and that by the exoskeleton, is also true of the mechanical power generated by the body and exoskeleton. This is because the joint and exoskeleton share a common angular velocity at the point of torque application. When the exoskeleton generates

negative mechanical power on the body, the body generates positive mechanical power on the exoskeleton. This positive mechanical power is converted into electrical power with an efficiency determined by the exoskeleton components including its transmission, generator and power conditioning circuitry (77). Thus, our controller automatically scales electrical power generation to be proportional to the available negative mechanical power at the joint, with the proportion determined by K.

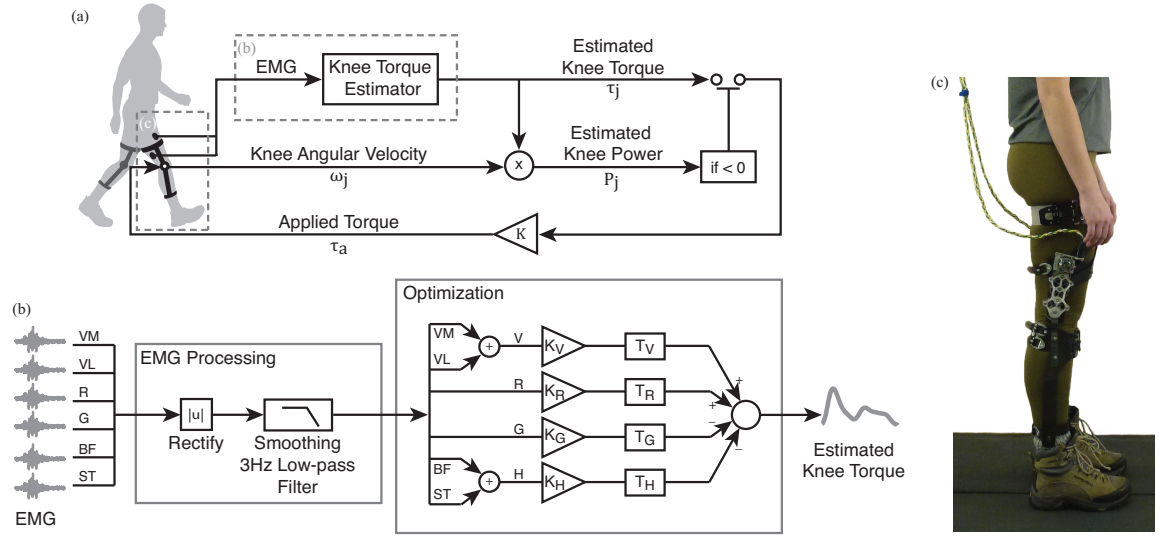

Figure 2.1: Myoelectric control system for an energy harvesting exoskeleton
(a) Controller design. Muscle activity is used to produce a real-time estimate of knee joint torque. The product of this estimate and knee angular velocity produces an estimate of knee joint power. A resistance proportional to knee joint torque (by a factor **K**) is applied only during negative work phases of gait, when knee joint power is negative. **(b)** Torque estimation. Raw EMG signals from the vastus medialis (VM), vastus lateralis (VL), rectus femoris (R), medial gastrocnemius (G), biceps femoris (BF) and semitendinosus (ST) are rectified and smoothed. The VM and VL are summed, as are the BF and ST, resulting in four muscle activity profiles. A constrained nonlinear optimization is then used to identify four optimal gains (K_V, K_R, K_G and K_H) and delays (T_V, T_R, T_G and T_H), and the resulting four profiles are summed to produce an estimate of knee joint torque. Note that the optimization of all gains and delays occur during a parameter identification period, are not continually optimized in real-time. **(c)** Exoskeleton hardware. The custom carbon fiber shell is mounted to the thigh and shank using nylon and polyethylene strapping. The steal gear train transmits rotation at the knee joint to the rotor of a magnetic motor. EMG electrodes, placed on the quadriceps and hamstring muscles, are used to measure muscle activity, which is in turn used to control harvesting. While the exoskeleton is identical to that used in the experiment, the picture is of a different subject.

It is not possible to predict an optimal value of K without human experiments. Very low values of K are undesirable because the resulting low applied torque would

leave some available negative mechanical work untapped for power generation. It is likely that very high values of K are also undesirable because a user's nervous system may not be able to adapt its control of muscle forces to take advantage of the assistance provided by the exoskeleton. This would result in a greater than required total torque at the knee, leading to a stiff-kneed gait with very little knee motion and thus very little mechanical power available for harvesting. If users are able to dramatically reduce the torque generated by their muscle, high values of K may still not be desirable because the resulting low EMG signals may become insufficient for control. Finally, it is likely that users will be more perturbed by the inevitable errors in estimated torque, especially timing errors, when the exoskeleton attempts to apply the large torques associated with high values of K. The ideal value for K lies somewhere between the two extremes, and can be determined using human experiments to compare power generation, comfort, and muscle activity at different values of K.

Overall, our simple controller structure is inherently adaptable to varying gaits and movements, as it does not rely on prior knowledge of standard knee joint kinematics or kinetics. Indeed, if knee joint torque and angular velocity are accurately estimated, the controller should engage and disengage power generation appropriately, regardless of the task. While we have chosen to estimate knee joint torque from muscle activity, and knee angular velocity from generator voltage (discussed below), our controller is not specific to these measures, or even to the knee joint; it could use other means to estimate joint torque and angular velocity in real-time, and can be applied to other biological joints.

2.4. Joint Torque and Power Model

Our model estimates knee joint torque and mechanical power using measured muscle activity and joint angular velocity. To design our model, we have used literature data, including knee joint angular velocity, torque and power (*86*), as well as lower limb muscle activity (*102*). As detailed below, we first identify unknown model parameters, including gains and delays, using knee joint flexor and extensor muscle activity during level walking at a moderate speed. We then tested our model's robustness to predicting knee joint dynamics across a range of magnitudes and timings by comparing our

estimated knee joint torque and power to literature values across a range of walking speeds.

2.4.1. Model Design

Our model incorporates muscle activity from three knee extensors—vastus medialis (VM), vastus lateralis (VL), and rectus femoris (R)—as well as from three knee flexors—biceps femoris (BF), semitendinosus (ST), medial gastrocnemius (G) (Figure 2.1b). The activity of these muscles can be easily measured using surface EMG. In the design of our model, we used average muscle activity profiles from the literature that were collected during level walking at 1.25m/s by Hof and colleagues (*102*). They instrumented the right leg of each subject and placed electrodes in accordance with the SENIAM committee (*103*). During processing, they band pass filtered their EMGs with a 20 Hz -10 kHz third order zero-lag Butterworth filter and then rectified and smoothed their signals with a 25 Hz third order zero-lag Butterworth low-pass filter. The EMG profiles made available in the literature had been averaged across subjects, with data from between 11 to 13 subjects per muscle. We further smoothed these signals with a 6Hz third order low-pass Butterworth filter. Next, activity from VM and VL were summed to create one vastus muscle activity profile (V). The BF and ST were also summed, creating a single hamstring muscle activity profile (H). No weightings were applied to the signals prior to summing. Using the resulting four muscle activity profiles (V, R, H, and G) we sought to produce an estimate of joint torque, which, when multiplied by angular velocity, would produce an estimate of joint power.

2.4.2. Parameter Identification

We used constrained nonlinear optimization to solve for four gains (K_V, K_R, K_H and K_G) and four time delays (T_V, T_R, T_H and T_G) that we applied to the V, R, H, and G profiles prior to summing these signals to produce an estimate of joint torque. These parameters were optimized such that the resulting estimate of joint torque, when multiplied by knee angular velocity, produced an estimate of joint power that best fit the literature knee joint mechanical power for the same walking speed (*86*). That is, the root mean square error between the estimated and literature joint power was minimized.

While it is also possible to optimize these parameters such that they produce the best-fit estimate of knee joint torque, we have chosen to optimize for power because our intended application is energy harvesting during phases of negative mechanical joint power. By optimizing for power we are in effect optimizing for torque that is weighted by angular velocity, with phases of high angular velocity assigned greater importance than those with low angular velocity. For other applications, such as powered exoskeletons, it may be more useful to simply optimize for torque. The optimization was implemented using Matlab's *fmincon* function (Mathworks, NA, USA). The constraints applied to the optimization required positive magnitudes for the knee extensor gains (K_V and K_R) and negative magnitudes for the knee flexor gains (K_H and K_G). Additionally, we restricted the magnitudes of the four time delays to lie within 0-100 ms, which encompasses reasonable predictions of the delay between measured muscle activity and produced joint torques (*94*, *95*).

Using this model and our optimized parameters, we were able to produce accurate EMG-derived estimates of knee joint torque and power that well matched literature profiles collected at the same walking speed (torque R^2: 0.92, power R^2: 0.94, Figure 2.2, Table 2.1). As expected, the vastus muscle profile (V) contributed most substantially to the large net knee extensor torque during mid stance, while the hamstring profile (H) accounted for the net flexor torque during late swing to early stance. The rectus femoris (R) and medial gastrocnemius (G) activity profiles made substantially smaller contributions, but did improve the optimized fit to the more subtle net extensor and flexor torque evident at mid gait cycle. The literature knee joint power data that we used to identify model parameters were collected on different subjects, and by different authors, than the measures of muscle activity. This provides an initial indication that we may not need subject-specific measures of joint power when identifying model parameters for individual users.

Table 2.1: Optimized model parameters and resulting torque and power R^2 values for literature and experimental data

	Time Delay (ms)				Gain (Nm/μV)				R^2	
	T_V	T_R	T_G	T_H	K_V	K_R	K_G	K_H	Torque	Power
Literature Right	83	0	7	83	0.42	0.14	-0.72	-0.33	0.92	0.94
Experimental Right	38	0	0	31	1.09	0.00	-0.34	-0.39	0.92	0.79
Experimental Left	19	67	0	23	0.98	0.32	-0.26	-0.39	0.92	0.81

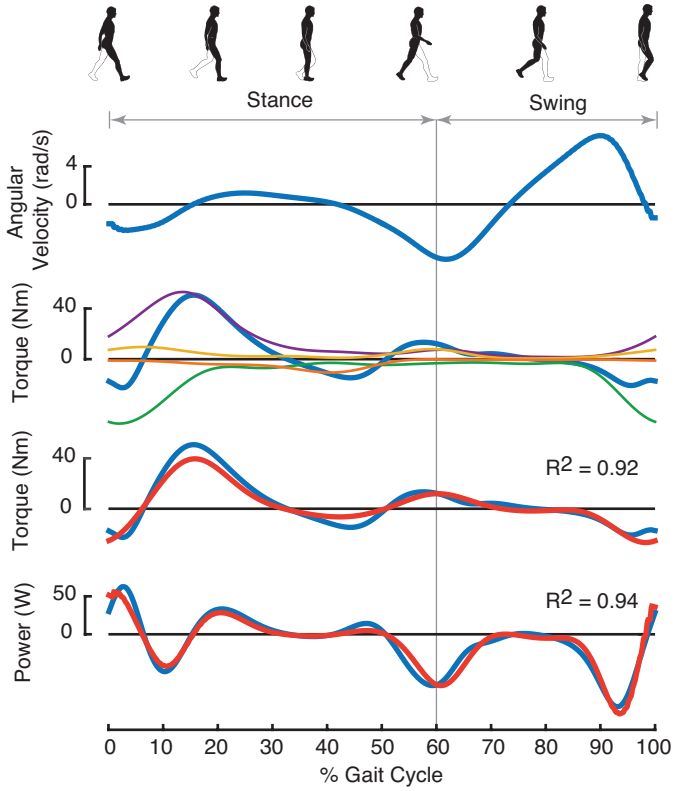

Figure 2.2: Parameter estimation using literature EMG
Literature knee joint angular velocity, torque and mechanical power (blue; all plots) **(*86*)**. Literature EMG signals **(*102*)** were used to identify optimal model parameters, including four gains and four delays, which when applied to muscle activity profiles produced the V, R, G, and H traces (purple, yellow, orange, and green, respectively; second plot). Summing these traces produces the torque estimate (red; third plot), while taking the product of angular velocity and the torque estimate produces the power estimate (red; fourth plot). All literature data were from level walking at 1.25m/s.

2.4.3. Parameter Validation

We next assessed if our optimized gains and delays could be used to produce accurate EMG-derived estimates of knee joint torque and power across a range of walking speeds. It is important for us that the solved parameter values generalize to walking conditions beyond which they were optimized for, as this allows us to use a relatively simple and short procedure for identifying model parameters. We used the gains and time delays identified at a walking speed of 1.25m/s to estimate torque and power profiles for speeds ranging from 0.9m/s to 2.0m/s. We used varying speeds to test our model's generalizability because changes in speed result in changes in both the

timing and magnitude of joint torque and power. While EMG and kinetic data are readily available in the literature across a range of speeds, exact speed matches were not. Here, we used EMG data from Hof and colleagues, collected at speeds of 0.75, 1.00, 1.25, 1.50, and 1.75m/s, and kinematic and kinetic data from Zelik and Kuo, collected at speeds of 0.70, 0.90, 1.25, 1.60, 1.80m/s (*86*, *102*).

We found that we could generate reasonably accurate estimates of torque and power for most walking speeds using parameters optimized at a single comfortable walking pace (Figure 2.3). Although torque and power estimates did worsen as speeds differed from 1.25m/s, the R^2 of our estimates remained above 0.70 for torque and 0.60 for power at all speeds. The magnitudes of the torque and power estimates were appropriately scaled across the range of speeds. Moreover, the timing of negative and positive torque and power phases were quite accurate despite large changes in stride times across different speeds. Overall, our findings indicate that using a relatively small number of muscles and a simple procedure for optimizing model parameters, it is possible to predict knee joint torque and power for walking over a two-fold range in speed.

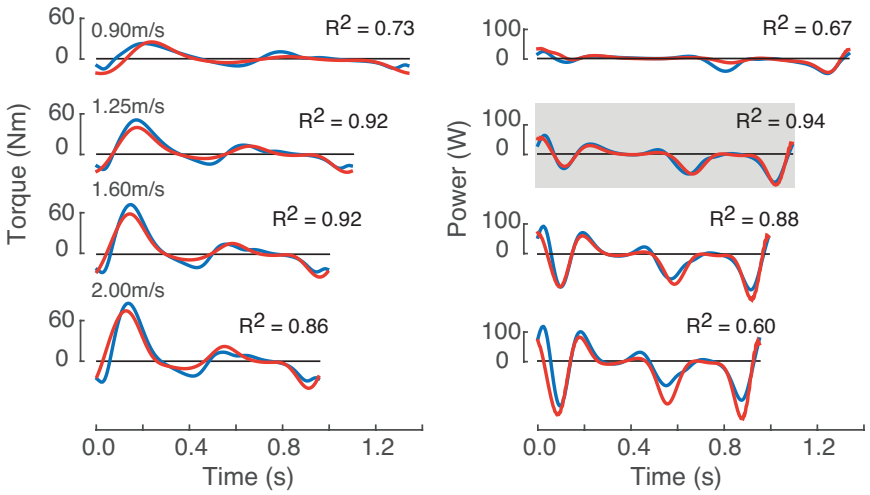

Figure 2.3: Parameter validation across walking speeds using literature EMG EMG profiles from the literature **(*102*)** were used to derive estimates of knee torque (red; left column) and power (red; right column) that were compared to literature knee joint torque (blue; left column) and mechanical power (blue; right column) for various walking speeds (0.90, 1.25, 1.60, and 2.00 m/s) **(*86*)**. Although model parameters were optimized only for power at 1.25 m/s (grey shading), these same parameters well predicted knee joint torque and power across a wide range in walking speed. The x-axes are expressed in time, as opposed to percent-normalized gait cycle, allowing better visualization of the absolute changes in timing for the various gait speeds presented.

2.4.4. Alternative Models

We tested a number of alternative models for estimating knee joint torque and power that leveraged different combinations of muscles. For example, we tried including only uni-articular knee extensors (VM and VL) and flexors (BF and ST). However, it was clear that, for level walking at 1.25 m/s, our poorest estimates of torque occurred during the end of stance and beginning of swing (30-70% gait cycle) and, as a result, we largely missed the substantial phase of negative joint power that peaks at around 60% of the gait cycle. This is not surprising, as the uni-articular knee extensors and flexors are nearly inactive during this portion of the gait cycle. The addition of G and R, which demonstrate peak activity in this otherwise silent phase, allowed for better fitting of these subtle mid gait cycle flexor and extensor peaks in torque. Overall, models that do not include G and R are still able to account for about 85% of the variation in torque and power, but their inclusion improves this to over 90%.

Our model estimates of torque and power are less impacted by the removal of other, more redundant, muscles. Muscle activities from the two vasti are quite similar. Therefore, it is possible to remove either the VL or VM and still explain over 90% of the variation in torque and power. The same is true for the two hamstrings; either the BF or ST can be removed. We have chosen to sum the activity from VM and VL, as well as that from BF and ST, because, for our purposes, it was easy to instrument both. However, in situations where hardware or accessibility to muscle electrode sites is limited, it appears that our model could function equally well with EMG recordings from only four non-redundant muscles per leg.

2.5. Experimental Testing

Here we preformed preliminary experiments to test the ability of our controller, and the joint torque and power model that it relies on, to control energy harvesting exoskeletons worn by a human subject. Our primary aim was to assess if our myoelectric controller could be used to accurately identify when the knee is generating negative mechanical power, and automatically adjust the magnitude of electrical power generation to match the available mechanical power.

Performing human experiments allowed us to test our controller in ways not possible using only available literature data. For one, we assessed if our simple parameter estimation procedure sufficiently predicted knee joint toque and power profiles when relying on EMG data from a single subject, as opposed to data averaged over multiple subjects. We were also able to test if, when the controller is turned on, our estimates of knee joint torque and power were still reliable, despite the potentially perturbing effects of the exoskeleton resistance. We were also able to explore what fraction of total knee joint torque, defined by K, was optimal for the user—a question we are unable to assess without instrumenting a human with the exoskeleton. Lastly, when attempting to validate our solved controller parameters, we were able to asses not only changes in torque timing and magnitude across steady-state walking speeds, for which literature EMG data were available, but also across different inclines and in a number of non-steady walking conditions.

2.5.1. Hardware

We used wearable energy harvesting exoskeletons that couple knee joint movement to generator rotation, allowing us to convert mechanical to electrical power. These novel exoskeletons differ from those on which we have previously reported (*76*, *84*)—they perform bi-directional energy harvesting, generating electrical power during both knee joint flexion and extension. Each exoskeleton weighs 1.1 kg and is comprised of a custom carbon fiber shell and custom steel gear train coupled to an off-the-shelf rotary magnetic generator (BLDC40S-10A, NMB Technologies Inc.) (Figure 2.1c). During walking, the relatively low angular velocity and high torque characteristics of knee motion are transformed by the gear train to produce relatively high angular velocity and low torque at the generator. This rotational motion in the generator's rotor induces voltage in the windings and, if the controller allows it, electrical current in the windings (*84*). The induced current generates its own magnetic field that resists the motion of the knee with a torque proportional to the current magnitude. We limited the maximum torque to 11 Nm based on the designed strength of the gear train. We estimated the torque applied to the knee from the product of the measured generator current, the generator's torque constant (3.36×10^{-2} Nm/A) and the exoskeleton gear ratio (110:1). We also estimated the magnitude of knee angular velocity from the product of measured generator voltage and the generator's velocity constant (0.33Rad/s/V). We determined the direction of generator rotation from the voltage phase relationship between the generator's three phases.

2.5.2. Subject Instrumentation

We performed testing on a single able-bodied subject (body mass: 88 kg; height: 180 cm) during a single six-hour testing session. Simon Fraser University's Office of Research Ethics approved the protocol, and the participant gave their written, informed consent before experimentation. We placed EMG electrodes bilaterally on the subject's knee joint extensors (VM, R, VL) and flexors (BF, ST, and G) (DE-2.1 EMG sensors, Bagnoli Desktop EMG, Delsys Inc., MA, USA). EMG electrodes were placed in accordance with recommendations from the SENIAM committee (*103*), and the ground electrodes (Dermatrode Reference Electrode, Delsys Inc., MA, USA) were placed on

the kneecaps. The subject then donned an exoskeleton on each leg. All walking was carried out on an instrumented treadmill (FIT, Bertec Inc., OH, USA). We used custom software to measure muscle activity, generator voltages and generator currents in real-time. Subjects first performed a ten second resting baseline EMG trial, where they sat on a chair with legs outstretched and relaxed. These data were used to determine any offset in the recorded EMG and were subtracted in real-time during subsequent walking trials. During walking, EMG signals were full-wave rectified and smoothed using a 3Hz third order low pass Butterworth filter in real-time (Figure 2.1B). Our model was used to calculate desired exoskeleton torque based on measured EMG, and desired generator current based on desired torque. The software commanded the desired current to a custom current control unit, which performed high-frequency closed-loop control of the current drawn from each exoskeleton to match the desired current, and thus match the actual torque to the desired torque. We implemented the real-time software using Simulink and Real-Time Windows Target (Mathworks, NA, USA). All signals were sampled and commanded at 1000 Hz (NI DAQ PC1-6071E, National Instruments Corporation, TX, USA).

2.5.3. Parameter Identification

To identify optimal model parameters for our test subject, they walked on the level at 1.5 m/s for 6 minutes while wearing the exoskeleton with the controller turned off. EMG signals (Figure 2.4 and Figure 2.5) from the last 3 minutes were then used to solve for the optimal muscle gains (K_V, K_R, K_H and K_G) and time delays (T_V, T_R, T_H and T_G) for each leg that best fit literature knee power profiles (*86*) for a similar walking speed (1.6 m/s).

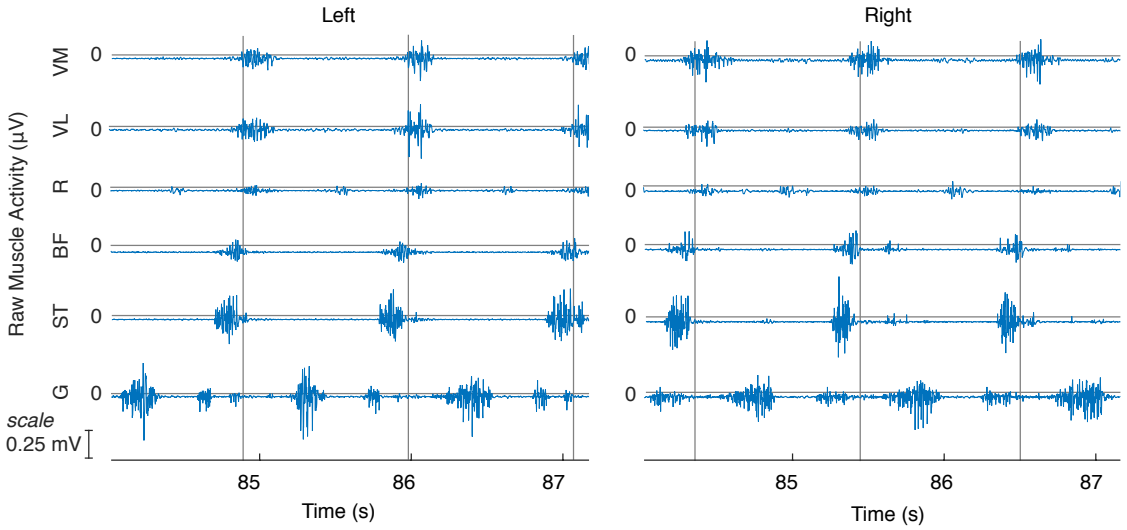

Figure 2.4: Sample raw EMG collected during level walking at 1.5m/s
Muscles include the vastus medialis (VM), vastus lateralis (VL), rectus femoris (R), biceps femoris (BF) and semitendinosus (ST) and medial gastrocnemius (G) for the left and right legs. Vertical grey lines represent heelstrikes for the respective leg.

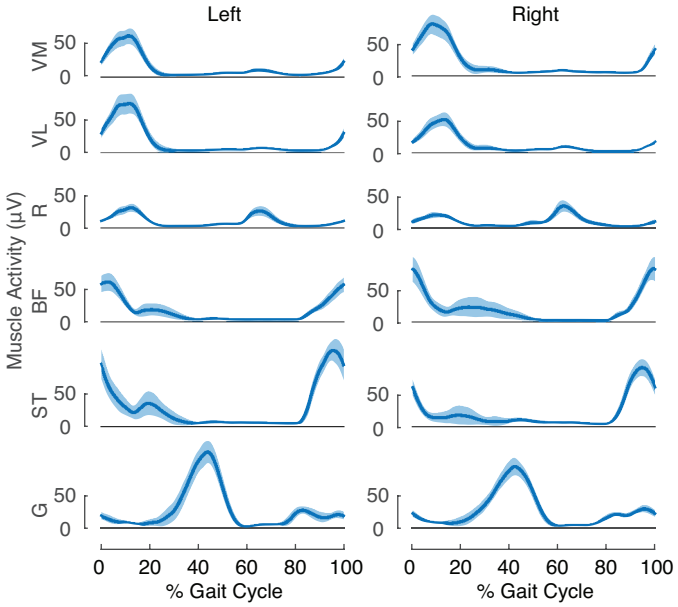

Figure 2.5: Processed EMG collected during level walking at 1.5 m/s
Muscles include the vastus medialis (VM), vastus lateralis (VL), rectus femoris (R), biceps femoris (BF) and semitendinosus (ST) and medial gastrocnemius (G) for the left and right legs. Shaded regions represent ± 1 SD.

Using these optimized parameters, we were again able to produce accurate estimates of both knee torque and power (Figure 2.6, Table 2.1). Our estimates of knee

joint torque using EMG from our single test subject matched the literature knee joint torque just as well as the estimate derived from literature EMG, which was averaged across multiple subjects (R^2: 0.92 for both literature and experimental data). Our experimental estimates of joint power were somewhat worse, but still explained approximately 80% of the variability in literature mechanical knee joint power.

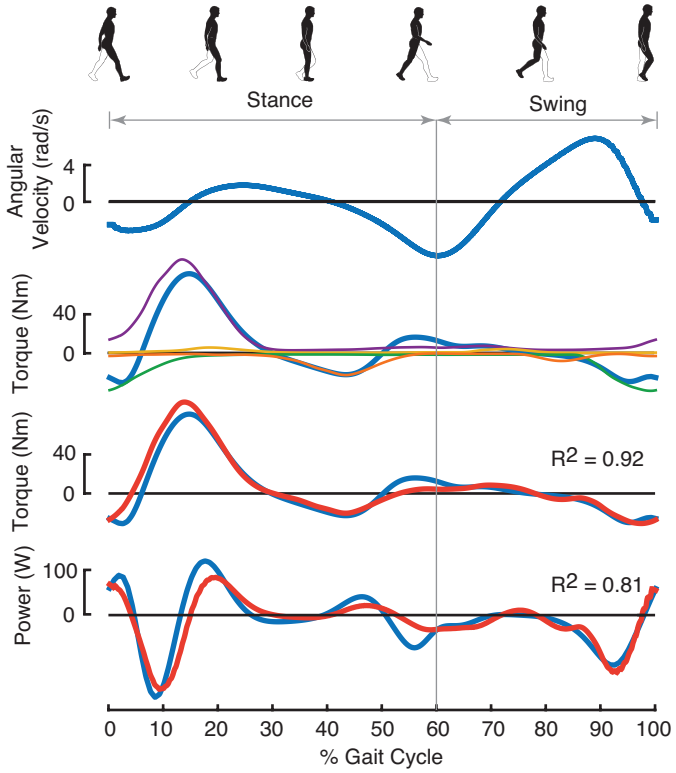

Figure 2.6: Parameter estimation using experimental EMG
Literature knee joint angular velocity, torque and mechanical power (blue; all plots) ***(86)***. Measured EMG signals ***(102)*** were used to identify optimal model parameters, including four gains and four delays, which when applied to muscle activity profiles produced the V, R, G, and H traces (purple, yellow, orange, and green, respectively; second plot). Summing these traces produces the torque estimate (red; third plot), while taking the product of angular velocity and the torque estimate produces the power estimate (red; fourth plot). All EMG data were measured during level walking at 1.5 m/s. Data presented is from the left leg.

A comparison of the optimized parameters from the left and right legs showed many similarities, and one clear difference (Table 1). The knee flexors, including H and

G profiles, were similarly weighted for the two legs and exhibited comparable time delays. The same was true for the dominant extensor profile, V. However, while the extensor R profile made a substantial contribution to the extensor torque for the left leg, it was assigned a zero weighting for the right leg. This finding was consistent regardless of what 3-minute window of EMG data was used for parameter identification. Indeed, we collected walking data with the controller turned off at various points throughout the 6 hour testing session and found that the solved gains and delays for each leg were remarkably consistent. This gives us confidence in our optimized parameters. Thus, the differences between optimized parameters for the left and right legs may highlight our controller's adaptability, not only to particular subjects, but even asymmetries in electrode placement or muscle activity between legs.

2.5.4. Optimal Torque Fraction

Here we identify an optimal fraction of total knee joint torque to be applied by the exoskeleton (Equation 2.2). Our optimized gains and time delays are used to estimate joint torque and power, and the exoskeleton only applies a resistive torque, proportional to joint torque, when joint power is negative. We use a proportionality constant (K) between estimated and applied torque to tune this fraction (Equation 2.2).

To determine the optimal torque fraction applied by the exoskeleton, we had the subject walk at a range of values for K (0, 0.125, 0.25, 0.375, 0.5, 0.75, 1, 2, and 4) that spanned torque fractions from 0 to 4/5. Order was randomized. They walked at each K for 3 minutes at 1.5 m/s on the level, and data from the last 1 minute were used for analysis. For each K, the subject also verbally rated their level comfort on a scale of 1 to 10 (10 being the most comfortable and 1 being the least).

We found a parabolic relationship between harvested power and torque fraction applied by the exoskeleton (Figure 2.7). Harvested power appeared to peak at a K of around 1, which corresponds to a torque fraction of 1/2. However, because comfort scores dropped between a K of 0.5 and 1 (from a score of 6 to 3), we selected a K of 0.5 for all subsequent testing. Muscle activity of the knee flexors and extensors showed trends consistent with these subjective comfort scores, where EMG activity steadily

increased for gains above 0.50 (Figure 2.8). This chosen gain of 0.5 corresponds to a torque fraction of 1/3, and harvested power was still 90% of the maximal produced at a gain of 1.

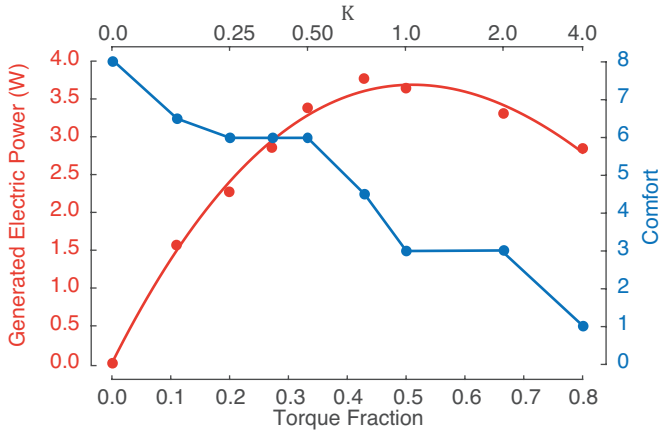

Figure 2.7: Effect of torque fraction on power generation and comfort
Generated electric power (red) and comfort scores (blue) across a range of torque fractions applied by the exoskeleton. The proportionality constant (K) determines the fraction of the total knee joint toque applied by the exoskeleton (Torque Fraction, Equation 2.2). Electric power data presented is from the left leg.

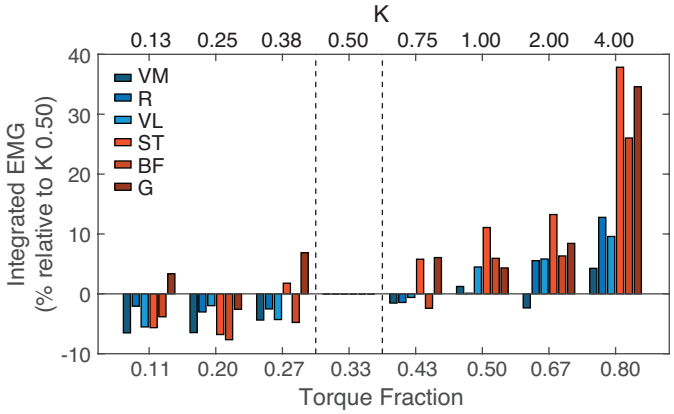

Figure 2.8: Effect of torque fraction on muscle activity
Integrated EMG throughout the gait cycle for the knee extensors (blue shades) and flexors (red shades) for a range of torque fractions applied by the exoskeleton. Muscle activity is normalized to activity from the chosen torque fraction of 1/3 (K= 0.50).

2.5.5. Parameter Validation

We next assessed if our optimized model parameters and K could be used to control energy harvesting for a human walking at different steady state and non steady state gaits. To be useful in real-world walking conditions, our controller must be adaptable to various self-selected gaits, such as different walking speeds, as well as imposed changes in gait, such as those adopted when one encounters a sloped terrain. Moreover, our controller would ideally be adaptable to sudden single step changes in gait, such those taken when stepping over an object or down from an object. We sought to determine if our controller could accurately identify when the knee is generating negative mechanical power, and then automatically adjust the magnitude of electrical power generation for these range of conditions.

Adaptability to Steady State Gaits

To produce different steady state gait patterns that varied the timing and magnitude of negative mechanical knee joint power, we had the subject walk at a range of speeds and slopes. They walked for 2 minutes at speeds of 0.9, 1.25, 1.6, and 2 m/s on the level, in randomized order. They also walked for 2 minutes at slopes of -15°, 0°, and +15° at a speed of 1.5 m/s. We averaged across strides the harvested power from the final one minute of data and compared it to the corresponding literature mechanical power profiles. Level walking literature profiles were from Zelik and Kuo (*86*), while sloped walking profiles were from Lay et al. (*89*, *90*).

Our controller was able to automatically modulate the timing and magnitude of energy harvesting for various steady state gaits (Figure 2.9 and 2.10). For level walking, electrical power was produced during four phases of the gait cycle, all of which correspond to phases of negative mechanical knee joint power from the literature. The controller, which was calibrated only during level walking at 1.5 m/s, was also able to identify phases of negative joint power across a range of speeds and slopes (Figure 2.9 and 2.10, respectively). For example, during decline walking the controller appropriately ceased harvesting at mid-stance (~35% gait cycle)—a phase in which harvesting

occurred on the level. And within each phase, the controller automatically harvested increased levels of electrical power when greater power was available. This can be clearly seen during decline walking and at higher walking speeds.

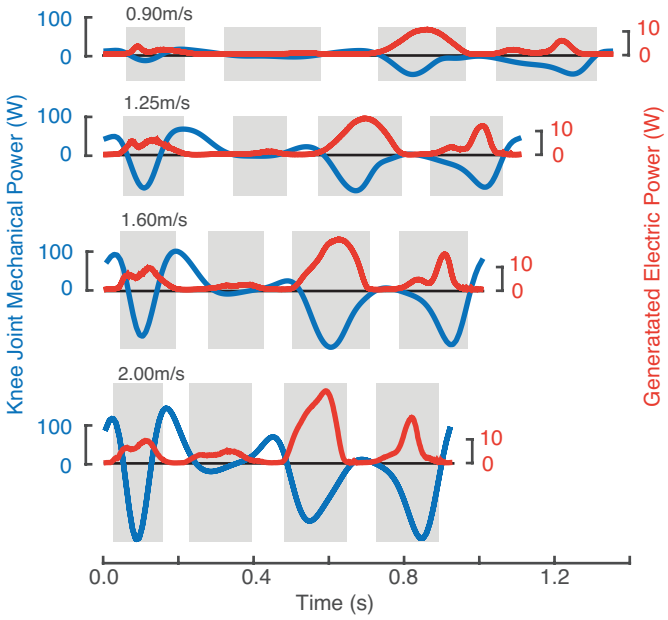

Figure 2.9: Controller adaptability to steady state walking at various speeds
Generated electric power (red) compared to literature knee joint mechanical power (blue) for various walking speeds. Shaded regions represent phases of the gait cycle during with the exoskeletons engaged power generation. The x-axes are expressed in time, as opposed to percent-normalized gait cycle, allowing better visualization of the absolute changes in timing for the various gait speeds presented. Data presented are from the left leg.

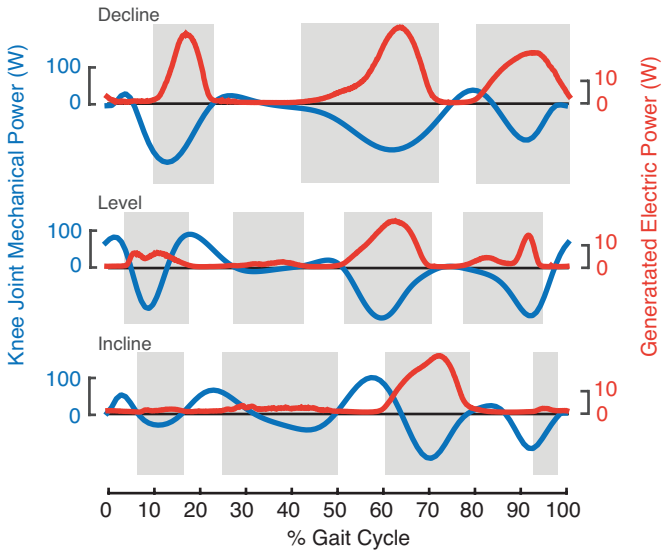

Figure 2.10: Controller adaptability to steady state walking at various slopes
Generated electric power (red) is compared to literature knee joint torque and mechanical power (blue) for decline (-15°), level (0°) and incline (+15°) walking at 1.5 m/s. Shaded regions represent phases of the gait cycle during with the exoskeletons engaged power generation. Data presented are from the left leg.

Adaptability to Non-steady State Gaits

We used three tasks to assess our controller's adaptability to sudden changes in gait. In the first task, we rapidly changed the treadmill speed every 20 seconds during a 2 minute level walking trial. The speed alternated between 1.25 m/s and 1.6 m/s, with an acceleration of 0.1 m/s^2. In the second task, again during a 2 minute level walking trial, we held the treadmill speed constant at 1.5 m/s while the subject simulated stepping over a knee high object, such as a log, every 20th step with the left leg leading. The third task was of similar design to the second except every 20th step the subject lunged down on the left leg, as though bending so that their head could clear an overhead object.

The first task allowed us to assess our controller's responsiveness to rapid changes in gait. Within one step of a speed change, the power harvested immediately increased for increases in speed and decreased for decreases in speed (+1.32 ± 0.28W and -1.10 ± 0.17 W, respectively). The second task, where the subject performs a high step with their left leg, is a task for which we would expect minimal negative knee joint power. Indeed, we found that for these steps, the controller turned harvesting off throughout the 20-80% of the gait cycle when we anticipate the leg is being lifted and

accelerated (Figure 2.11). In the third task, where the subject performs a lunge with their left leg, we would expect high negative knee joint power following heel strike as the subject flexes the knee to lower their body. Indeed, we found that for these steps, significant harvesting occurred in the 0-30% phase of the gait cycle (Figure 2.11).

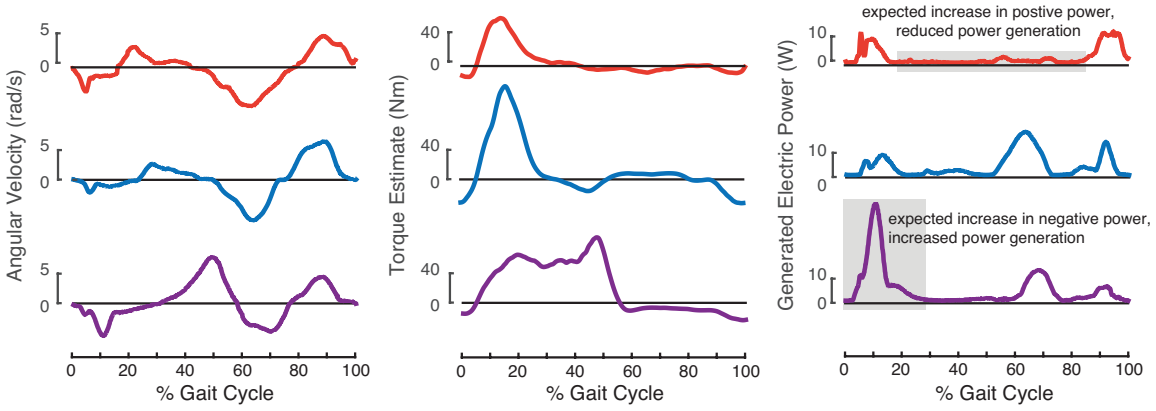

Figure 2.11: Controller adaptability to non-steady state gaits
Knee joint angular velocity (left column), torque estimate (middle column), and generated electric power (right column) for a high step (red; top row), normal step (blue; middle row), and downward lunge (purple; bottom row). Generated electric power is relatively low during mid gait cycle for the high step, when net knee joint mechanical power is expected to be positive, and is markedly increased during early gait cycle for the lunge, when net knee joint power is expected to be negative during lowering (regions indicated with grey shading). Walking speed was 1.5 m/s and data presented are from the left leg.

2.6. Discussion

We have demonstrated that myoelectric control can be used to automatically adapt the timing and magnitude of electrical power generation for an energy harvesting exoskeleton. Our controller design engages power generation only when estimated knee joint mechanical power is negative. When engaged, the exoskeleton scales the resistive torque in proportion to estimated knee joint torque, thereby automatically scaling electrical power generation in proportion to the available negative mechanical power at the joint. Real-time estimates of knee joint torque and power are crucial to our controller's function and are produced using a simple model embedded within our controller that relies on muscle activity from knee joint flexors and extensors. We found that this model was able to predict knee joint dynamics across a range of timings and

magnitudes. We demonstrated this using literature EMG data available for a range of walking speeds and found that estimates of knee joint torque and power well matched the corresponding literature profiles (torque R^2: 0.73-0.92; power R^2: 0.60-0.94). We also preformed preliminary experiments, which demonstrated that our myoelectric controller can be used to identify when the knee is generating negative mechanical power, and automatically adjust the magnitude of electrical power generation. It appeared to work well for a range of steady state walking speeds and inclines, as well as number of non-steady state walking conditions.

One limitation of this preliminary test of our controller is that we did not measure the knee joint torque and mechanical power for our particular subject. Instead, we relied on average literature profiles from able-bodied subjects. Our approach does have the benefit of more closely replicating exoskeleton use in a real-world setting, where capturing subject specific joint kinetics using inverse dynamics (*104*, *105*), may be difficult and cumbersome. However, future work may still benefit from subject-specific joint kinetics during parameter identification, allowing model parameters to be optimized to a user's particular knee joint torque and power. This may be especially important for users that display atypical gait patterns, such as those with mobility impairments. We expect knee joint kinetics were quite similar to literature values for our able-bodied test subject, but even in our specific case, we may have benefited from subject-specific measures. For example, we found that the R muscle activity for the right leg was not needed to predict literature values of knee joint torque (gain of 0 assigned). However, it is also possible that for this particular subject and leg, the R muscle activity was responsible for an atypical extensor torque that was not evident in the literature torque profile. Further testing is needed to determine when differences between individuals, and between limbs within an individual, necessitate user specific knee joint kinetics for parameter estimation. Another benefit of collecting subject-specific kinetics is that they could be used to further validate our controller's performance. EMG-derived estimates of knee joint torque and power from each trial would ideally be compared to the knee joint kinetics measured during that particular trial. This is because the interaction with the active exoskeleton may have caused actual knee joint kinetics to differ from generic literature profiles during steady state walking. Moreover, it would have provided us with joint kinetics for non-steady state walking conditions (conditions that are absent from the

literature). Our use of literature values for parameter estimation and subsequent assessment of our controller performance demonstrate the potential usefulness of this type of control, which is likely to only improve with subject-specific measures.

Even with subject-specific joint torque and power profiles, the biomechanics and control of muscle action makes predicting optimal phases of harvesting difficult. As detailed by Li and Donelan, muscle co-contraction, bi-articular muscle architecture and elastic energy storage complicate the relationship between net joint power and true muscle power (*84*). And for effective generative braking, a controller needs to assist muscles, not joints, in performing negative mechanical work. There are a number of ways our myoelectric controller could be adapted to deal with these physiological complexities. For one, our controller could be used in combination with a state-machine that disengages or engages electrical power generation during phases of negative joint power that don't reflect true negative muscle power. For example, if it is determined that the negative joint work performed at the beginning of walking's stance phase is typically stored and returned to straighten the knee during the middle of stance, a modified controller may leverage measures of muscle activity to detect this event and turn off electrical power generation for this phase. With this hypothetical modification, our myoelectric controller would be used for the remainder of the walking cycle to modulate the timing and magnitude of power generation. Integrating our myoelectric controller within a state-machine certainly reduces the simplicity and generality of our controller, but the combination of the two may outperform either on their own.

Rather than modifying our controller to compensate for the complex relationship between joint and muscle power, it may instead be feasible to keep our controller exactly the same and control the action of the exoskeleton based on estimates of muscle torque and power, rather than joint torque and mechanical power. Much development has been directed towards musculoskeletal models that combine EMG with forward dynamic models to predict individual muscle velocities, forces and mechanical powers (*91*, *106*, *107*). Future work may combine these models with our parameter identification procedure to find the optimal parameters for relating measured muscle activity to muscle torque and power. Using these muscle-optimized parameters with our myoelectric controller may improve the accuracy and efficiency of harvesting while preserving its

generality and adaptability. It is also possible that these more complex musculoskeletal models are integrated within our controller in place of our simple model and used to estimate muscle force and power not just within the parameter identification procedure, but for all conditions. This would likely require a more extensive muscle set as well as real-time estimates of kinematics and kinetics from all lower limb joints. Given the success of our simplified controller, we suspect that any improvements in performance would not outweigh the drawbacks of added model and instrumentation complexity.

Our controller structure lends itself naturally to adaptive control. The controller initially has a small number of parameters, and we fix all but one of these using a parameter identification procedure. The remaining free parameter is the gain between estimated torque and applied torque (K)—it determines the relative contribution of the exoskeleton to the total joint torque and power. In our experiments, we evaluated a range of its values and found that there is a tradeoff between subject comfort (which is high at low values of K) and electrical power generation (which is high at high values of K). One use of this gain is to allow a user to manually adjust this single parameter to optimize their current needs—comfort or power. Rather than yield control to the user, the controller may instead employ adaptive control, adjusting this gain to meet some programmed objective. For example, the objective may be to maximize power generation while maintaining user comfort. As a user becomes more experienced with the exoskeleton and learns to take advantage of the assistance it provides, their muscle activity may reduce for a given value of K (*67*). Sensing this, an adaptive controller could increase K to match the prior levels of muscle activity, increasing electrical power generation while attempting to maintain user comfort. Alternatively, the controller may regulate power generation by adapting K in order to keep a battery at some minimum charge. Whatever the programmed objective, it is convenient to have a single adjustable parameter.

Muscle fatigue can pose a challenge for myoelectric controllers, as EMG signal characteristics can change without a corresponding decline in the generated muscle force. As a muscle fatigues the build up of metabolic by-products can slow the conduction velocity of motor unit action potentials, shifting their spectral power to lower frequencies (*108*, *109*). This shift to lower frequencies is captured by surface EMG and

can be characterized using measures or mean or median power frequency (*108*). This spectral shift also affects the amplitude of the signal in the time domain. Tissues between the emanating signal and the detection site, be it muscle or fat, act as low pass filters. Because the frequencies of the signals have shifted to the lower end of the spectrum, more signal energy is able to pass through the tissues and an increase in signal amplitude is recorded during fatigue (*108*). Our myoelectric controller relies on these time domain EMG amplitudes and may therefore be disrupted as fatigue progresses. If all muscles in the algorithm fatigue at a common rate, with their amplitudes increasing by a common gain, the shape of the joint power estimate produced by our controller would remain unchanged. The estimate would simply increase in amplitude, but the timing of regions of positive and negative power would not be affected. This would essentially function like applying a torque fraction (K) that is higher than optimal for the user. Here, an adaptive control strategy, again based on comfort or harvested power, could be used to compensate for fatigue by reducing torque fraction (K). In the more probable case that muscles fatigue at varying rates, the shape and zero crossings of the power estimate would be disrupted leading to poor control. Here, a different corrective strategy would be required. One benefit of our controller design is that individual muscle parameters can be re-optimized during a short level walking period, potentially allowing the user to rapidly account for fatigue. However, if fatigue levels are gradually changing over time, this may not be a desirable solution, as the user would need to re-optimize frequently. Instead, it is possible that future versions of our controller correct for EMG amplitude changes using the spectral characteristics of the EMG signal. For example, as median power frequency declines for a particular muscle, the gain on that muscle could be reduced to compensate for an increasing amplitude (*110*).

While we have focused here on energy harvesting, our methods also apply to powered exoskeletons. For one, electrical motors in actuated exoskeletons may be used as generators to recover energy from the natural motion of walking. But more importantly, it is also possible that our EMG-derived estimates of joint torque and power be used to control exoskeletons that do not seek to harvest electrical power, but rather to assist movement. These exoskeletons need not be limited to those acting at the knee joint; our model of joint torque and power may work equally well using muscles that act

about other joints. By translating the user's own neural signals, our controller design appears to adapt well to complex and varied movements and environments.

Chapter 3.

Humans can continuously optimize energetic cost during walking

3.1. Abstract

People prefer gaits that minimize energetic cost. Although aspects of this preference are likely established over evolutionary and developmental timescales, here we test whether people can continuously adapt their gait to optimize energetic cost in real-time. To accomplish this, we used robotic exoskeletons to manipulate people's energetically optimal step frequency, creating novel energetic landscapes in which prior predictions about energetic optima were obsolete. We found that subjects adapted their step frequency to converge on the new energetic optima within minutes, and remarkably, in response to relatively small cost savings (< 5%). When transiently perturbed from their new optimal gait, subjects relied on an updated prediction to rapidly re-converge within seconds. Our collective findings indicate that energetic cost is not just an outcome of movement, but plays a central role in continuously shaping it.

3.2. Introduction

Within the constraints imposed by a particular task, people prefer to move in ways that minimize energetic cost(*33*, *34*, *36*, *37*, *39*, *40*, *111*). For example, a person's walking speed may be constrained by the need to catch a departing bus, but within this speed constraint, they will choose to use their energetically optimal step frequency. This phenomenon has been established for decades, and now represents a central principle of movement science(*111-113*). But the processes by which people discover their optimal patterns are not clear. Much theorizing has focused on optima being established

over evolutionary timescales, through changes to body shape, muscle action, and the hardwiring of neural circuitry (*40-43*). Energy optimization may additionally occur over the course of a lifetime, as years of experience could allow people to learn the optimal way to move in familiar situations and allow training to tune physiology to be more economical (*44*, *114*). An alternative hypothesis—one that underpins many modern theories of motor control—is that people can adjust their movements to continuously optimize energetic cost (*14*, *43*, *47*, *115-117*). Only recently has energetic cost been assessed during standard adaptation paradigms, and it was indeed found that cost was lower after adaptation than before in both reaching and walking tasks (*47*, *49*). These studies, while tantalizingly suggestive, were not designed to test whether energetic cost minimization was a control objective of the central nervous system, leaving the possibility that the measured reductions in energetic cost were correlated with alternative nervous system goals.

Here we directly address the continuous optimization hypothesis using robotic exoskeletons to create novel energetic landscapes and then test if walking subjects adopt the necessary gait adaptions to find new optima. Of all possible energetic landscapes, we chose to manipulate the relationship between step frequency and energetic cost, because step frequency is a fundamental characteristic of gait, people have strong preferences for particular step frequencies, and these preferred frequencies are energetically optimal (*38*, *118*). We manipulated the relationship using lightweight robotic exoskeletons to apply torques that resisted the motion of the knee joints (Figure 3.1A-B). To shift the energetic optimum to lower step frequencies, we had the exoskeleton controller use a “penalize-high” control function that applied a resistance, and therefore an added energetic penalty, that was minimal at low step frequencies and increased as step frequency increased (Figure 3.1C-D). To shift the energetic optimum to higher step frequencies, we used a “penalize-low” control function, where the slope of the penalty was reversed (Figure 3.1C-D). The control functions were designed to create a clear energetic gradient for step frequencies in the neighborhood of subjects’ initial preferred step frequency, yet keep all resistive torques low enough to allow relatively natural gaits. To distinguish between energetic cost optimization and simply minimizing the resistance applied to the limb, we also designed the control functions to ensure that the energetic cost optima occurred at step frequencies distinct from those that minimized

exoskeleton resistance. It is not possible to design control functions that specifically rule out all alternative objectives to energetic cost minimization. But to be indistinguishable from energy minimization, optimizing these alternative objectives would need to yield step frequency adaptations in the same directions, and by about the same magnitudes, as those predicted by our novel energetic landscapes.

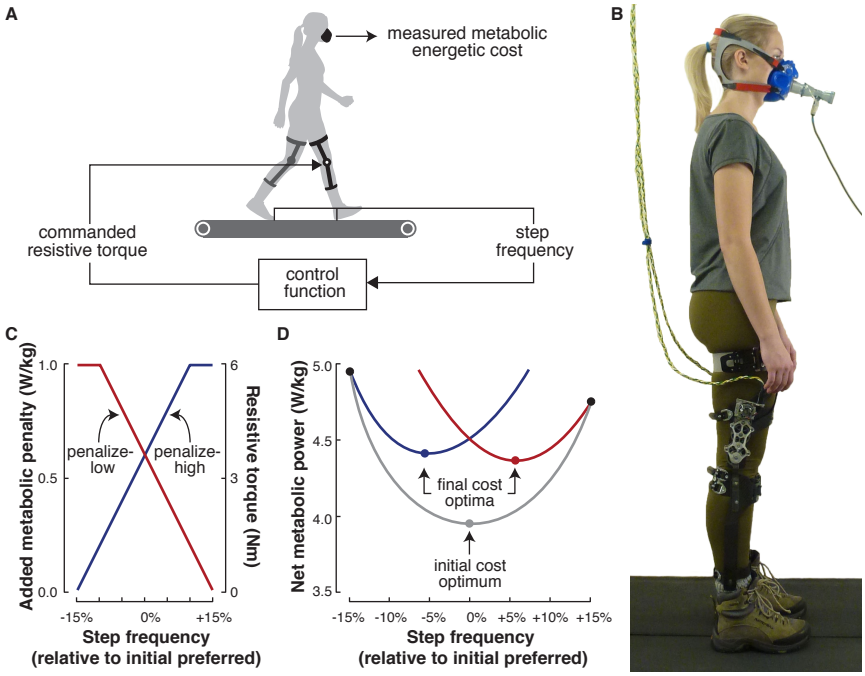

Figure 3.1: Experimental design
(A-B) By controlling a motor attached to the gear train of our exoskeletons, we can apply a resistance to the limb that is proportional to the subject's step frequency. **(C)** Design of the penalize-low (red) and penalize-high (blue) control functions. **(D)** Schematic energetic landscapes. Adding the energetic cost of the penalize-low control function to the natural cost curve (grey) produces a cost curve with the optimum shifted to higher step frequencies (red curve). The optimum can instead be shifted to lower step frequencies (blue curve) by adding the energetic cost of the penalize-high control function to the natural cost curve.

3.3. Results

Natural gait variability does not reliably initiate optimization

We first sought to determine if our subjects would adapt to a new energetically optimal step frequency given limited experience with the novel energetic landscape and

without being perturbed away from their natural gait. Subjects were assigned to both the penalize-high and penalize-low control functions, in random order, on two separate testing days. On each day, during an initial baseline trial, subjects first walked for 12 minutes while wearing the exoskeletons, but with the controller turned off (Figure 3.2A, baseline). This allowed us to determine their "initial preferred step frequency", which we defined from the final three minutes of walking. All walking took place on an instrumented treadmill (FIT, Bertec Corporation, MA, USA) at 1.25 m/s and we measured step frequency from treadmill foot contact events. All subjects appeared to settle into a steady state step frequency within 9 minutes. On average subjects walked at 1.8 ± 0.1 Hz (mean ± SD), and from step to step subjects' step frequency varied about this average by 1.1 ± 0.3 % (mean ± SD). We then turned the controller on, resulting in an applied resistive torque that was dependent on step frequency, and the subjects walked for an additional 12 minutes (Figure 3.2B, first adaptation). During this time, subjects showed no adaptation in step frequency (penalize-high: $p = 4.3\times10^{-1}$, penalize-low: $p = 4.4\times10^{-1}$). They continued to walk at their initial preferred step frequency even though we designed the controller such that minor adjustments to step frequency would result in a more economical gait.

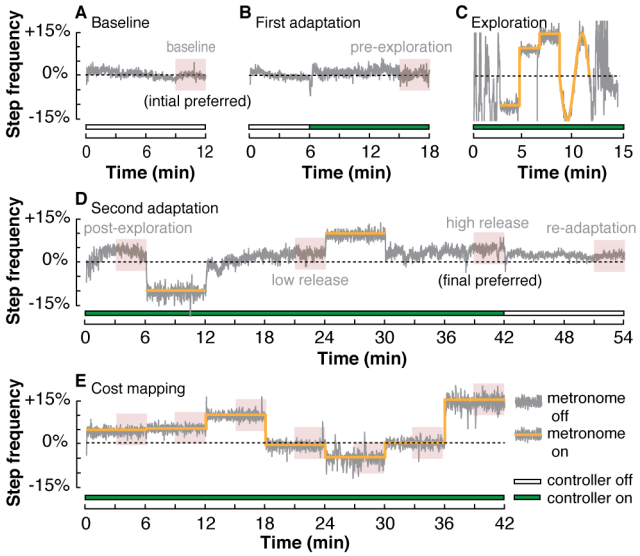

Figure 3.2: Experimental protocol
Measured step frequency from a representative subject for a single day of testing with the penalize-low control function. Subjects completed five testing periods: Baseline, First adaptation, Exploration, Second adaptation, and Cost mapping (A-E, respectively), with a rest period (5-10 minutes) between each period. For all periods, regions of red shading illustrate the time windows during which we assessed steady-state step frequencies and metabolic costs.

Broad experience with the energetic landscape initiates optimization

We next gave our subjects experience with the novel energetic landscape across a wide range of step frequencies and then once again looked for adaptations toward the novel energetic minima. This was accomplished by instructing subjects to self-explore walking with high and low step frequencies, as well as match their steps to different steady-state and sinusoidally varying metronome tempos (Figure 3.2C, exploration). Following this 15 minute exploration period, subjects were again allowed to self-select their step frequency (Figure 3.2D, second adaptation) and we found that subjects immediately made large adaptations in step frequency toward the energetic minima (Figure 3.3A). To robustly determine if this was a new preferred step frequency, we had subjects match a metronome tempo for 6 minutes that perturbed them toward both higher resistive torques (penalize-high: +10%; penalize-low: -10%) and lower resistive torques (penalize-high: -10%; penalize-low: +10%) (Figure 3.2D, second adaptation).

Following each perturbation, subjects were allowed to self-select their step frequency for another 12 minutes and we found that they returned to a step frequency that was shifted toward the energetic optima (Figure 3.3). We defined the average of the final 3-minutes of self-selected step frequency after the last perturbation as the "final preferred step frequency". On average, when given the penalize-high control function, subjects decreased their step frequency by 5.7 ± 3.9 % (mean ± SD), while for the penalize-low control function subjects' step frequency increased by 6.9 ± 4.3 %. These final preferred step frequencies were distinct from what subjects initially preferred (penalize-high: $p = 1.3\times10^{-3}$, penalize-low: $p = 6.2\times10^{-4}$). And, they were distinct from those that would minimize the resistive torque being applied to the limb (penalize-high: $p = 5.2\times10^{-5}$, penalize-low: $p = 2.4\times10^{-4}$).

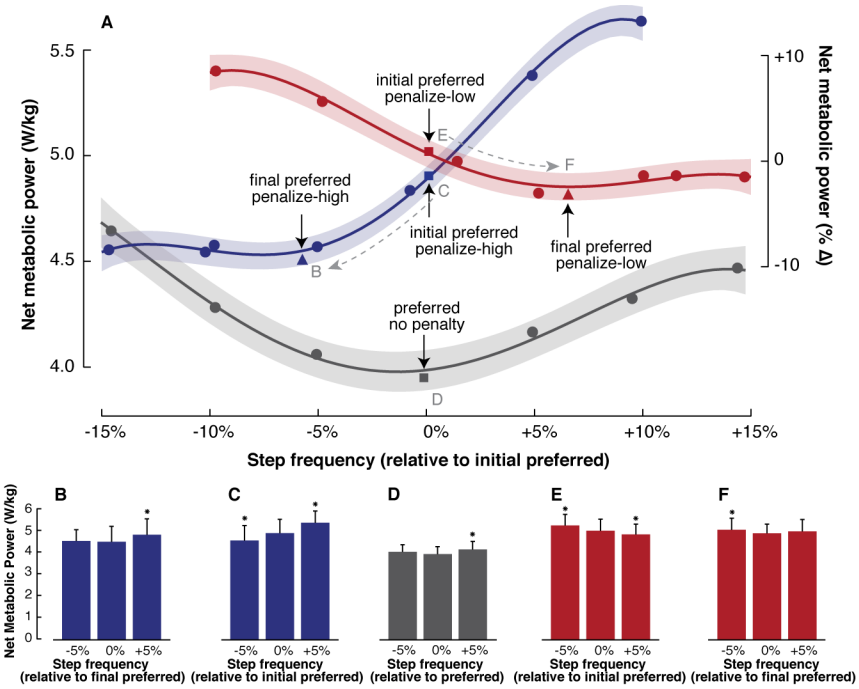

Figure 3.3: Optimization of energetic cost
(A) Energetic landscapes, averaged across all subjects, for the penalize-high (blue) and penalize-low (red) control functions, as well as for the controller off condition (grey). The lines are 4th order polynomial fits, and the shading their 95% confidence intervals, shown only for illustrative purposes. Dashed grey arrows illustrate the directions of adaptation from initial preferred to final preferred step frequencies. Comparisons of energetic costs, averaged across all subjects, around the initial preferred step frequencies (C-E) and final preferred step frequencies (B, D, and F). Error bars represent 1 standard deviation. Asterisks indicate statistically significant differences in energetic cost when compared to the cost at the initial or final preferred step frequency (0%).

Gait adaptations converge on energetic optima

We next sought to determine how our subjects' final preferred step frequency compared to the energetically optimal step frequency by mapping their energetic landscape. We again turned the controller on and had subjects walk to steady-state metronome tempos for 6-minutes each (Figure 3.2E, cost mapping), including tempos about the initial preferred step frequency (+5%, 0%, -5%) and about the final preferred step frequency (+5%, 0%, -5%). We measured metabolic energetic cost using respiratory gas analysis equipment (VMax Encore Metabolic Cart, ViaSys, IL, USA). As hypothesized, our subjects had indeed increased or decreased their self-selected step frequency, whichever was required by the new landscape, to converge on the new

energetic optima (Figure 3.4). These adaptations were to achieve relatively small cost savings. The energetic cost at the final preferred step frequency was 8.1 ± 7.0 % lower than the energetic cost at the initial preferred step frequency for the penalize-high control function ($p = 4.1\times10^{-3}$) and 4.0 ± 3.8 % lower for the penalize-low control function ($p = 9.7\times10^{-3}$). Subjects achieved most of the costs savings immediately after the exploration period, yet continued to fine-tune their step frequency for vanishingly small energetic savings (Figure 3.3). Evaluating the energetic cost at the final preferred step frequencies, and at step frequencies on either side of the final values, suggested that subjects converged to, or at least near, their minimum costs; no further cost savings appear to be gained by additional adjustments to preferred step frequency (Figure 3.4B and 3.4F).

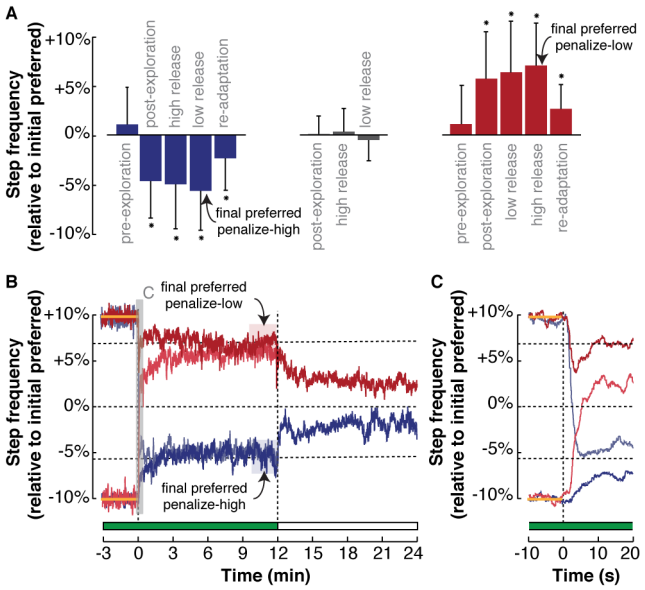

Figure 3.4: Time course of step frequency adaptations
(A) Steady-state step frequencies, averaged across subjects (mean ± SD), throughout the course of the protocol. Results for the penalize-high control function are shown in blue, the penalize-low control function in red, and the controller off condition in grey. Asterisks indicate average step frequencies that are statistically different from 0% (the initial preferred step frequency). (B) Step frequency time-series data, averaged across subjects, for the release high and low from the second adaptation period. For the penalize-high controller, the release from high and low step frequencies is shown in light and dark blue, respectively. For the penalize-low controller, the release from low and high step frequencies is shown in light and dark red. The horizontal bar indicates when the controller is turned on (green fill) and off (white fill), and the yellow lines indicate the prescribed metronome frequencies. (C) Average step frequency time-series data for a 30-second window about the metronome release (at time 0).

Gait adaptations use updated predictions of energetically optimal gaits

Following perturbations using the metronome tempos, our subjects converged towards their new preferred step frequency within seconds (Figure 3.3B-C). In cases where subjects were held at metronome tempos that resulted in high resistive torques (penalize-high: +10%; penalize-low: -10%) and then released, they immediately bypassed their initial preferred step frequency, which was now energetically suboptimal, to quickly converge on the new preferred and energetically optimal step frequency. All subjects bypassed the initial preferred step frequency in less than 10 seconds. When

held at metronome tempos that resulted in low resistive torques (penalize-high: -10%; penalize-low: +10%) and then released, subjects actually elected to increase the resistance on their limb, again within seconds, in order to reach the energetic optima. We have previously argued that the time scale of such rapid adaptations to energetically optimal gaits requires the prediction of energetic cost, rather than its direct optimization [29]. That subjects rapidly converge on new energetic minima indicates that subjects had updated their prediction of the optimal gait for each control function. This is also observable when the high or low penalty was removed for a final 12 minutes (Figure 3.2D, second adaptation); subjects' step frequency remained shifted toward the control function optima for minutes despite a return to the natural energetic landscape and its former energetically minimal gait (Figure 3.3).

3.4. Discussion

We have shown that during walking people can adapt established motor programs to minimize energy use. We used robotic exoskeletons to shift people's energetically optimal step frequency to frequencies higher and lower than normally preferred. After just minutes of exploratory experience with these novel cost landscapes, we found that subjects adapted their step frequency to converge on the new energetic optima. They did so in opposite directions (-5.7% and +6.9%) based on the landscape profiles, and remarkably, in response to relatively small energetic cost savings (< 5%). Following this, when transiently perturbed from their new optimal gait, subjects rapidly re-converged on the optima within seconds. It appears that, despite a lifetime of experience walking under natural conditions, people can readily adapt fundamental characteristics of their gait to minimize energy expenditure.

Motor variability has traditionally been thought of as an inevitable, if not potentially burdensome, consequence of imperfect neural control. However, recent findings have reframed motor variability as an asset—one that can facilitate and enhance motor learning. For example, song birds are able to leverage small variations in their pitch to continuously optimize their song performance (*119*), while humans actively reshape the structure of their motor output variability to elicit faster learning of reaching tasks (*120*). We found that natural gait variability did not initiate the optimization process

in our particular experiment. Instead, subjects persevered at their initial preferred step frequency after the controller was turned on, even though minor adjustments to step frequency would have resulted in a more economical gait. Only after the exploration period, which enforced large variations in step frequency, did subjects demonstrate large adaptations toward the new energetic optima (Figure 3.3A). One possible explanation for this need for exploration is that people's natural variability in step frequency is not expansive enough to elucidate a clear energetic gradient. Alternatively, people may not initiate optimization based on energetic gradients, but may instead require that exploration provide explicit experience with the new optimum in order for people to adapt to it. In either case, these may be smaller issues when walking in a real world setting because natural changes in speed and terrain may generate the variability in gait required to either initiate optimization or provide experience with new optimal movement patterns.

Our findings suggest that new optima are encoded in an updated prediction of the energetically optimal gait and leveraged to rapidly select preferred step frequency (*2*, *121*). When subjects were held away from their preferred step frequency using a metronome and then released, they returned to their new preferred step frequency within seconds (Figure 3.3B and 3.3C). These gait adjustments are likely too fast to be governed by blood gas sensors, muscle metaboreceptors, and other known direct sensors of energetic cost, which are known to be relatively slow (*122*, *123*). Furthermore, optimization itself tends to be slow if its algorithm requires the time consuming steps of averaging and iterative convergence (*2*). That the subjects made an updated prediction of the optimal gait is also observable at the end of the experiment, when subjects preferred step frequency remained shifted towards the control function optima for minutes despite a return to the natural energetic landscape (Figure 3B). This aftereffect differs from the aftereffects seen in force-field reaching or split-belt walking paradigms (*21*, *124*), where the resulting trajectories are mirror images of those observed when initially exposed to the novel environment. When our controller was turned off, rather than displaying this overshoot and rapid correction, we instead found that subjects adjusted to the rapid reduction in exoskeleton torque and persevered at the optimum for the previous adaptation. These aftereffects appeared to last an order of magnitude longer than those typically reported in other walking paradigms (*24*, *25*, *124*,

125). This implies that sensorimotor predictions about energetically optimal movements are particularity resilient, at least without an exploratory phase to initiate re-optimization. The slow step frequency adjustments during re-adaptation are not in conflict with the fast adjustments observed when subjects are released from a metronome after exploring their new energetic landscape. During the latter, subjects are able to quickly predict their optimal gait within a now familiar energetic landscape. But the former requires optimizing within a new energetic landscape, or at least recognizing that this new landscape is familiar.

In recent years, optimal control models of biological movement have successfully explained complex and varied behaviour (*43*, *126*). Nearly all such models explain coordination as arising out of the desire to minimize an objective function with two primary terms, one representing error and a second representing effort. To date, scientific focus has been directed primarily at the first term; various measures of task error have been proposed and then subjected to careful experimental testing (*14*, *43*, *115-117*, *127*, *128*). In contrast, we know relatively little about what the nervous system considers as effort, as well as the importance of this effort relative to other objectives in determining our preferred coordination. In the context of optimal control, our results suggest that the nervous system manages metabolic energetic cost as one measure of effort, and in walking, its minimization is important relative to other objectives. This is consistent with recent findings demonstrating that energetic cost was lower after adaptation than before in both reaching and walking tasks (*47*, *49*).

This present work benefitted from three previous attempts, including one by our group, to directly manipulate subject's energetic cost functions during walking (*2*, *80*) or reaching (*48*). None had been able to show clear adaptation to new energetic minima, but a careful study of their protocols and controllers guided us in designing ours. First, we focused on ensuring that the energetic cost gradient about subjects initial preferred step frequency was clear, substantial, and sloped in the appropriate direction by comparing the energetic cost at the initial preferred step frequency to the energetic cost at step frequencies 5% slower and faster than this preferred value (Figure 4C and 4E). Second, we kept context as consistent as possible on each testing day. That is, we did not alternate between the penalize-high and penalize-low conditions in order to avoid

contradictory experience with the exoskeleton which may interfere with learning (*129*). Third, we tried to limit the complexity of our controller. Measured step frequency was directly coupled to a resistance that was applied throughout the stride. Other more complex controllers that involve filtering, delays, or more arbitrary couplings may be outside the realm of normal experience and therefore more difficult to learn (*130*). Last, and perhaps most importantly, we encouraged and enforced subjects to explore different ways of walking, giving them board experience with the energetic landscape. Our experimental results indicate that this exploration is very important, if not necessary, to initiate adaptation.

At an applied level, the drive to continuously seek energetic optima presents challenges and opportunities for rehabilitating and augmenting human movement. Traditional rehabilitation of stroke-induced asymmetries, as well as other gait disorders, is often focused on restoring 'normal' symmetric limb trajectories (*26*, *131*). But the achieved symmetries are transient (*26*, *131*). Our findings perhaps suggest that the asymmetric gait is preferred because it is energetically optimal (*132*). Rehabilitation may instead take advantage of continuous cost optimization by reshaping underlying energetic landscapes with training or assistive devices to align the otherwise competing goals of symmetrical and optimal gaits. Our findings also have important implications for the recent and exciting push to design and build robotic exoskeletons to improve human performance. To date, users of these well-designed and powerful devices have only gained modest performance improvements (*70*), perhaps because, like our subjects, users persevere with aspects of their normal, and now suboptimal, coordination. A successful partnership between human and machine may require the exoskeleton to not only reshape the user's energetic world, but also guide them through their new landscape to their improved, and energetically optimal, performance.

More broadly, our finding that energetic cost is continuously optimized gives rise to a number of fundamental questions. First, how is energetic cost sensed? It may be directly sensed, either globally by known blood gas receptors (*50*-*52*) or locally by muscle receptors sensitive to the byproducts of metabolism (*53*, *54*). It may instead, or in addition, rely on indirect information that the body has learned is related to energetic cost. These energetic proxies may include ventilation rate, motor efference copy, or

some combination of muscle proprioceptor activity. Experimentally perturbing blood gas sensors or muscle afferents in isolation may provide insight into the relative importance of each type of sensor for real-time cost optimization. Second, what is the nature of the optimization process? Walking requires the time-varying coordination of tens of thousands of motor units, resulting in an optimization of dauntingly high dimension. To overcome this 'curse of dimensionality', our nervous system may be primed to quickly search only a reduced subspace—such as particular combinations of speeds and step frequencies or particular combinations of muscle activities—rather than attempting to continually tune the contributions of individual motor units (*8*, *133*) The nervous system may also employ a 'local search' strategy or other optimization tricks to speed the search for new energetic optima. For example, a gradient decent process could be used to converge on optima. Finally, does continuous energetic cost optimization generalize to movements other than walking? Theories of motor control and learning often rely on energy optimization to explain the coordination of discrete movements like reaching, and postural tasks like standing and sitting (*127*, *128*). While our research provides clear evidence that the nervous system can indeed perform such continuous cost optimization, future experiments will be needed to test whether the nervous system can leverage this capability in the control of discrete and low cost movements. It is sensible that motor programs remain malleable because people's bodies, and the tasks they are presented with, can change. Continuous energetic optimization may assist motor adaptation by keeping movements close to energetically optimal, helping people to efficiently adapt to changing terrains, compensate for injury or motor deficits, and learn new tasks.

3.5. Experimental Procedures

Controller Design

We manipulated energetic cost using robotic exoskeletons mounted about the knee joints. Each exoskeleton weighed 1.1 kg and was composed of a custom carbon fiber shell and custom steel gear train coupled to an off-the-shelf rotary magnetic motor (BLDC40S-10A, NMB Technologies Inc.) (Figure 3.1A-B). Rather than powering the motor to induce motion, we used the motor as a generator to provide controlled

resistance to knee flexion and extension. During walking, the relatively low angular velocity characteristic of knee motion was transformed by the gear train to produce relatively high angular velocity at the motor. This rotational motion in the motor's rotor induced voltage in the motor's windings and, when allowed, electrical current (*84*). The induced current generated its own magnetic field that resisted the motion of the knee with a torque proportional to the current magnitude. We used a custom control unit to measure and control the flow of electrical current through the motor, and therefore the magnitude of the resistive torque applied to the knees (Figure 3.5A-C). In the penalize-high and penalize-low controller settings, the commanded resistive torque sent to the control unit was proportional to the subject's step frequency measured from the previous step. While the commanded torque within each step was a constant, the applied torque only reached the commanded value for the periods of the step cycle when the knee angular velocity, and thus motor voltage, was sufficiently high (Figure 3.5A-B). In the controller off setting, the commanded current, and thus commanded resistive torque, was zero. Step frequency for an individual step was calculated as the inverse of the time between foot contact events, identified from the time derivative of the ground reaction force center of pressure in the fore-aft direction (*134*) from the instrumented treadmill (FIT, Bertec Inc.). Ground reaction forces, as well as measured motor current and voltage, were sampled at 200 Hz (NI DAQ PCI-6071E, National Instruments Corporation). Step frequency, and the newly desired knee torque were commanded in real-time at 200 Hz using custom software (Simulink Real-Time Workshop, Mathworks). We estimated the actual torque applied to the knee from the product of the measured motor current, the motor's torque constant (3.36×10^{-2} Nm/A) and the exoskeleton gear ratio (110:1 gear ratio).

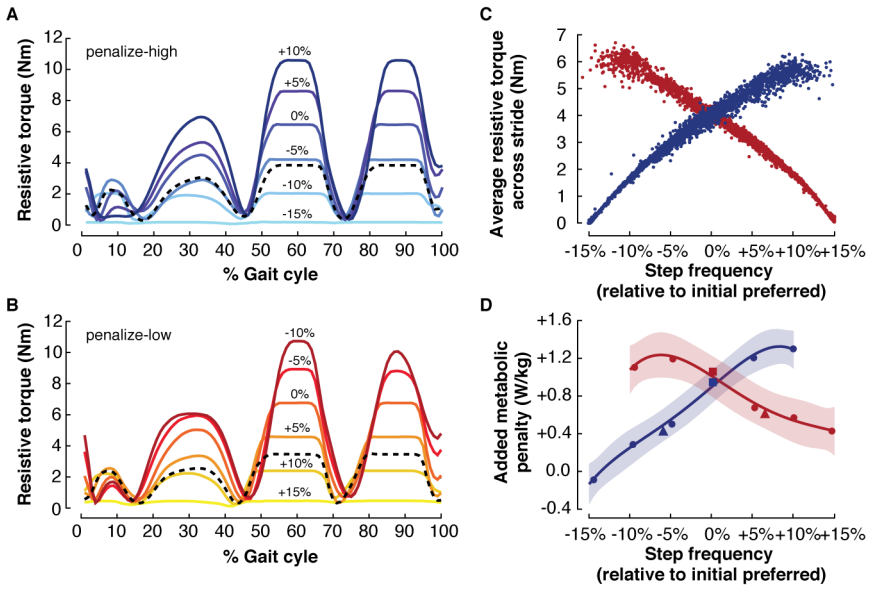

Figure 3.5: Controller performance
(A) Resistive torque applied throughout the gait cycle for a representative subject walking at a range of step frequencies (+10 to -15% of the initial preferred step frequency) under the penalize-high controller. The black dotted line illustrates the resistive torque profile at their final preferred step frequency. (B) The equivalent plot for the penalize-low controller. (C) The average resistive torque across a stride for a range of step frequencies in the same representative subject. Blue data points are for the penalize-high controller and red are for the penalize-low. (D) Added energetic penalty, averaged across subjects, for both the penalize-high (blue) and penalize-low controllers (red). Square data points represent initial preferred step frequencies and triangles represent the final preferred step frequencies. Data points were produced by subtracting the energetic landscape under the controller off condition (Figure 4A; grey curve) from that produced under the penalize-high and penalize-low controllers (Figure 4A; blue and red curves, respectively). The lines are 4th order polynomial fits, and the shading their 95% confidence intervals.

We faced a number of tradeoffs when designing the control functions used to relate step frequency to applied resistance. Firstly, we sought to create a clear energetic gradient about the subject's preferred step frequency. In principle, this is best achieved with steep sloped relationships between step frequency and commanded torque. Secondly, we thought it desirable that the step frequency that minimizes energetic cost be distinct from that which minimizes resistive torque at the knee. This is best achieved with shallow sloped control functions because steep slopes obscure the underlying curvature of subject's natural energetic landscape (Figure 3.1C-D, Figure 3.5). Finally, to guard against straight-kneed gaits, we sought to limit the maximum resistive torque applied to the limb to be within the ranges of knee torques that people typically use

during the swing phase of walking (*86*). With these criteria, we used pilot experiments to test candidate control functions. We settled on a penalize-high control function that applied no resistance at -15% of initial preferred step frequency with resistive torque increasing to a maximum of ~ 6Nm, averaged over the step cycle, at step frequencies greater than +10%. Our chosen penalize-low control function was sloped in the opposite direction, applying ~ 6Nm of torque, averaged over the step cycle, for step frequencies less than -10% of initial preferred with resistive torque decreasing to zero for step frequencies greater than +15%. Although it may have been possible to generate more bowl-like energetic cost landscapes with a non-linear penalty, we deemed our controller and resulting landscapes to be sufficient. Indeed, it is a difficult task to design a single control function that produces a precise energetic landscape across different subjects.

Subjects

Testing was performed on nine healthy adults (body mass: 65.3 ± 9.8 kg; height: 167.2 ± 10.0 cm; mean ± SD) with no known gait or cardiopulmonary impairments. Simon Fraser University's Office of Research Ethics approved the protocol, and participants gave their written, informed consent before experimentation.

Detailed Protocol

Each subject completed three days of testing, each lasting three hours with no more than two and half hours of walking to reduce fatigue effects. Subjects were asked to fast for 4 hours prior to testing. On the first testing day, subjects experienced either the penalize-high or penalize-low control function, assigned in random order. On the second day, they experienced the opposite control function. And on the third and final testing day, as a control condition, subjects were tested while wearing the exoskeleton but with the controller turned off resulting in negligible added resistance from the exoskeleton friction and inertia. Subjects were given between 5-10 minutes of rest in between each of the walking periods, including baseline, first adaptation, exploration, second adaptation, and cost mapping (Figure 3.2A-E, respectively). The second adaptation period, and the 12 minutes of re-adaptation that followed the second adaptation period, was not included on the third testing day because the controller always remained turned off.

At the beginning of each testing day, subjects were instrumented with the exoskeletons and indirect calorimetry equipment (VMax Encore Metabolic Cart, VIASYS®). We then determined their resting metabolic rate during a six minute quiet standing period. The average metabolic rate during the final three minutes of this period was subtracted from all subsequent energetic data collected during walking, allowing us to control for day-to-day variability in subjects' resting energy use. Throughout this study, the term energetic cost is used interchangeably with metabolic rate. Prior to and during the baseline and first adaption periods (Figure 3.2A-B), subjects were simply instructed to walk. At no point during testing were subjects provided with any information about how the controller functioned, or how step frequency influenced the resistance applied to the limb.

Prior to the exploration period (Figure 3.2C), we explained to the subjects that for a given walking speed it is possible to walk in a variety of different ways, including with very long slow steps or very short fast steps. They were encouraged to explore these different ways of walking during the next period. They were also informed that at times a metronome would play different steady state tempos, or slowly changing tempos, and that they should do their best to match their steps to the tempos. During the exploration period, three different steady state tempos were played for three minutes each. These tempos included +10%, -10%, and -15% of the initial preferred step frequency on the penalize-high day; -10%, +10%, and +15% on the penalize-low day; and ±10% (in random order) and 0% on the controller off day. The sinusoidal varying metronome tempo had a range of ±15% of the initial preferred step frequency and a period of three minutes.

Prior to the second adaptation period (Figure 3.2D), we explained to subjects that in the next period they would walk for 42 minutes with the exoskeleton turned on, after which the exoskeleton would be turned off and they would walk for an additional 12 minutes. For Day 3, when the controller was always off, they were told that they would be walking for only 42 minutes. We explained that at times the metronome would be turned on, during which they should match their steps to the tempo, and that when the metronome turned off, they no longer had to remain at that tempo. Besides these instructions, subjects were given no further directives about how to walk. The first

metronome tempo was used to hold subjects at step frequencies that resulted in high resistive torques (+10% penalize-high, -10% penalize-low) (Figure 3.1C). Therefore, when the metronome was turned off, we could determine if subjects would overshoot their initial preferred step frequency, which was now energetically suboptimal, to settle on a new preferred, and energetically optimal, step frequency (Figure 3.1D). The second metronome tempo was used to hold subjects at step frequencies that resulted in low resistive torques (+10% penalize-high, -10% penalize-low). Therefore, when the metronome was turned off, we could determine if subjects would elect to increase the resistance on their limb in order to settle on an energetically optimal step frequency.

During the final cost mapping period (Figure 3.2E), subjects matched their steps to steady state metronome tempos including: 0%, ±5%, ±10% of their initial preferred step frequency, the step frequency that corresponded to minimal resistance (-15% for penalize-high, +15% for penalize-low), and 0%, ±5% of the final preferred step frequency. Subjects matched each tempo for six minutes and we presented these tempos in a randomized order.

Outcome Measures

All step frequency outcome measures, including the baseline (initial preferred), pre-exploration, post-exploration, low release, high release (final preferred), and re-adaptation step frequencies were averages of a three minute window of data, always taken at the end of a period or just prior to a change in condition (Figure 3.2). For the cost curve mapping, we used the average of the last three minutes of energetic data for each steady-state step frequency. We used one-tailed paired t-tests to compare the step frequency outcome measures to the initial preferred step frequency. We used one-tailed because we hypothesized that step frequency adaptations would be toward lower costs. We also used one-tailed paired t-tests to compare the energetic cost at +/-5% of the initial and final preferred step frequencies to that at the initial and final preferred step frequencies. Once again, one-tailed tests were used because we expected energetic penalties consistent with the design of our controller. We used a significance level of 0.05 for all tests.

Chapter 4.

How humans continuously optimize energetic cost during walking

4.1. Abstract

We have recently demonstrated that people can continuously optimize their gait in order to minimize energy expenditure. Here, we test multiple competing hypotheses about how the nervous system initiates this optimization and the process used to converge on new optima. To accomplish this, we used robotic exoskeletons to shift people's energetically optimal step frequencies to frequencies lower than normally preferred. We found that only a small subset of subjects with high levels of natural gait variability, and therefore more varied information about the energetic gradient, are able to spontaneously initiate this optimization. Conversely, the majority of subjects require perturbations toward the optimum, yet not explicitly to it, in order to initiate the optimization. These perturbations appear critical—subjects that were given complete experience with the energetic landscape, but were not perturbed did not initiate optimization. Once optimization is initiated, we found evidence consistent with the nervous system employing a 'local search' process to discover and converge on novel optima. Subjects' step frequency adaptations following perturbations reveals that over time the old cost optima is abolished and subject learn to rapidly predict the new optima, suggesting that optimization leads to the formation of new motor memories.

4.2. Introduction

Human gait is shaped by an underlying drive to continuously minimize energy expenditure. We have recently demonstrated this using a paradigm where robotic

exoskeletons are used to alter the energetic consequences of various gaits (*135*). We made abnormal ways of walking energetically optimal and found that when given broad experience with the novel energetic landscapes subjects discovered the optimal gaits and opted to walk at them, even when the energetic benefits were small. This is consistent with recent findings demonstrating that energetic cost is lower after adaptation than before in both reaching and walking tasks (*47*, *49*). Although our experiment is the first to provide direct experimental evidence for continuous energy optimization, a weakness of its design is that it did not allow us to decipher the conditions conducive to optimization. When first exposed to the novel energetic landscape, subjects did not spontaneously optimize their gait. Instead, they did so immediately after an exploration period in which they were given broad and varied experience with the landscape that was both self and metronome guided. While it was clear that optimization terminated with subjects converging on the energetically optimal gait, it was not clear what experience from the exploration period was critical to *initiate* this optimization or what *process*, or strategy, was used to discover the novel optimum. Further insight into the functioning of the body's internal optimization could advance modern theories of motor control and inform the design of training and rehabilitation programs.

Initiating energy optimization likely requires a cue, signalling to the nervous system that a more optimal gait may exist. When the energetic consequences of movement are sufficiently altered, the nervous system must sense this and begin to deviate from past motor programs. It is logical that a criterion or threshold exists, below which the nervous system does not initiate optimization. And, there are a number of possible ways energy optimization could be initiated. In the most sensitive of cases, optimization would be initiated spontaneously based on very small sensed gradients in cost arising from natural variability in gait (*119*, *120*). Alternatively, it may be that larger perturbations, which move subjects further away from their preferred gait and result in more substantial and salient changes in cost, are necessary to initiate optimization. It is also possible that initiation requires experience with multiple cost points along an energetic gradient, rather than perturbations to discrete new costs. Perhaps this more expansive and complete experience is required for gradients to become clear and trusted. In our previous experiment we did not find that subjects spontaneously initiate

optimization, suggesting that the energetic gradient elucidated by their natural gait variability falls below the initiation threshold in our paradigm (*135*). However, subjects did adapt to novel energetic optima after an exploration period that included larger perturbations away from their preferred gait as well as broad and continuous experience with the energetic landscape. Because our past experiment was not designed to differentiate between these remaining two possibilities—that initiation requires discrete perturbations or broad gradient experience—either remains as a possible catalyst for optimization.

After optimization is initiated, the nervous system must converge on the energetically optimal gait. Once again, there are a number of possible processes it could employ to do so. For one, the nervous system may employ a very simple rule such as 'chose best'. In other words, if perturbed to a new gait and the new gait is energetically cheaper, it will remain at that gait. Under such a rule one would not converge to a novel optima unless explicitly directed to it. Rather than this somewhat passive strategy, the nervous system may employ more active exploration. For example, once optimization is initiated, the nervous system may begin exploring a random sampling of gaits within a given subspace. Alternatively, the nervous system may employ more clever techniques such as a local search process, which could be advantageous under many circumstances. In such a case, if a gait parameter changes and the nervous system detects a lower cost movement, it will continue to change that gait parameter as long as it continues to reduce cost. While our previous experiment demonstrated that people can converge on novel optima during walking, the design could not rule out any one of these optimization processes. Subjects adapted to novel energetic optima after an exploration period that included explicit experience with the energetic optima, sufficient for a chose best strategy, as well as broad and varied experience with the energetic landscape that was both self-directed and enforced (*135*), greatly obscuring our ability to capture the time course of any underlying strategy of the nervous system.

The purpose of this study was to test what conditions are needed for energy optimization to occur. We use the same paradigm used previously to demonstrate people that can continuously optimize energetic cost during walking (*135*). In brief, lightweight robotic exoskeletons capable of applying resistive torques at the knee joints

(Figure 4.1A-B) were used to shift people's energetically optimal step frequency to frequencies lower than normally preferred. The exoskeleton controller was set to a "penalize-high" control function that applied a resistance, and therefore an added energetic penalty, that was minimal at low step frequencies and increased as step frequency increased (Figure 4.1C-D). The control function was kept identical to that which we used in our previous experiment, allowing us to leverage past mappings of energetic landscapes. The "penalize-high" control function was previously shown to create positively sloped energetic gradient in the neighborhood of subjects' initial preferred step frequency (Figure 4.1E-F). On average subjects decreased their step frequency by approximately 6% to converge on the energetic minima and reduce cost by 8% (Figure 4.1E-G). This step frequency was distinct from the step frequency that would minimize resistive torque on the limbs, giving us confidence that subjects were optimizing for cost and not simply minimizing the resistive torques applied to the limbs. Here, we used a series of experiments to tightly control the type of experience subjects get with the energetic landscape and study how this effects optimization. We had two main goals. First, we sought to determine what experience is necessary to *initiate* optimization. Towards this goal, we designed experiments to distinguish between three alternative hypotheses: a) the nervous system spontaneously initiates optimization in response to a novel energetic landscape, b) the nervous system initiates optimization following perturbations to discrete cost points on a novel energetic landscape, or c) the nervous system initiates optimization in response to broad experience with multiple costs along a novel energetic landscape. Second, we sought to determine what optimization *process* is used to converge on a novel optimum. We again tested three alternative hypotheses: a) the nervous system uses a 'chose best' strategy where the body remains at the gait with the lowest experienced cost, b) the nervous system uses a 'sampling' strategy where the body intermittently explores a range of gaits, or c) the nervous system uses a 'local search' strategy where the body progressively alters a given gait parameter as long it continues to result in cost reductions.

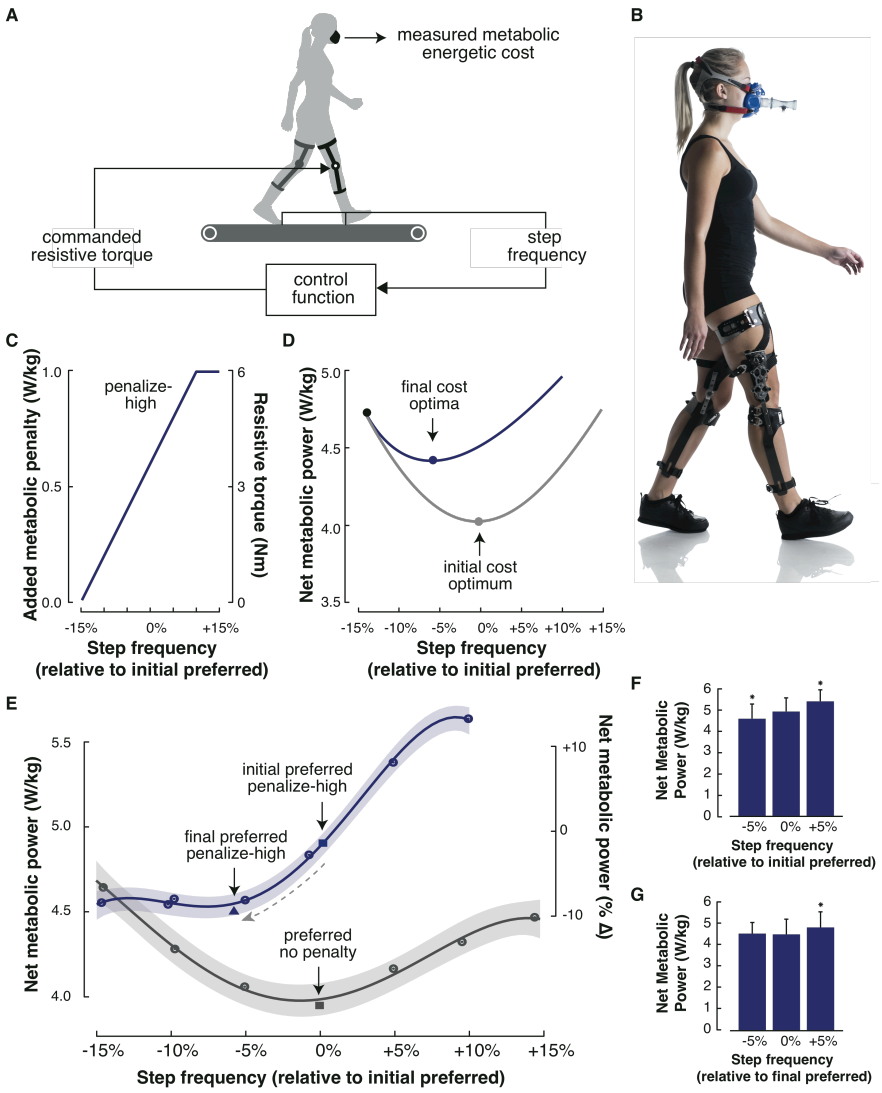

Figure 4.1: Experimental design

(A-B) By controlling a motor attached to the gear train of our exoskeletons, we can apply a resistance to the limb that is proportional to the subject's step frequency. (C) Design of the penalize-high (blue) control function. (D) Schematic energetic landscapes. Adding the energetic cost of the penalize-high control function to the natural cost curve (grey) produces a cost curve with the optimum shifted to lower step frequencies (blue curve). (E) Measured energetic landscapes, reproduced from Selinger et al. (2015), for the penalize-low (blue) control function and controller off condition (grey). The lines are 4th order polynomial fits, and the shading their 95% confidence intervals, shown only for illustrative purposes. The dashed grey arrow illustrates the direction of adaptation from initial preferred (blue square) to final preferred step frequencies (blue triangle). (F) The penalize-high control function creates a positively sloped energetic gradient about the subjects' initial preferred step frequency. (G) Subjects adapted their step frequency to converge on the energetic minima. Error bars represent 1 standard deviation. Asterisks indicate statistically significant differences in energetic cost when compared to the cost at the initial or final preferred step frequency (0%).

4.3. Results

High natural gait variability can spontaneously initiate optimization

We previously found that natural gait variability did not reliably initiate optimization (*135*). Here, we have repeated this test in a larger sample of subjects and found that a small subset are in fact able to spontaneously initiate optimization and converge on novel energetic optima. Subjects first walked for 12 minutes while wearing the exoskeletons, but with the controller turned off (Figure 4.2A, baseline). The final 3 minutes of walking data was used to determine subjects 'initial preferred step frequency'. All walking took place on an instrumented treadmill at 1.25m/s and we measured step frequency from treadmill foot contact events. Consistent with our previous experiments, all subjects appeared to settle into a steady state step frequency within 9 minutes and on average subjects walked at 1.8 ± 0.1 Hz (mean ± SD). Next, to guard against the possibility that in future trials subjects could be unaware they are able to alter, or fearful to alter, their step frequency when walking on a treadmill at a constrained speed, we habituated subjects to walking at a range of step frequencies (Figure 4.2B, habituation). During this habituation, the controller remained off; therefore, subjects did not gain experience with the novel energetic landscape. We then turned the controller on, resulting in an applied resistance that was dependent on step frequency, and the subjects walked at a self-selected step frequency for an additional 12 minutes (Figure 4.2C, first adaptation). During this time, 6 of the 36 subjects displayed gradual adaptations in gait, all toward lower, less costly, step frequencies (Figure 4.3A). They did so with an average time constant of 65.7 seconds (95% CI [60.5, 70.8]). By the final 3 minutes, these 'spontaneous initiators' had settled on a step frequency of -7.9 ± 2.5 % of their initial preferred step frequency (Figure 4.3C). This is indistinguishable from the location of the expected optima (p = 0.66). The others, or 'non-spontaneous initiators', remained at their initial preferred step frequency (0.8 ± 2.7 %, Figure 4.3C), despite it being suboptimal. Perhaps most interestingly, when we analyzed individual subjects' step-to-step variability, prior to the controller even being turned on, we found that spontaneous initiators displayed higher variability in step frequency than non-

spontaneous initiators (1.5 ± 0.3 % and 1.1 ± 0.3 %, respectively, $p = 1.8\times10^{-2}$, Figure 4.3B). High natural gait variability, which would result in a more expansive and therefore more clear sampling of the novel energetic gradient, appears to be a predicator of spontaneous initiation.

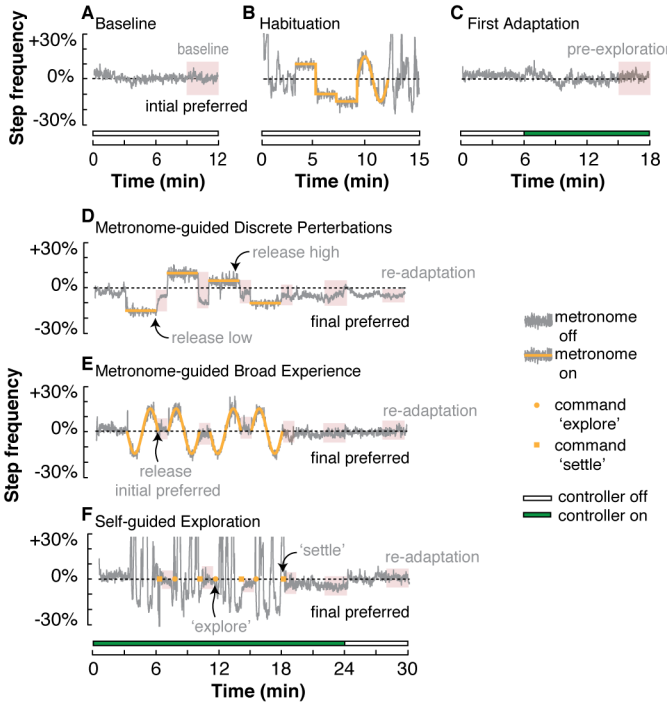

Figure 4.2: Experimental protocol
Each subject completed four testing periods. The first three, Baseline (A), Habituation (B), and First Adaptation (C), were the same from all subjects. For the 4th testing period, subjects were assigned to either the metronome-guided perturbations to discrete cost points (D), metronome-guided broad experience with the cost landscape (E), or self-guided exploration of the cost landscape. Rest periods of 5-10 minutes were provided between each testing period. For all periods, regions of red shading illustrate the time windows during which we assessed steady-state step frequencies. Data shown in A-B and E are from one representative subject, while data in D and F are from two other representative subjects.

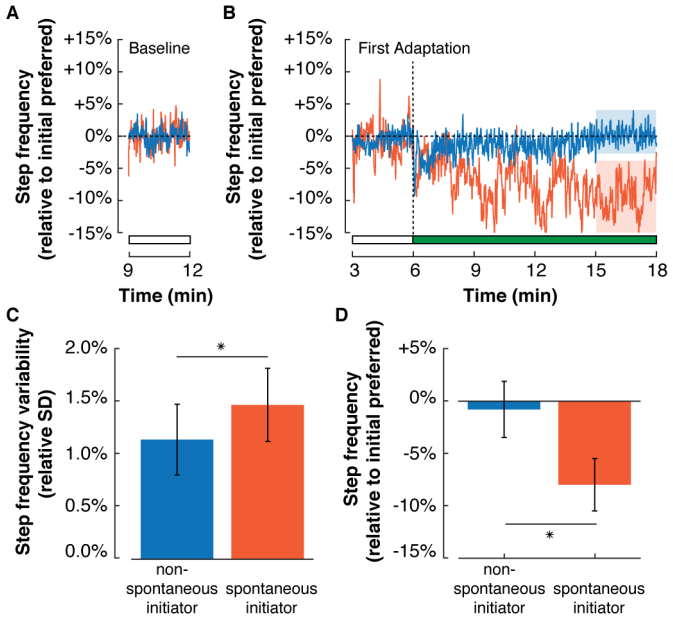

Figure 4.3: Non-spontaneous and spontaneous initiators
(A) Self selected step frequency during the final 3 minutes of the Baseline testing period for representative non-spontaneous initiator and spontaneous initiator (blue and orange, respectively). (B) Step frequency data during the First Adaptation period for the same two representative subjects. The horizontal bar indicates when the controller is turned on (green fill) and off (white fill). (C) Across all subjects, spontaneous initiator displayed greater average step frequency variability than non-spontaneous initiator during the Baseline testing period. (D) By the final 3 minutes of the First Adaptation period, spontaneous initiators appeared to adapt their step frequency to converge on the energetic minima, while non-spontaneous initiators did not. Error bars represent 1 standard deviation. Asterisks indicate statistically significant differences.

Perturbations toward optima can initiate optimization

We previously found that following a 15 minute period of exploration subjects made large adaptations in step frequency toward energetic minima (*135*). During this exploration period, subjects were instructed to self-explore walking with high and low step frequencies as well as match their steps to different steady-state and sinusoidally varying metronome tempos. Here, we sought to determine what aspects of this exploration were critical to initiate optimization. Eight 'non-initiating optimizers' were assigned to one of three experiments in which their exploration included either metronome-guided perturbations to discrete cost points on a novel energetic landscape (Figure 4.2D), metronome-guided experience with many costs along a novel energetic landscape (Figure 4.2E), or self-guided exploration of high and low step frequencies

(Figure 4.2F). To gain insight into the progress of optimization, 1-minute probes of subjects' self-selected step frequency occurred at the 6th, 10th, and 14th minute, along with a final 6 minute probe at the 18th minute. We found that if, prior to the probe, subjects were perturbed toward low step frequencies they appeared to initiate optimization and adapt toward the novel optima (Figure 4.4A-B). Yet, if they were perturbed toward high step frequencies they appeared to converge back toward the initial preferred step frequency (Figure 4.4A-B). This finding was consistent regardless of if the perturbation was self or metronome directed. Moreover, if immediately before the probe subjects were returned to the initial preferred step frequency, as was the case with the metronome-guided experience of many cost points, they showed no adaptation (Figure 4.4C). This was in spite of them having broad experience with the energetic landscape. These findings suggests that initiating optimization, by perturbing subjects in the direction of the optima and then allowing them to self-select their gait following these new initial conditions, is critical, while expansive experience with the landscape is not.

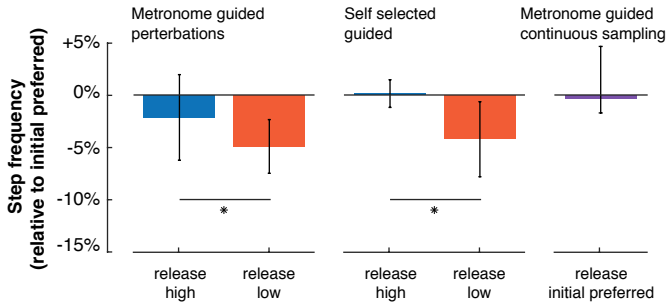

Figure 4.4: Effect of perturbation direction
For each subject, data from the final 30 seconds of each of the 1 minute self-selected step frequency probes, following either a high or low perturbation, were averaged, prior to averaging across subjects. Because there was no high or low perturbation for the metronome-guided broad experience, data from the final 30s of each probe were averaged. Error bars represent 1 standard deviation. Asterisks indicate statistically significant differences.

A local search strategy is used to discover and converge on novel optima

To achieve the statistical power necessary to investigate the interaction between perturbation direction and time, we next added an additional six non-spontaneous initiators to the discrete perturbations experiment, bringing our total to 14 for this condition. For the six added subjects, the first or final perturbations were set to be either the highest (+10%) or lowest (-15%) step frequency, with the other three perturbations

assigned in random order. We then compared the first to final release from the highest (+10%) and lowest (-15%) perturbations. We found that following the first perturbations at the high step frequency, subjects appeared to use prediction to rapidly move away from this high cost step frequency (Figure 4.5A). But, their prediction was erroneous—having not yet experienced lower costs gaits, they return to their initial preferred step frequency (Figure 4.5B). They did so with an average time constant of 2.0 seconds (95% CI [1.5 2.5]). Following the initial perturbation to low step frequency, subjects more slowly descended the cost gradient, with an average time constant of 10.8 seconds (95% CI [9.2 12.5]) and eventually converged on the new optima (Figure 4.5A). Because this was the first perturbation, all of which were from -15%, these subjects had no prior explicit experience with the novel optima, yet were able to adapt to it (Figure 4.5B). Although perturbing subjects in the direction of the optima is critical for initiating optimization, prior explicit experience with the new optima is not necessary for convergence—subjects appear to use a strategy consistent with gradient decent to discover and converge on novel optima.

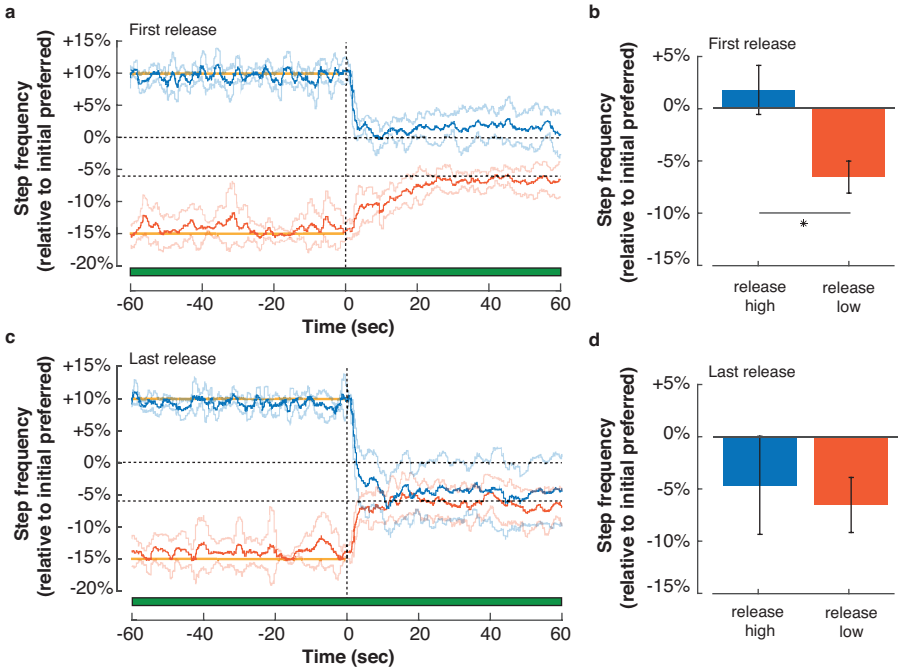

Figure 4.5: Effect of perturbation direction at beginning and end of exploration
Step frequency time-series data, averaged across subjects, for the first (A) and final perturbations (C) toward either high or low step frequencies. The horizontal bars indicate when the controller is turned on (green fill) and off (white fill), and the yellow lines indicate the prescribed metronome frequencies during the perturbation. Steady state step frequencies, averaged across subjects, during the final 30 seconds of the probe for the first (B) and final (D) perturbations toward either high or low. Error bars represent 1 standard deviation. Asterisks indicate statistically significant differences.

Optimization terminates with new predictions of optimal gaits

Given more time and experience with the energetic landscape, optimization leads to new predictions about energetically optimal gaits. Following the final perturbation, subjects rapidly converge on the novel optima, with an average time constant of two to three seconds, regardless of perturbation direction (perturb high: 2.8 seconds, 95% CI [2.3 3.2]; perturb low: 2.5 seconds, 95% CI [1.9 3.1]; Figure 4.5C-D). These findings are consistent with those of our previous experiment where subjects rapidly converged on the new preferred and energetically optimal step frequencies following the exploration period (*135*). However, in this experiment, we are able to see the formation and updating of these predictions. Following the final perturbation from low step frequencies, subjects no longer display slow adaptations consistent with optimization, but instead rapidly predict the optimal gait. And, following the final perturbation from high step frequencies,

subject's erroneous prediction has been corrected. Optimization appears to culminate in the formation of new motor memories and the abolishment of old.

Subjects preferred step frequency did not remain shifted toward the optima when the controller was turned off. On average, subject's 'final preferred step frequency' was -4.8 ± 3.1 %; however, they gradually returned to a step frequency indistinguishable from the initial preferred step frequency when the controller was turned off (-0.8 ± 3.0 %, $P = 4.8\times10^{-1}$, Fig. 6). They did so with a time constant of 10.5 seconds (95% CI [8.8 12.2]). This outcome differs from that in our previous experiment where subjects' step frequency remained shifted toward the control function optima for minutes despite a return to the natural energetic landscape (*135*).

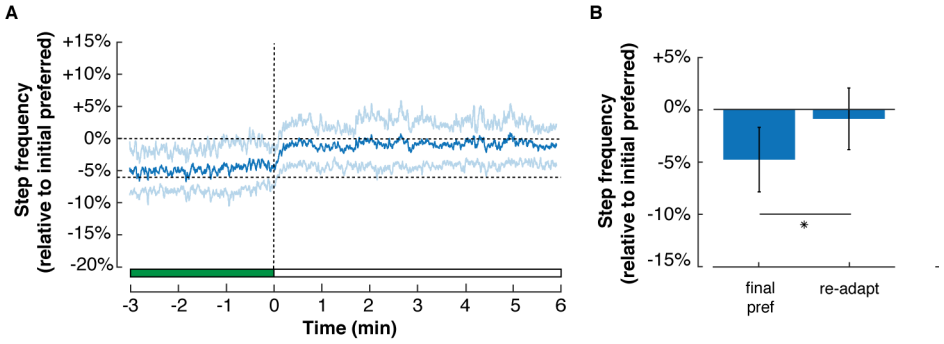

Figure 4.6 Final preferred step frequency and re-adaptation
Final preferred step frequency and re-adaptation. (A) Step frequency time-series data, averaged across subjects from both the high and low final release, for the final 12 minutes of the exploration period. The horizontal bars indicate when the controller is turned on (green fill) and off (white fill). (B) Steady state step frequencies, averaged across subjects, for the final preferred step frequency (minutes -3 to 0) and re-adaption step frequency (minutes 3 to 6). Error bars represent 1 standard deviation. Asterisks indicate statistically significant differences.

4.4. Discussion

We have tested multiple competing hypotheses about how the nervous system initiates optimization and the process used to converge on new energetic optima. To do so, we used robotic exoskeletons to alter people's energetically optimal gaits. We found that a small subset of subjects with naturally high gait variability can spontaneously initiate optimization. The majority of subjects, however, require perturbations toward the

new optima to initiate optimization. Interestingly, for these subjects perturbations appear to be critical—if they were not perturbed they did not initiate optimization, even if they were given broad experience with the entire landscape, including explicit experience with the optima. When optimization was initiated, subjects gradually adapted their gait, in a manner consistent with a local search strategy, to converge on the new optima. Given more time and experience, this slow optimization was replaced by a new and rapid prediction of the optimal gait. Optimization appears to terminate in the formation of new motor memories.

High motor variability may be an asset that leads to the discovery of optimal movements. We found that only a small subset of subjects adapted toward low and more energetically optimal step frequencies prior to any enforced exploration. High natural variability in step frequency, even before the exoskeletons were turned on, was predictive of which subjects would adapt. This may be because subjects with higher variability sample a more expansive range of the cost landscape. When measurements are noisy, this variability could clarify estimates of the energetic gradient and aid the nervous system in optimizing performance (*119*, *120*). It is possible that this variability is simply a consequence of noisy sensorimotor control, which fortuitously benefits the optimization process, or it may reflect meaningful motor exploration by the nervous system. Recent work showing that humans actively reshape the structure of their motor output variability, to elicit faster learning of reaching tasks, suggests the latter (*120*). Experiments could be performed to test if our spontaneous adaptors tend to exhibit high variability in all situations, for example during over ground walking without the exoskeletons, or if their variability was increased when donning the exoskeleton in the lab. Interestingly, motor variability that may facilitate the discovery of a less costly movement, can itself elicit an energetic penalty. For example, if one is currently at an optima for a given gait parameter, strides that deviate from that optima will necessarily increase cost. This trade-off creates an interesting conflict for a nervous system that seeks to minimize cost, and perhaps explains why most subjects do not spontaneously initiate optimization in our paradigm—exploration itself can be costly.

Enforced exploration in the form of perturbations toward lower costs can initiate optimization. We found that those subjects that did not spontaneously adapt toward the

optima could be enticed to do so by perturbations away from their preferred gait and toward the optima. Conversely, perturbations toward high costs did not initiate optimization. This suggests that sensing a lower cost gait is an important cue for the nervous system to abandon past predictions and begin to optimize. Surprisingly though, subjects did not initiate optimization if they were given broad metronome-guided experience with the energetic landscape, including experience with the optima and other lower costs gaits. Taken together these findings suggest that initiation of optimization is occurring during self-directed gait following a perturbation. Fully guided exploration, in our case with a metronome, appears ineffectual, suggesting that nervous system must actively direct it's own optimization and cannot simply recall past experience. A confounding factor that makes the comparison between the discrete perturbation and broad experience conditions difficult is that in the former subjects were given minutes of experience with one gait while in the later they were given seconds of experience with many gaits. Sensed cost, which may be both noisy and delayed (*46*, *136*, *137*), could therefore be more difficult for the nervous system to assess during the broad experience condition. However, that subjects initiated optimization during the self-guided exploration condition, where changes in gait were even more rapid and frequent, suggests that sufficient sensing of cost was not the barrier. Future testing of additional experimental conditions, including steady-state experience that ends in a return to the preferred gait and broad varying experience that ends in a perturbation away from the preferred gait, could conclusively rule out this alternative interpretation.

Identifying the dimension of an optimization problem may be an important aspect of initiation. Walking is a task of dauntingly high dimension. Various gait parameters, including walking speed, step frequency, and step width must be selected, and numerous combinations of muscle activities can be used to satisfy any one desired gait. When presented with novel contexts, the nervous system must identify which parameter, or parameters, to change in order to improve economy. This difficultly may partly explain why non-spontaneous adaptors do not initiate optimization when the exoskeletons are turned on and they are shifted to a higher cost gait. Although it may be clear that costs are higher, it may unclear how to lower them. Perturbations toward lower step frequencies, and therefore lower costs, may allow the nervous system to identify that this is the relevant dimension along which to optimize. In our experiments, we have only

presented subjects with a one-dimensional optimization problem and intentionally applied perturbations along this dimension. It would be interesting to determine if in higher dimension problems, perturbations along one dimension can initiate optimization along others.

A slow optimization process leads to the rapid prediction of energetically optimal gaits, offering a window into the formation of motor memories. When initially perturbed toward lower cost movements, our subjects gradually descended the cost gradient to converge on energetically optimal gaits. This adaptation was consistent with a gradient descent process. By the end of the exploration period, the same perturbation resulted in subjects rapidly returning to the optima. Our lab has previously investigated the selection of preferred step frequency and speed in both walking and running under natural energetic circumstances (*2*, *45*, *60*). This work has suggested that the nervous system beneficially combines these two processes to select economical gaits, relying on prediction to rapidly improve gait economy during changing walking contexts and optimization to accurately fine-tune the gait mechanics over time. Here, we add to this framework by showing that optimization not only works in tandem with prediction, but also appears to inform the process and birth prediction. While our current design allows us to study these processes following the first and final perturbations from the same points on the cost landscape, limited subject numbers prevent us from doing so for the more intermediate perturbations throughout the exploration period. Future experiments with additional subjects could allow us to more precisely quantify the progression of motor prediction formation.

The time course of re-adaptation may provide insight into the nervous system's confidence in the newly generated prediction. In our current experiment when the exoskeletons were turned off, returning subjects to their natural energetic landscape, subjects slowly converged back toward their natural optima. They did so at a rate consistent with the slow descent of the cost gradient evidenced after the first perturbation toward low costs, suggesting subjects are re-optimizing their gait. These findings differ from those of our previous experiment, where subjects step frequency remained shifted toward the control function optima for minutes despite a return to the natural energetic landscape. In reaching paradigms, others have found that the

persistence of motor memories can reflect the type of experience subjects get with a novel environment (*138-141*). For example, Huang and Shadmehr (2009) found that prior experience with a rapid change in the environment increased the decay rate of memories, evidenced by faster time constants during re-adaptation (*138*). Conversely, prior experience in an environment that changed gradually reduced the decay rates. They propose that decay of motor memory reflects the brain's implicit estimate of how likely it is that the environment will change with time. In the context of our experiments, this suggests the nervous system was more confident that the new energetic landscape was unlikely to change in our original experiment and therefore relied more heavily on the newly formed prediction. One reasonable explanation for this is that prior to re-adaptation subjects in our original experiment experienced the new energetic landscape for twice as long as those in our current experiment. It is also possible that the combination of discrete perturbations, broad landscape experience, and self-guided exploration had an additive or interactive effect on the produced motor prediction in our original experiment.

Our collective findings provide insight into the body's internal optimization process. Specifically, we determined that high natural gait variability and perturbations toward lower cost movements can initiate the optimization process. Once initiated, the body can gradually converge on novel energetic optima, perhaps suggesting that it implements a local search strategy. This optimization appears to culminate in the formation of new predictions of the energetically optimal gait. While this work has begun to unveil the processes that underlie optimal gait selection, it remains unclear how the body senses energetic cost in order to do so. It may be directly sensed, either globally by known blood gas receptors (*50-52*) or locally by muscle receptors sensitive to the byproducts of metabolism (*53*, *54*). It may instead, or in addition, rely on indirect information that the body has learned is related to energetic cost. These energetic proxies may include ventilation rate, motor efference copy, or some combination of muscle proprioceptor activity. Experimentally perturbing blood gas sensors or muscle afferents in isolation may provide insight into the relative importance of each type of sensor for real-time cost optimization. A complete understanding of how the body senses and optimizes energetic cost will shed light on how people adapt to changing terrains, compensate for injury or motor deficits, and learn new tasks.

4.5. Experimental Procedures

Subjects

Testing was performed on a total of 36 healthy adults (body mass: 63.9 ± 9.8 kg; height: 1.69 ± 0.10 cm; mean ± SD) with no known gait or cardiopulmonary impairments. Simon Fraser University's Office of Research Ethics approved the protocol, and participants gave their written, informed consent before experimentation.

Initially, 27 subjects were randomly assigned to one of three testing conditions (9 subjects per condition) in which their exploration period included either metronome-guided perturbations to discrete cost points on the energetic landscape (Figure 4.2D), metronome-guided broad experience with multiple costs along the energetic landscape (Figure 4.2E), or self-guided exploration of high and low step frequencies (Figure 4.2F).

A preliminary analysis revealed that 5 of the 27 subjects (1 from the discrete perturbations condition, 1 from the broad experience, and 3 from the self-guided condition) appeared to gradually adapt their gait toward the optima during the first adaptation period, prior to exploration period (Figure 4.2C). These subjects, whom we refer to as 'spontaneous initiators', were therefore not included in the analysis for the exploration conditions and were instead analyzed as a separate group. To be considered a spontaneous initiator subjects had to meet two criteria. First, during the final 3-minutes of the first adaptation period their average step frequency was required to fall below 3 SD in steady state variability determined from the initial preferred step frequency. For most subjects, this equates to a minimum decrease in step frequency of approximately 3-5%. Second, the decrease in step frequency could not be an immediate and sustained mechanical response to the exoskeleton turning on. The final adapted step frequency had to be significantly lower than the step frequency assumed in the 10th to 40th second after the exoskeleton turned on (one-tailed t-test, $P>0.05$). To rebalance conditions, an additional 2 subjects, both of whom were non-spontaneous initiators, were added to the self-guided exploration condition.

An analysis of data from the three explorations conditions indicated that the perturbation direction prior to the 1-minute probes had a lasting effect on the subjects'

self-selected step frequency. To investigate the interaction between perturbation direction and time, we wanted to compare the time course of adaptation during the first and final probes following perturbations from the same step frequencies. To achieve the statistical power necessary to do so, we added an additional 7 subjects to the discrete perturbations experiment. For the added subjects the first or final tempos were set to be either the highest (+10%) or lowest (-15%) step frequency, with all other tempos assigned in random order. One of the added subjects met the criteria for a spontaneous initiator and was therefore not included in this investigation between perturbation direction and time. In total for the analysis, 5 subjects were perturbed toward +10% and 4 toward -15% prior to the first probe. Prior to the final probe, 4 subjects were perturbed toward +10% and 5 toward -15%.

In total, 6 of the 36 tested subjects were identified as spontaneous initiators (body mass: 60.8 ± 10.6 kg; height: 1.68 ± 0.11 cm; mean ± SD), while 14 were included in the analyses for the discrete perturbation condition (body mass: 63.0 ± 10.7 kg; height: 1.69 ± 0.11 cm; mean ± SD), 8 for the broad experience condition (body mass: 67.7 ± 9.1 kg; height: 1.71 ± 0.09 cm; mean ± SD), and 8 for the self-guided condition (body mass: 64.2 ± 8.6 kg; height: 1.67 ± 0.07 cm; mean ± SD).

Detailed protocol

Each subject completed one testing session, lasting three hours with no more than two and half hours of walking to reduce fatigue effects. All subjects experienced the penalize-high control function, which has previously been show to shift energetic optima to low step frequencies (*135*) (Figure 4.1C-G). Subjects were given between 5-10 minutes of rest in between each of the walking periods, including baseline, habituation, first adaptation, and one of the three assigned exploration conditions (Figure 4.2, A-F respectively, described in detail below).

At the beginning of testing, we instrumented subjects with the exoskeletons and indirect calorimetry equipment (VMax Encore Metabolic Cart, VIASYS®). We then determined their resting energetic cost during a six-minute quiet standing period. Following this, during the baseline period (Figure 4.2A), subjects were simply instructed to walk for 12-minutes.

Next, subjects completed a habituation period were they were familiarized with walking at a range of step frequencies (Figure 4.2B). This trial was included to reduce the possibility that in future trials subjects could be unaware they are able to alter, or fearful to alter, their step frequency when walking on a treadmill at a constrained speed (Figure 4.2B). During this habituation, the controller remained off; therefore, subjects did not gain experience with the novel energetic landscape. We explained to the subjects that for a given walking speed it is possible to walk in a variety of different ways, including with very long slow steps or very short fast steps. They were encouraged to explore these different ways of walking during the habituation period. They were also informed that at times a metronome would play different steady state tempos, or slowly changing tempos, and that they should do their best to match their steps to the tempos. During the habituation period, three different steady state tempos were played for three minutes each. These tempos included +10%, -10%, and -15% of the initial preferred step frequency. The sinusoidally varying metronome tempo had a range of ±15% of the initial preferred step frequency and a period of three minutes.

Prior to the first adaptation period, we explained to subjects that they would next walk for 6 minutes with the exoskeleton turned off, at which point the exoskeleton would turn on and they would walk for a remaining 12 minutes (Figure 4.2C). They were given no other directives about how to walk and at no point during testing were subjects provided with any information about how the controller functioned, or how step frequency influenced the resistance applied to the limb.

For the final exploration period, subjects completed one of the three conditions including, metronome-guided perturbations to discrete cost points on the energetic landscape (Figure 4.2D), metronome-guided broad experience with multiple costs along the energetic landscape (Figure 4.2E), or self-guided exploration of high and low step frequencies (Figure 4.2F). All subjects were informed that they would be walking for 30 minutes and that the exoskeleton would be on for the first 24 minutes and off for the final 6 minutes. To gain insight into the progress of optimization under each condition, 1-minute probes of subjects' self-selected step frequency occurred at the 6^{th}, 10^{th}, and 14^{th} minute, along with a final 6 minute probe at the 18^{th} minute (Figure 4.2 D-F).

Those assigned to the metronome-guided perturbations to discrete cost points condition were informed that at times the metronome would be turned on, during which they should match their steps to the steady-state tempo, and that when the metronome turned off, they no longer had to remain at that tempo (Figure 4.2D). Besides these instructions, subjects were given no further directives about how to walk. The metronome was turned off at four different time points, each serving as a probe of subjects self-selected step frequency. Prior to each probes, a different metronome tempos were played, including -15%, -10%, +5% and +10% of initial preferred step frequency. We chose these tempos such that they spanned the energetic landscape but did not include perturbations explicitly to the expected optima or the preferred step frequency (approximately -5% and 0%, respectively). Order of the tempos was randomized. The exception to this being that for the 7 subjects added to this condition, either the first or last tempo was randomly assigned as +10% or -15%, with the remaining 3 perturbations assigned in random order.

Those assigned to the metronome-guided broad experience condition were given the same instructions as those in the discrete perturbation condition, except that they were informed that the metronome tempo would change slowly over time (Figure 4.2E). A sinusoidally varying metronome tempo was played for three minutes, four separate times, which were once again separated by probes of self-selected step frequency. The sinusoidal tempo had a range of ±15% of the initial preferred step frequency, a period of three minutes, and began and therefore ended at 0% of the initial preferred step frequency. These subjects therefore did not experience perturbations; they were guided through the complete landscape but always returned to their preferred gait prior to a probe.

Those assigned to the self-guided exploration condition were informed that at times the experimenter would verbally give them the command ‘explore’, at which point they should explore walking at a range of different step frequencies (Figure 4.2E). They were informed that they should continue to do so until given the command ‘settle’, at which point that should settle into a steady step frequency. They were given no

directives about what their steady state step frequency should be. Subjects were instructed to explore four separate times, each lasting three minutes and once again separated by probes of self-selected step frequency. When the command settle was given subjects could be at any self-selected step frequency, therefore the perturbation direction and magnitude were not predetermined.

Outcome measures

Each subject's initial preferred step frequency was calculated as the as the average step frequency during the final 3 minutes of the baseline period. Individual subject's variability in step frequency, calculated as a coefficient of variation, was also assessed during this time period. Similarly, the pre-exploration step frequency was calculated as the average step frequency during the final 3 minutes of the first adaptation period. During this period, the spontaneous initiators were found to adapt toward the optima. To determine the average rate at which they did so, step frequency time series data from the 6^{th} to the 18^{th} minute for the subjects was grouped together and fit with a single term time-delayed exponential. Prior to fitting data was down-sampled to a step rate of 1.8Hz, so as not to overestimate data points and inflate calculated confidence intervals. We used one-tailed t-tests with a significance level of 0.05 to compare the pre-exploration step frequency, as well as variability in step frequency, of the spontaneous and non-spontaneous initiators (Figure 4.3C-D). One-tailed t-tests were used because we expected the spontaneous initiators to present with lower steady-state step frequencies and higher variability.

During the three exploration conditions, 1-minute probes of subjects' self-selected step frequency occurred at the 6^{th}, 10^{th}, and 14^{th} minute, along with a final 6 minute probe at the 18^{th} minute. When statistical comparisons were made between high and low perturbations or initial and final perturbations, data from the 30^{th} to the 60^{th} second of each of the self-selected step frequency probes were used for analysis. We used t-tests with a significance level of 0.05 (Figure 4.4 and Figure 4.5B and 5D). When investigating the rate at which subjects adapted their step frequency following the various perturbations, step frequency time series data from the first 60 seconds of the probes from subjects of the same condition were once again fit with a single term time-delayed exponential, using the same process steps as previously described. For plotting

purposes, we averaged across subjects of the same condition and calculated the across subject standard deviation at each time point.

Because there was no effect of perturbation direction following the last release, subjects from the high and low release conditions were grouped. The final preferred step frequency was calculated as the average step frequency during the 21st to 24th minute of the exploration period, just prior to the controller being turned off. The re-adaptation step frequency was calculated as the average step frequency during the final 3 minutes of the exploration period, when the controller was turned off. When investigating the rate at which subjects re-adapted their step frequency back to the initial preferred, step frequency time series data from the entire re-adaptation period were once again fit with a single term time-delayed exponential and the average and standard deviation profiles were calculated for plotting purposes.

Chapter 5.

Estimating instantaneous energetic cost during non-steady state gait

5.1. Abstract

Respiratory measures of oxygen and carbon dioxide are routinely used to estimate the body's steady state metabolic energy use. However, slow mitochondrial dynamics, long transit times, complex respiratory control mechanisms, and high breath-by-breath variability obscure the relationship between the body's instantaneous energy demands (instantaneous energetic cost) and that measured from respiratory gases (measured energetic cost). The purpose of this study was to expand on traditional methods of assessing metabolic cost by estimating instantaneous energetic cost during non-steady state conditions. To accomplish this goal, we first imposed known changes in energy use (input), while measuring the breath-by-breath response (output). We used these input/output relationships to model the body as a dynamic system that maps instantaneous to measured energetic cost. We found that a first-order linear differential equation well approximates transient energetic cost responses during gait. Across all subjects, model fits were parameterized by an average time constant (τ) of 42 ± 12 s with an average R^2 of 0.94 ± 0.05 (mean ± SD). Armed with this input/output model, we next tested whether we could use it to reliably estimate instantaneous energetic cost from breath-by-breath measures under conditions that simulated dynamically changing gait. A comparison of the imposed energetic cost profiles and our estimated instantaneous cost demonstrated a close correspondence, supporting the use our methodology to study the role of energetics during locomotor adaptation and learning.

5.2. Introduction

Steady state measurements of metabolic energetic cost have provided valuable insight into why and how we walk the way we do. Energetic cost, in this context, refers to the input energy required to power the cellular processes underlying the body's movement. This energy is liberated from glucose, fats, and other stored foodstuffs in a reaction that requires oxygen and produces carbon dioxide (*142*). Consequently, energetic cost is typically measured indirectly by quantifying the oxygen and carbon dioxide in respiratory gases (*143*, *144*). These measurements have demonstrated that we select the most fundamental characteristics of our gait—such as speed, step frequency and step width—so as to minimize energetic cost per distance travelled (*33*, *38*, *145-152*). Cost measurements have also allowed the quantification of energetic penalties imposed by various gait disabilities, and the evaluation of the effectiveness of rehabilitation interventions at mitigating these added costs (*145*, *146*, *148*). Equipment and wearable devices, be it backpacks (*153*, *154*), prosthetics (*155*, *156*), orthoses (*157*, *158*), or running shoes (*159*), have been assessed, iteratively designed, and ultimately improved based on cost measurements.

The relationship between the body's instantaneous energy demands (instantaneous energetic cost) and that measured from respiratory gases (measured energetic cost) is complicated. Consider, for example, oxygen consumption measured at the mouth. Muscles meet their instantaneous energy demands for force generation using ATP, a form of stored energy. While ATP is immediately replenished using another form of stored energy, creatine phosphate, the mitochondrial dynamics that use oxygen and foodstuffs to replenish creatine phosphate are rather slow (*160-162*). There are still further delays before mitochondrial oxygen consumption is reflected in respiratory gases due to blood circulation from muscle to lungs (*163*), oxygen exchange between the blood and the lungs, and then lung ventilation itself. The relationship between instantaneous and measured cost cannot be determined by simply adding up these component time delays because blood gases are under tight neural control (*164*), and these controllers impose their own dynamics. For example, rapid increases in ventilation are often seen at the onset of exercise (*164*), preloading the body in anticipation of future mitochondrial oxygen requirements. Consequently, energetic cost as measured at the mouth can

occur in advance of any actual energy use by muscle. An additional complicating factor is the discrete nature of breathing—while muscles may be continuously consuming the body's oxygen, the lungs only replenish oxygen with each breath and each breath may be of drastically different volume. Irregularities in both depth and timing of breaths create noisy breath-by-breath estimates of energetic cost that do not reflect true fluctuations in muscle energy use (*137*, *165*). In summary, the relationship between instantaneous and measured energetic cost is complicated by mitochondrial dynamics, body transit delays, and respiratory control mechanisms, and then further obscured by high breath-by-breath variability.

It is due to these complexities that energetic cost is traditionally only measured during long bouts of constant intensity conditions. By discounting non-steady state regions of cost measurements, the rate at which the oxygen is entering the body is allowed to reach equilibrium with the rate at which cellular processes are consuming it. By averaging over minutes of data, high breath-by-breath 'noise' is overcome and the measured energetic cost then accurately matches the instantaneous energetic cost. While these processing techniques have served us well over the past century, they restrict the research questions that can be effectively answered. Long-duration steady state conditions, such as those experienced on a treadmill, are the exception rather than the norm during real-world walking (*166*, *167*). In truth, we are continually adjusting our gait to meet the demands of a changing environment and the energetic cost under these real-world conditions is essentially unknown.

Here, we expand on traditional methods of assessing energetic cost with the primary purpose of developing a technique to estimate instantaneous energetic cost during non-steady state gait. We first characterized the dynamic relationship between instantaneous and measured energetic cost. To accomplish this, we enforced known changes in instantaneous energy use (input)—by prescribing changes to subjects' walking speed and step frequency—and measured the respiratory responses in measured energetic cost (output; Figure 5.1A). We then modeled the body as a dynamic system that maps instantaneous to measured energetic cost (Figure 5.1B). Next, we used this model to test two approaches for estimating instantaneous energy use from respiratory measures. The *inverse model approach* is perhaps the most intuitive—the

actual measured energetic cost is smoothed and then passed through the inverse of the identified model to produce an estimate of the instantaneous energetic cost (Figure 5.1C). The *forward model approach* estimates instantaneous energetic cost as the input that when passed forward through the identified model produces an estimate of measured cost that best fits the actual measured energetic cost response (Figure 5.1D). We have chosen to present both approaches, as each has distinct strengths and limitations and for particular study designs, one may be better suited than the other.

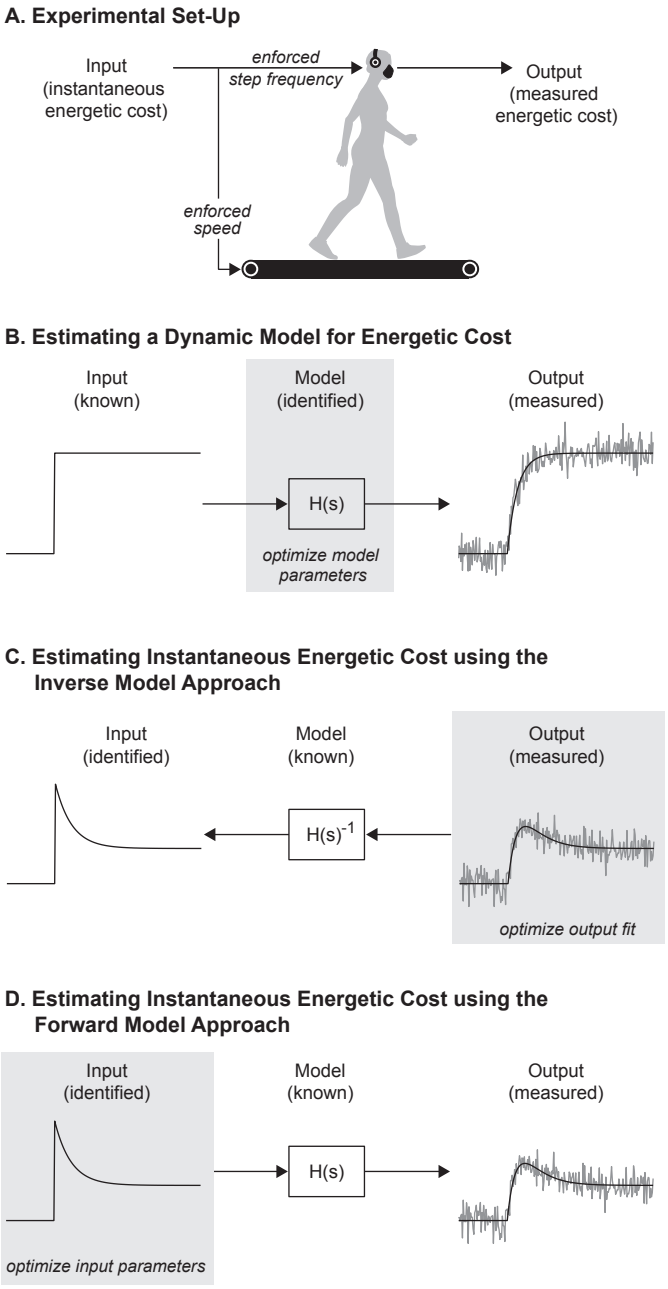

Figure 5.1: Experimental design
(Caption continued on next page)

A. Experimental Set-up. To evoke known changes in instantaneous energetic cost, subjects' walking speed (treadmill speed) and step frequency (metronome frequency) was enforced and the resulting breath-by-breath energetic cost response was measured using indirect calorimetry. B. We then modeled the relationship between instantaneous energetic cost (input) and measured energetic cost (output). Using this model we estimated instantaneous energetic cost from the measured energetic cost response using two approaches. C. When using the inverse model approach, noisy output data was fit with a constrained polynomial, which was then passed through the inverse of our identified model to produce an estimate of instantaneous energetic cost. D. When using the forward model approach, we assumed the general shape of the input profile is known and described it by a set of parameters, which were then optimized so that the input profile, when run forward through our identified model, generated an output profile that best fit our measured output. Grey shaded boxes have been used to highlight what parameters were optimized for each processing technique.

5.3. Methods

Simon Fraser University's Office of Research Ethics approved the protocol, and participants gave their written, informed consent before experimentation.

5.3.1. Enforcing rapid changes in instantaneous energetic cost

Ten adult subjects (body mass: 67.1 ± 6.0 kg; height: 173.7 ± 5.2 cm; mean ± SD) with no known musculoskeletal or cardio-pulmonary impairments participated in these experiments. Subjects were instrumented with indirect calorimetry equipment (VMax Encore Metabolic Cart, ViaSys, IL, USA) and all walking was performed on an instrumented treadmill (FIT, Bertec Corporation, MA, USA). To habituate subjects to the experimental set up, they walked at a range of treadmill walking speeds (0.75, 1.00, 1.25, 1.5, and 1.75 m/s) for a minimum of 10-minutes at each speed (*168-170*). Subjects next completed a series of enforced rapid changes in gait. The treadmill speed (walking speed) and metronome frequency (step frequency) were rapidly and simultaneously increased or decreased using custom written software (Simulink Real-Time Workshop, Mathworks Inc., MA, USA), in order to evoke a step-like change in instantaneous energetic cost (Figure 5.1A). We chose to not only alter speed, but also step frequency because people often take tens of seconds to adjust their step frequency to steady state following perturbations in treadmill walking speed (*2*, *168*). Metronome frequency was set at the subjects' preferred step frequency at each speed, defined as the average step

frequency during the final 3-minutes of walking in the habituation trials. Step frequency for an individual step was calculated as the inverse of the time between foot contact events, identified from the characteristic rapid fore-aft translation in ground reaction force center of pressure (*134*). The treadmill speed alternated between 6-minute periods at a base speed of 1.25m/s and 6-minute periods above or below this base speed (1.5 or 1.75 m/s, and 0.75 and 1.00 m/s, respectively). This resulted in eight different changes in gait (conditions), including step-like changes up-to and down-from the non-base speeds of 0.75, 1.00, 1.5, 1.75 m/s. Speed presentation order was randomized. We designed these changes to have differing direction (increase or decrease in speed) and magnitude (absolute speed change of 0.25 or 0.50 m/s) in order to test if the identified energetic cost dynamics differed across conditions. To compensate for the variable nature of breath-by-breath measurements and to further control for order effects, we had subjects complete a second day of testing in which they repeated the enforced gait changes twice with a newly randomized order, giving us a total of three repeats for each of the eight conditions. Subjects walked for less than two hours per day to reduce fatigue effects.

5.3.2. Modeling the relationship between instantaneous and measured energetic cost

Whipp and colleagues have previously modeled ventilatory gas dynamics during non-steady state cycling (*137*, *171*). Given step-like changes in work rate, they found that for some conditions, the oxygen uptake and carbon dioxide output could be adequately described by first-order differential equations with an accompanying time delay. Here, we use their model as a starting point for our modeling efforts while recognizing that gas kinetics during walking and cycling are not constrained to have identical dynamics. We modeled the relationship between the instantaneous energetic cost (our input) and the measured cost (our output) as a single dynamic process comprising a time-delayed first-order linear ordinary differential equation. The mathematical representation of this model expressed in the frequency domain, takes the form:

$$Y(s) = H(s)X(s), \tag{5.1}$$

where

$$H(s) = \frac{A}{\tau s+1} e^{-\delta s}, \tag{5.2}$$

$X(s)$ is the input instantaneous energetic cost, and $Y(s)$ is the output measured energetic cost. The parameter τ is a time constant characterizing the rate of change, A represents the amplitude of the change, and δ is a fixed time delay between energy use by muscle and that which we measure at the mouth. One may understand this model as a low-pass filter, where a rapid change in input (instantaneous energetic cost) will result in a slow and smoothed output response (measured energetic cost), and the amount of slowing and smoothing will increase with the magnitude of τ. Thus, if one were to see very quick changes in measured respiratory energetic cost, it would mean there was an exceptionally large and rapid change in the underlying instantaneous energetic cost. One might also understand this model in terms of its response to a step input, where the produced response would take the form of an exponential rise to steady state with a delay between the step input and the beginning of the response. The larger the value of τ, the longer the time required for the exponential rise.

To fit this model to our data, we analyzed three minutes of metabolic data prior to each gait change and six minutes of data following the gait change. The magnitude of each trial was normalized to unity to allow us to compare and average gait changes of differing magnitude and direction. To accomplish this normalization, we first subtracted the steady state value before the gait change (the average of minutes -3 to 0) and then divided by the amplitude of the change (the average of minutes 3 to 6). Note that this normalization process does not affect any dynamics in the measured cost response. To solve for our unknown model parameters (τ and δ), we used weighted least-squares optimization to minimize the residuals between our model and measured data. The optimization uses the Levenberg-Marquardt algorithm and was implemented with MATLAB's *nlinfit* function. Due to prior normalization, best-fit amplitudes had a value of one (A =1). In order to avoid known convergence issues with delayed dynamic models (*172*), we visually confirmed the accuracy of the fitted time delays. We assessed the goodness-of-fit of our estimated parameters by calculating the R^2 value between the model and our measured data. As a test of model sufficiency we also evaluated whether

the addition of a second process, modeled as an additional time-delayed first-order linear differential equation, produced a better fit to our data.

To test whether the same model holds regardless of magnitude or direction, for each subject we first separately fit our model to all trials of the same direction (increase or decrease in speed) or magnitude (absolute speed change of 0.25 or 0.50 m/s) and tested for differences using a Student's paired t-test. For all tests, we accepted $p < 0.05$ as statistically significant. For each subject, we also performed cross validations by fitting the increase in speed trials with the model parameters solved from the decease in speed trials (and visa versa), as well as the 0.25 m/s magnitude trials with the parameters solved from the 0.50 m/s magnitude trials (and visa versa).

5.3.3. Estimating instantaneous energetic cost during dynamically changing gait

We next assessed if the subject-specific models that we previously identified could be used to estimate instantaneous energetic cost from measured breath-by-breath energetic cost. To accomplish this, we had four representative subjects (body mass: 69.5 ± 9.8 kg; height: 175.2 ± 2.1 cm; mean ± SD) return for a third and fourth day of testing. Our goal was to enforce instantaneous energetic cost profiles that differed from those upon which our model was based. To design varying instantaneous energetic cost input profiles, we leveraged the fact that subject's energetic cost will increase as their step frequency deviates from preferred (*38*, *118*). To quantify this relationship, on the third testing day our test subjects walked on the treadmill at 1.25m/s for six minutes at nine enforced step frequencies that were at, above, and below preferred (0, ±5, ±10, ±15, ±20 % deviation from preferred step frequency). For each enforced step frequency, we took an average of the final three minutes of steady state energetic cost data, leaving us with nine data points that we then fit with a cubic polynomial (Figure 5.2B). Note that during these steady state regions, the average measured energetic cost is equivalent to the average instantaneous energetic cost, as the gas exchange measured at the mouth has reached equilibrium with the gas exchange occurring at the muscle tissue level.

Next, the solved polynomial was used to design step frequency profiles that, at constant treadmill speed of 1.25 m/s, would evoke three distinct input muscle energy use

profiles—a step, a ramp, and an adaptation profile (Figure 5.2A). The step profile, although the same shape as the original input profile on which we based our model, imposed different physical constraints on the subject, as treadmill speed was held constant and only step frequency was rapidly increased. The profile was designed to produce a final steady state magnitude change of approximately 1 W/kg. The ramp profile was markedly different from that of the step in that step frequency was gradually increased over the course of minutes, again resulting in a final magnitude change of approximately 1 W/kg. The adaptation profile was designed to mimic a fast adaptation, where a subject's instantaneous energetic cost may initially step up in response to a perturbation and then rapidly decay. For our adaptation profile, cost was stepped up by approximately 1.3 W/kg and then decayed with a time constant of 60 seconds to a final steady state that was approximately 0.3 W/kg above the initial steady state. For each trial, treadmill speed was held constant at 1.25 m/s and the subject was asked to match their steps to the changing metronome frequency (Figure 5.2C) while we measured energetic cost. The subjects completed three repeats for each input profile shape in randomized order on the fourth testing day.

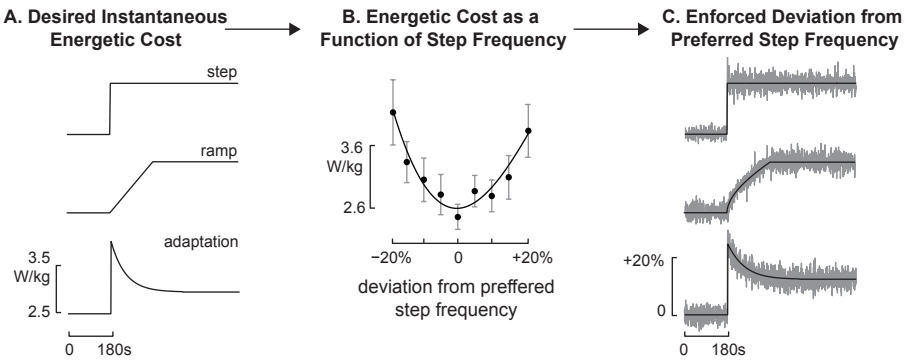

Figure 5.2: Enforcing known input changes in instantaneous energetic cost
A. We sought to enforce three differing but known input changes in instantaneous energetic cost. B. In order to identify what step frequency profiles would evoke these desired changes in instantaneous energetic cost, we identified each subject's relationship between energetic cost and deviation from preferred step frequency. C. Using the solved relationship between energetic cost and step frequency, we designed step frequency profiles that would evoke our desired change in instantaneous energetic cost. The black line illustrates the step frequency commanded with a metronome and the grey line illustrates the subjects actual step frequency.

We then used two different approaches to estimate instantaneous energetic cost from measured cost, each approach having distinct strengths and drawbacks. Recall that for each subject, we have solved for an individualized model that maps instantaneous to measured energetic cost. Therefore, the inverse of this model will do the opposite: map measured to instantaneous energetic cost. This is the basis of our inverse model approach (Figure 5.1C). By passing a subject's measured energetic cost data though their inverse model, we can directly compute the instantaneous energetic cost. However, it was necessary to first smooth the measured data. Passing unsmoothed data through the inverse model, which functions like a high pass filter, would effectively amplify high frequency components in the measured signal and these high frequency components tend to be dominated by the breath-by-breath noise. Although a low pass filter could be used to first attenuate noise, it would indiscriminately attenuate all high frequency inputs, which may include rapid changes in instantaneous energetic cost that we are seeking to identify. Instead, to estimate the shape of the underlying energetic cost profiles, less the noise, we fit each trial of measured data with a polynomial. A constrained least squares optimization, implemented using MATLAB's *lsqlin* function, was used to solve for the best-fit polynomial parameters. Polynomial order was set such that no systematic pattern was observed in the residuals. The fitted

curve was required to pass through the initial steady state value (0 after normalization) at the point of perturbation and had to reach steady state (1 after normalization) in the last 3 minutes of the trial. These constraints are reasonable given that the prescribed step frequencies were at steady state during these regions. We did not constrain the initial slope of the polynomial allowing for rapid initial changes in the smoothed cost.

Our forward model approach can be used in situations where the experimenter has a good first approximation of the shape of the instantaneous energetic cost profile (Figure 5.1D). This shape is described with a set of parameters that are then optimized so that the generated input profile, when run through the subject-specific model, produces an estimate of measured cost that best fits the actual measured energetic cost response. We used a Nelder-Mead Simplex method, implemented with MATLAB's *fminsearch* function, to solve for the optimal parameter values. For the step input, a single parameter was optimized: the time of onset of the step. For the ramp input, two parameters were optimized: the time of onset and the time of offset of the ramp, which together dictate the slope of the ramp. For the adaptation input, three parameters were optimized: the time of onset, the amplitude of the peak, and a decay constant. Note that the initial and final steady state amplitudes were not optimized, as normalization fixes them at 0 and 1, respectively.

The inverse and forward model approaches where applied to individual repeats of the step, ramp, and adaptation profiles for each subject, as well average profiles, which were produced by averaging the measured energetic cost data across the three repeats of a given profile prior to applying the inverse model or forward model approach. We also averaged data across all four subjects and again applied the inverse and forward model approach, this time using the average model parameters across our four subjects. In all cases, we assessed the goodness-of-fit between model-produced estimates of instantaneous energetic cost and the enforced instantaneous energetic cost profile by calculating an R^2 value for each approach.

5.4. Results

We found that the dynamic relationship between instantaneous energetic cost and measured energetic cost could be modeled using a first-order linear ordinary differential equation (Equation 5.2). We first tested whether this simple model held irrespective of the direction and magnitude of the change in gait. For each subject, we grouped across all trials of the same direction, and found that the time constants describing both increases and decreases in speed, were similar in magnitude and not statistically different (*p=0.500*, Table 5.1). We found the same pattern when we grouped trials of the same magnitude and compared responses to 0.25 m/s speed changes to those induced by 0.50 m/s speed changes (*p=0.094*, Table 5.1). When the increase in speed trials were fit with the time constant solved from the decease in speed trials (and visa versa), and the 0.25 m/s magnitude trials with the time constant solved from the 0.50 m/s magnitude trials (and visa versa) R^2 values, averaged across subjects, remained above 0.85. Because the underlying dynamics did not depend strongly on the magnitude or direction of the change in gait, in subsequent analyses all trials for an individual subject are grouped together before fitting.

Table 5.1: Time constants and model fits for changes in gait of different direction and magnitude, averaged across subjects

Change in Gait	Time Constant, τ (seconds)		Fit (R^2)	
	Mean	STD	Mean	STD
Direction up	38.04	8.52	0.87	0.10
Direction down	44.97	17.43	0.89	0.10
Magnitude 0.25 m/s	42.64	18.94	0.87	0.08
Magnitude 0.50 m/s	41.85	9.71	0.93	0.07
All	41.78	12.05	0.94	0.05

Our model described the dynamics of respiratory metabolic cost reasonably well for most subjects. When compared to the average response, the model accounted for 82-99% of the measured variability (Figure 5.3). Adding a second dynamic process, modeled as an additional time-delayed first-order linear differential equation, did not appreciably improve our fits; no improvement was visually evident and on average only an additional 0.9% ± 1.0% of the variability was explained (mean ± SD).

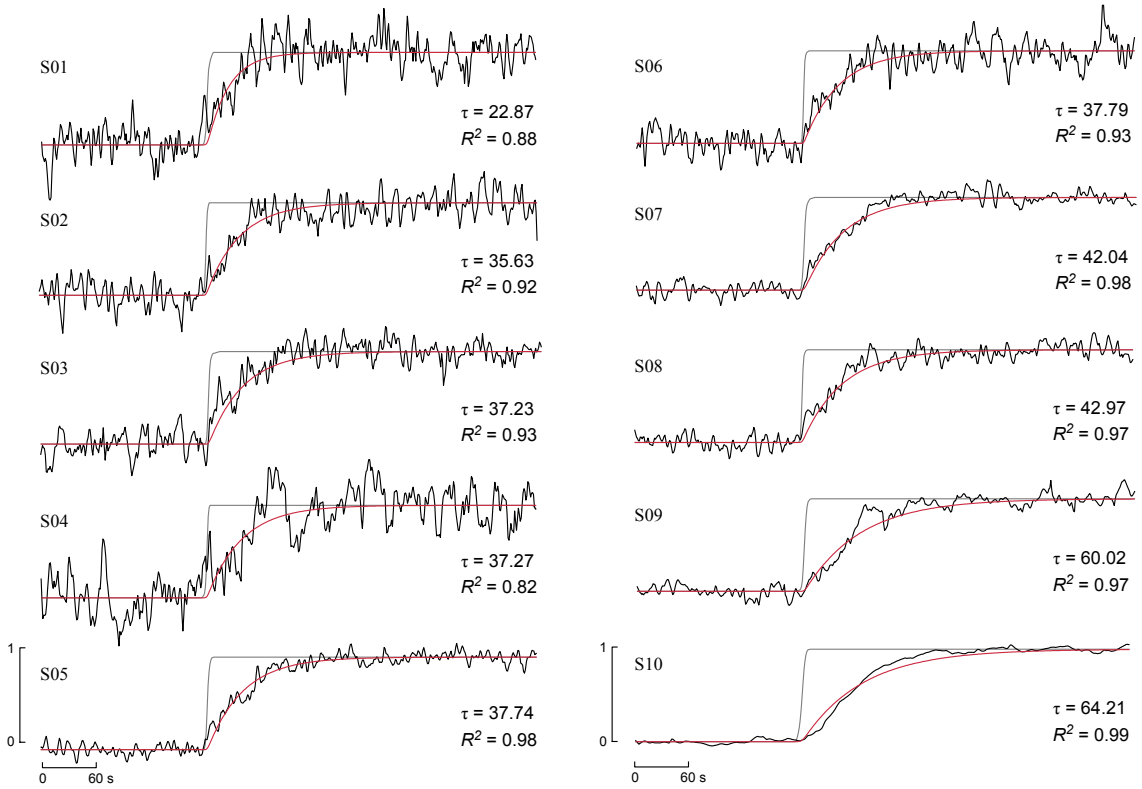

Figure 5.3: Modeling the measured energetic cost response
The average measured energetic cost response (black line) to 24 rapid changes in instantaneous energetic cost (grey line) is shown for each subject. The red line illustrates the model that best fits each subject's response. Model time constants (τ) and R^2 values for each fit are presented on the right hand side of each panel. Before we averaged the data, we normalized all instantaneous and measured energetic cost changes to unity by subtracting the initial steady state values and dividing by the amplitude of the final steady state values.

Across all subjects, model fits yielded an average time constant (τ) of 41.8 ± 12.1 seconds (mean ± SD). This means that 95% of the response to a step-like change in input is completed within three time constants, or 125.4 ± 36.3 seconds (mean ± SD). We did not identify time delays (δ) that were discernable from zero for any of the ten subjects. Due to normalization, all amplitudes (A) displayed in Figure 5.3 have a value of 1. Therefore, the mathematical representation of our model (Equation 5.2) simplifies to a transfer function of the form:

$$H(s) = 1/(\tau s + 1), \tag{5.3}$$

Using the time constants we measured for each subject, this model enabled accurate subject-specific estimates of instantaneous energetic cost from respiratory energetic cost measures. Using both our inverse and forward model approaches, we were able to produce estimates of instantaneous energetic cost from measured energetic cost that well matched the enforced step, ramp, and adaptation profiles (Table 5.2 and Figure 5.4). For the step and ramp input profiles, both approaches performed exceptionally well. The R^2 values between the enforced instantaneous energetic cost profile and the model-produced estimates of instantaneous energetic cost were typically greater than 0.9 for individual trials. As a result, averaging measured energetic cost data across the three repeats or across subjects prior to applying either approach did little to improve our estimates of instantaneous energetic cost. Thus, for the step and ramp profiles, it appears possible to accurately estimate instantaneous cost from a single trial of measured energetic cost data. Single trial estimates of instantaneous energetic cost were less accurate for the adaptation profile. Individual trial R^2 values ranged widely from 0.38 to 0.96 and 0.26 to 0.96 for the inverse model approach and forward model approach, respectively. However, averaging measured energetic cost data across the three repeats prior to applying the inverse model or forward model approaches typically resulted in R^2 values above 0.75, while then averaging across all subjects resulted in R^2 values above 0.85.

Table 5.2: R^2 values between the enforced and the model-produced estimates of instantaneous energetic cost for both the inverse model and forward model approach.

Input	Trial	S03		S05		S07		S10		All Subjects	
		Inv.	For.	Inv.	For.	Inv.	For.	Inv.	For.	Inv.	For.
Step	best	0.97	0.99	0.99	0.99	0.98	0.99	0.97	0.99		
	median	0.96	0.99	0.99	0.98	0.97	0.99	0.88	0.96		
	worst	0.98	0.92	0.94	0.87	0.94	0.93	0.83	0.74		
	average	0.98	1.00	0.99	0.99	0.98	0.98	0.96	0.92	0.98	0.97
Ramp	best	0.99	1.00	0.99	1.00	0.99	0.99	0.94	1.00		
	median	0.98	1.00	0.97	0.98	0.98	0.99	0.89	0.91		
	worst	0.86	0.79	0.89	0.93	0.98	0.99	0.69	0.60		
	average	0.97	1.00	0.99	0.99	0.99	1.00	0.87	0.99	0.97	0.98
Adapt	best	0.84	0.70	0.84	0.82	0.90	0.96	0.92	0.88		
	median	0.79	0.61	0.77	0.86	0.64	0.46	0.82	0.50		
	worst	0.72	0.40	0.79	0.78	0.38	0.26	0.77	0.46		
	average	0.81	0.76	0.84	0.88	0.75	0.66	0.92	0.79	0.87	0.85

Note, R^2 values from the three repeats, for each of the step, ramp, and adaptation input profiles, have been ordered from highest to lowest for each subject. To produce the average value, we averaged the measured energetic cost data across the three repeats prior to applying the inverse model or forward model approach. We also averaged across all subjects and all repeats to produce the final two columns of data. Subject S03 has been used as a representative subject in Figure 4, with the median trials being used as representative individual trials.

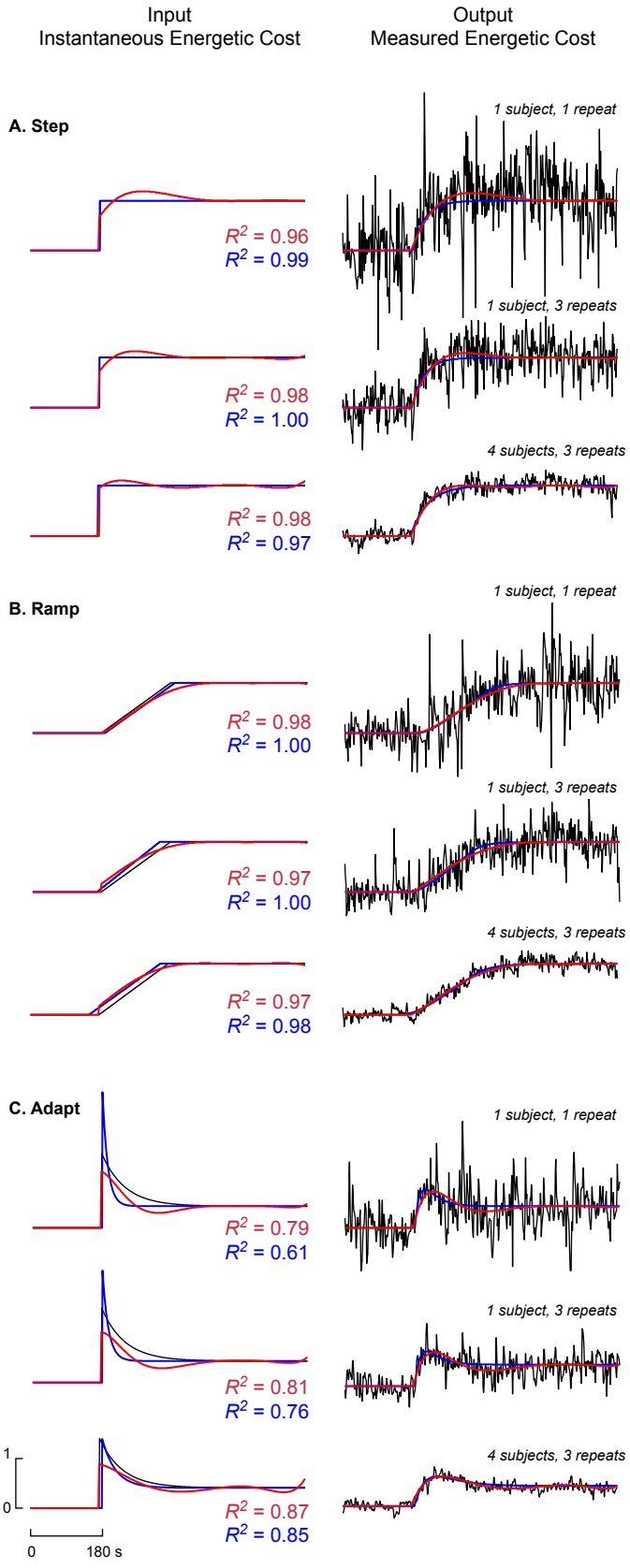
Input
Instantaneous Energetic Cost
Output
Measured Energetic Cost
A. Step
1 subject, 1 repeat
R^2 = 0.96
R^2 = 0.99
1 subject, 3 repeats
R^2 = 0.98
R^2 = 1.00
4 subjects, 3 repeats
R^2 = 0.98
R^2 = 0.97
B. Ramp
1 subject, 1 repeat
R^2 = 0.98
R^2 = 1.00
1 subject, 3 repeats
R^2 = 0.97
R^2 = 1.00
4 subjects, 3 repeats
R^2 = 0.97
R^2 = 0.98
C. Adapt
1 subject, 1 repeat
R^2 = 0.79
R^2 = 0.61
1 subject, 3 repeats
R^2 = 0.81
R^2 = 0.76
4 subjects, 3 repeats
R^2 = 0.87
R^2 = 0.85
1
0
0
180 s

Figure 5.4: Estimating changes in instantaneous energetic cost
The enforced instantaneous energetic cost (input, left panel) and measured energetic cost responses (output, right panel) are shown in black for the step (A), ramp (B) and adaptation (C) input profiles. The red lines represent estimates from the inverse model approach, and the blue lines represent estimates from the forward model approach. For some conditions, the lines illustrating the estimates obscure the black line input profiles. The first row of data is from a single representative trial for a representative subject (S03). The second row of data has been averaged across the three repeats for the same representative subject. The third row contains data averaged across the three repeats and four subjects. R^2 values calculated between the enforced instantaneous energetic cost profiles and the inverse model approach estimates of muscle energy use are shown in red text, while that for the forward model approach estimates are shown in blue text. The normalized Y-axis scale represents a change in energetic cost of approximately 1 W/kg.

5.5. Discussion

We found that a simple first order linear differential equation can approximate transient energetic cost responses during gait. When rapid step-like changes in instantaneous energetic cost were enforced, we observed a single underlying response featuring no discernable delay. On average, subjects took two minutes to reach 95% of the steady state metabolic cost value, with all but one subject reaching 95% steady state within three minutes. These same underlying dynamics held regardless of the magnitude or direction of the change in gait. Despite the collective effect of many sources of complexity—including mitochondrial dynamics, gas stores, transit delays, and cardio-pulmonary control—a simple model explains the transient energetic cost response during walking.

This model allowed us to produce reasonably accurate estimates of instantaneous energetic cost from respiratory cost measures. Our two approaches—the inverse model approach and forward model approach—resulted in similar estimates of instantaneous energetic cost, and when compared to our enforced cost profile, R^2 values were typically greater than 0.90. Both methodologies were able to capture rapid changes in instantaneous energetic cost that were prescribed during the step trials, as well as gradual changes and discontinuities that were prescribed during the ramp trials. The poorest estimates of instantaneous energetic cost were found for the adaptation trials, where fitting the rapid decay proved problematic in some trials. These sorts of transient

changes in cost are more readily distorted by breath-by-breath noise because there are fewer data points available within the transient period with which to fit model parameters. Our adaption trial decayed to steady state with a time constant of 60 seconds, which equates to only about 20 breaths. Better estimates may be possible with improved noise removal techniques, improved fitting techniques, or as we found here, through averaging over a greater number of trial repeats or subjects. Overall, the two approaches produced similar and seemingly accurate estimates of instantaneous energetic cost. However, each approach is subject to distinct limitations and requires different assumptions on the part of the user.

The inverse model approach requires little advance knowledge of the underlying instantaneous energetic cost profile, but is greatly complicated by breath-by-breath noise. High frequency components of breath-by-breath variability in measured energetic cost are effectively amplified when passed through the model inverse, obscuring estimated instantaneous energetic cost. To reduce their contribution, while retaining our ability to fit fast changing inputs, we first fit the noisy metabolic cost data using a polynomial. We constrained the polynomial to pass through an initial steady state value at the point of perturbation, and to reach steady state at the end of the trial. For an experimenter, these constraints require that the protocol be designed such that the subject begins and ends in steady state. (These particular constraints are not universal for every experimental paradigm—researchers should identify whatever constraints on the measured data are imposed by the experimental paradigm and use them to their fitting advantage.) Although we made no assumptions about the shape of the profile between the beginning and end steady state regions, complex profiles would not be fit well by a low order polynomial. In such situations higher order polynomials, splined polynomials, or all together different functions may be necessary to accurately fit the measured energetic cost profiles. This will inevitably introduce subjectivity, as the experimenter will be required to make decisions about what profile changes are ‘true’ and what is simply ‘noise’.

Estimating instantaneous energetic cost using the forward model approach requires some advance knowledge of the profile shape. This knowledge may be based on the study design or additional measurements. For example, if the study design calls

for a novel force to be rapidly applied to a limb one may reasonably assume an abrupt increase in instantaneous energy use, followed by an exponential decay as the subject adapts to the new force. One need not know the timings and magnitudes of the initial increase and subsequent decay as the forward approach employs optimization to estimate their values. Alternatively, one may deduce the profile shape from a measured physiological variable, such as the time course of adjustments to step frequency or muscle activity. It is also possible that the experimenter has a range of hypotheses about what the input profile shape may be. These hypotheses can be evaluated by optimizing each candidate input profile and testing which one provides the best fit. To illustrate this, we fit optimal step, ramp, and adaptation profiles to each of the three responses and found that each response was best fit by its respective profile shape (e.g. the enforced ramp was best fit by a ramp profile). Because the experimenter must make assumptions about the underlying profile shape, the forward approach introduces a bias based on the experimenter's expectations. Moreover, there may be situations where the experimenter does not have a reasonable first approximation of the input profile shape.

In addition to the approach specific limitations described above, there are four more general limitations to our methodology and analysis. First, we treat our enforced instantaneous energetic cost profiles as a gold standard to which we compare our model estimates. Although we attempted to enforce a specific cost profile by controlling walking speed and step frequency, other uncontrolled gait parameters, for example stance time or muscle activity, may have caused instantaneous energetic cost to deviate from our desired input profile. As a consequence, our estimates may be better or worse than presented. Second, the identified model and its average parameters only apply to adult humans. Differences in size and phylogenetic history are both likely to alter the dynamic relationship of other animals from that in adult humans. Similarly, the identified model and its average parameters only apply to walking. While we found that a single process accurately captures the identified dynamic relationship between instantaneous and measured energetic cost, Whipp and colleagues have found that there are two important processes in particular cycling conditions, perhaps reflecting a difference in cardio-pulmonary control between the two tasks (*46*, *56*). A fourth limitation of our model is that it can only be applied to walking tasks within the tested metabolic cost range. At metabolic rates above 5 W/kg, many subjects may breach the anaerobic threshold,

causing oxygen stores to be depleted faster than they can be replenished and rendering our measured energetic cost a poor estimate of the underlying instantaneous energetic cost. At metabolic rates below 1.5 W/kg it is possible that more complex dynamics exist at the onset of exercise, as first described by Whipp and colleagues (*46*). Overall, our exact model can be used to estimate instantaneous energetic cost of walking at metabolic rates ranging from 1.5 W/kg to 5 W/kg, which, under natural conditions, corresponds to walking speeds ranging from 0.75 m/s to 1.75 m/s. Outside of this range, care should be taken to first identify the underlying dynamic relationship between instantaneous and measured energetic cost before applying our inverse or forward model approach. Within the constraints imposed by these limitations, there is still considerable flexibility with regards to what tasks can be used to identify the model between instantaneous and measured energetic cost—rapid changes in speed and step frequency are convenient, but not necessary. The most important feature is that the dynamics underlying the energetics of the non-steady state tasks of interest should not be appreciably different from those underlying the tasks used to identify the model. In other words, the mitochondrial dynamics, body transit delays, and respiratory control mechanisms—but not necessarily the biomechanical task—need to be the same or similar between the tasks.

Our methodology may prove useful for both post-hoc and real-time estimation of energetic cost. Its accuracy benefits from a personalized model for each subject, but for some situations, it may suffice to use the average dynamic model identified in the current experiments. As an initial test of this possibility, we simulated measured energetic cost to an adaptation input profile for a subject with an exceptionally slow time constant of 60s. We then compared instantaneous cost estimates using this subject-specific time constant to that obtained if we assumed our average time constant (42 seconds). Using the average time constant still made it clear that instantaneous cost adapted by demonstrating the characteristic rapid increase followed by a slower decay. As to be expected, R^2 values dropped when using the average time constant, but over 80% of the variability was still explained. This general model is particularly useful because it allows experimenters to return to previously measured energetic cost data and estimate instantaneous energetic cost without the need for a subject-specific model of cost dynamics. Another use for the identified dynamic model is real-time estimation of

instantaneous cost. Kalman filters, and similar algorithms, leverage dynamic models of the system to help correct for noise and delays (*173*, *174*). Real-time estimates of instantaneous energetics may prove useful for biofeedback, manipulating gait training based on energetic cost, or simply for online determination of when a research subject has reached steady state.

An ability to assess instantaneous energetic cost during non-steady gait could unveil new insights into walking. People rarely experience metabolic steady state conditions; less than 1% of real-world walking bouts last the requisite five minutes (*166*). The fields of locomotor adaptation and learning aim to shift our scientific focus from the steady state to this real-world behaviour. Energetic concepts—such as economy, efficiency, and least effort—are often used to explain adaptations to novel environments or tasks. Yet, as researchers work to understand the neuronal circuitry involved in gait adaptation, and quantify the timescales over which adaptation occurs, they have been unable to effectively make direct comparisons to energetic cost during the adaptation itself. An understanding of the role of energy use may help us understand how we adapt to changing environments, how we compensate for injury or motor control deficits, and how we learn new tasks. By presenting a methodology for assessing instantaneous energetic cost during adaptation and other non-steady gait conditions, we aim to provide our field with a tool with which we can investigate previously unanswerable questions.

5.6. Supplementary: Establishing Model Confidence

Identifying an appropriate model between instantaneous and measured energetic cost is a first and critical step when using both our inverse and forward model approach. When designing the experiments for identifying the model, users need to know how confident they need to be in the identified model parameters, and the number of trial repeats required to achieve this level of confidence. That is, does one need to know the time constant within one second or ten seconds of its actual value to accurately estimate instantaneous energetic cost? And to achieve the appropriate accuracy in estimating the time constant, does one need a small number of trials, or a prohibitively large number of trials?

To address the first question, we simulated the measured energetic cost to step, ramp and adaptation input profiles for hypothetical subjects with time constants over the range of time constants that we measured in our subjects (20, 40, and 60s). We constructed the simulated data for a particular combination of input profile and time constant by passing the profile through our model (Equation 5.3), parameterized with the time constant, then added white noise to reflect breath-by-breath noise, and finally down sampled the signal to a desired breathing frequency. We then applied the inverse and forward model approaches and compared the R^2 values found for instantaneous cost estimates from the time constant used to simulate the data (i.e. actual time constant) to that obtained if the time constant deviated by different amounts (i.e. estimated time constant). We used deviations of ± 2, 5, 10, 15, and 20 seconds. As the difference in R^2 values will depend upon the particular random breath-by-breath variability used in each simulation, we employed a standard bootstrap Monte Carlo procedure and repeated this process 100 times to estimate the average difference in goodness of fit between the actual time constant and the estimated time constant (*175*). We found that across all time constants, the goodness of fit did not depend strongly on the accuracy of the time constant, the level of noise, or the breathing frequency within the range of these parameter values that we measured in our subjects. Rather, the required confidence in the time constant can depend strongly on the shape of the input profile. Profiles with impulse like characteristics, such as the adaptation input profile, are much more affected by errors in the time constant than a more gradual profile such as the ramp. For example, when the estimated time constant was 15 seconds longer than the actual time constant of 40 seconds, the average R^2 value dropped from 0.96 to 0.87 for the adapt input profile. The same error in time constant had almost no effect on the R^2 for the ramp input profile. As a conservative guideline, we recommend designing the identification experiments to have the 95% confidence level of the time constant be within 5 seconds. If attempting to fit input profile shapes that differ from those we have tested, we recommended using the range of subject data from Table 3 to simulate the output metabolic power response, allowing one to run their own simulation to determine the desired level of confidence in a subject's time constant.

To determine the number of trial repeats required to achieve that confidence, we leveraged the work of Lamarra and colleagues who addressed precisely this question for

the purpose of identifying the time constants underlying gas kinetics during stationary cycling (*137*). In brief, their method uses Monte Carlo simulations to estimate the confidence interval for a given model parameter. This is dependent on both the experimental design, including factors such as the number of trial repeats and the magnitude of the induced change in metabolic power, as well as particular subject characteristic, including their time constant, variability in measured metabolic power, and breathing frequency. We modified their analysis by using our measured ranges for changes in steady state metabolic power, time constants, variability in metabolic power, and breathing frequency (Table 5.3), as these are more typical for walking than the values used in the original analysis. We found that the number of trial repeats (*n*) was largely insensitive to changes in time constant (τ) within the ranges of time constants we measured in our experiments. Consequently, we choose a single value of τ (40 seconds) to test the effect on trial repeats of breathing frequency and variability in metabolic power. Table 4 presents the results of this analysis as well as serving as a simplified look-up table for estimating the number of trial repeats across a range of subject characteristics for a nominal change in metabolic power of 1.5 W/kg (about that that would be seen if walking speed increased from 1.00 m/s to 1.5 m/s). As described by Lamarra et al (1987), the following formula can be used to determine n for a different change in metabolic power ($\Delta \mathrm{W}_{\mathrm{new}}$):

$$\mathrm{n}_{\mathrm{new}} = \mathrm{n}_{\mathrm{table}} \left(\frac{\Delta \mathrm{W}_{\mathrm{table}}}{\Delta \mathrm{W}_{\mathrm{new}}} \right)^2, \tag{5.4}$$

where $\Delta \mathrm{W}_{\mathrm{table}}$ has a value of 1.5W/kg and $\mathrm{n}_{\mathrm{table}}$ is determined from Table 5.4 based on subject breath-by-breath noise and breathing frequency. Intuitively, the number of required trial repeats decreases as the signal to noise ratio increases—either through a higher signal due to larger changes in metabolic power or lower noise due to smaller subject variability in metabolic power—and when breathing frequency increases thereby yielding more information on which to fit the model. As an example calculation, if we determine a subject has a breath-by-breath standard deviation in metabolic power of 0.5 W/kg and a breathing frequency of 20 breaths/min from a short steady state walking trial, and we are going to subject them to a change in metabolic power of approximately 1.5 W/kg, we would require 5 repeats to determine their τ with a 95% confidence interval of ±5 seconds. If we were only going to subject them to a 1 W/kg change in metabolic

power, Equation 5.4 indicates that we would need 11 trial repeats to determine the time constant to the same accuracy. It is worth noting that this method is very convenient—the number of trial repeats required to determine a subject's time constant can be estimated by making a small number of measurements (breathing frequency and variability in breath-by-breath metabolic cost) during a single steady state trial.

Table 5.3: Each subjects' time constant, standard deviation in breath-by-breath metabolic power, breathing frequency, and net metabolic power across the range of walking speeds tested.

Subject	Time Constant (seconds)	Metabolic Power STD (W/kg)*	Breathing Frequency (breaths/ minute)*	Net Metabolic Power (W/kg)				
				0.5 m/s	1.00 m/s	1.25 m/s	1.50 m/s	1.75 m/s
S01	22.87	0.93	25	1.32	1.62	2.29	3.12	4.44
S02	35.63	0.77	25	1.78	2.21	2.89	3.81	5.29
S03	37.23	0.47	30	1.52	1.99	2.50	3.33	4.60
S04	37.27	0.78	19	1.46	2.03	2.26	3.01	3.95
S05	37.74	0.34	22	1.59	1.94	2.49	3.34	4.97
S06	37.79	0.51	26	2.35	2.91	3.38	4.35	6.31
S07	42.04	0.31	20	1.68	2.07	2.63	3.54	5.32
S08	42.97	0.34	20	2.35	2.79	3.37	4.16	5.85
S09	60.02	0.32	17	1.24	1.60	2.30	3.54	5.21
S10	64.21	0.19	11	1.53	2.02	2.54	3.36	4.67
Mean	41.78	0.49	22	1.68	2.12	2.67	3.56	5.06
STD	12.05	0.25	5	0.39	0.43	0.42	0.43	0.69

These data can be used to simulate an expected output metabolic cost response, allowing one to assess the required confidence in a subject's time constant and the resulting number of trial repeats required to achieve this confidence. * These values have been reported for a walking speed of 1.25m/s. On average, standard deviation in metabolic power increases as walking speed increases at a rate of 0.31W/kg/m/s and breathing frequency increases at a rate of 3.3bpm/m/s.

Table 5.4: Simplified lookup table for the number of repeats (n) required to approximate τ with a 95% confidence interval of ±5 seconds across a range of breath-by-breath noise levels and breathing frequencies.

Metabolic Power STD (W/kg)	Breathing Frequency (breaths / minute) 10	15	20	25	30
0.1	0.4	0.3	0.2	0.1	0.1
0.2	1.6	1.1	0.8	0.6	0.5
0.3	3.5	2.3	1.7	1.4	1.1
0.4	6.1	4.1	3.1	2.4	2.1
0.5	9.5	6.3	4.8	3.8	3.2
0.6	13.6	9.1	7.0	5.5	4.7
0.7	18.4	12.3	9.5	7.5	6.4
0.8	24.0	16.0	12.4	9.8	8.4
0.9	30.3	20.2	15.7	12.4	10.7

τ is assumed to be near 40 seconds and the change in metabolic power (ΔW) is 1.5 W/kg. Values are reported to one decimal place to facilitate accurate scaling of these numbers when applying Equation 4.

Chapter 6.

Conclusions

Throughout this dissertation I have investigated the role of optimization, and in particular energy optimization, in the control of human gait. I began my dissertation with an applied focus, interested in the evolving partnership between human and machine. In my first study I developed a control system for a lower limb exoskeleton that leveraged the body's internal optimization by tapping directly into the sensorimotor loop. I developed a myoelectric controller that can accurately identify the user's desired motion, automatically gradate the actuation of an exoskeleton, and allow the controller to be adaptable to complex movements and environments. While this work focused on predicting the user's intent, I became increasingly curious about the user's response to the novel conditions imposed by an active exoskeleton. Here my focus shifted to a related, but more fundamental question: when the energetic consequences of movement are altered, be that due to a novel technology, environment, or constraints on the body, how does one adapt? In my second study, I tested the hypothesis that people continuously adapt their gait to optimize energetic cost in real-time. To accomplish this, I developed a controller for the robotic exoskeletons that altered the energetic consequences of various gaits. I made abnormal ways of walking energetically optimal and found that when given broad experience with the novel energetic landscapes subjects discovered the optimal gaits and opted to walk at them, even when the energetic benefits were small. In my third study, I conducted a series of experiments to test how the nervous system initiates this optimization and the process used to converge on new optima. Here I found that the nervous system can be primed to initiate optimization when perturbed toward lower cost gaits, following which it gradually converges on novel optima in a manner consistent with a 'local search' strategy. Given that energetic cost is not just an outcome of movement, but appears to play a central role in continuously shaping it, in my fourth and final study I developed a technique to estimate instantaneous energetic cost during non-steady state conditions. This

technique now makes it possible to study the role of energetics throughout the course of locomotor adaptation and learning.

6.1. Implications and Future Directions

My finding that real-time optimization of energetic cost is a fundamental objective of the nervous system has applications in the design and control of assistive robotic devices. Powered prostheses, orthoses and exoskeletons are being used to restore and augment human movement (*61-68*). Yet, identification of optimal control parameters, which often number in the double digits, is a significant challenge. In most cases, these parameter settings are heuristically tuned for a specific user by a trial and error process that relies on experimenter observation and user feedback (*176*). This process can be prohibitively time consuming, due to many possible parameter combinations, as well as unreliable given its subjective nature. For example, in my first project we optimized a single parameter, torque fraction, based in part on subjective feedback. Because we tested nine parameter settings and allowed the subject to walk at each for three minutes, optimizing this single parameter required approximately 30 minutes. Had we optimized a second parameter with this many possible settings in combination with the first, we would have had to assess 9^2, or 81 conditions, requiring over 4 hours of walking. To address this problem, we have collaborated with researchers from the University of Michigan and are developing an automated 'body-in-the-loop' method to optimize assistive device settings (*176*). In brief, rather using brute force to explore all possible parameter settings, we propose to allow the computer to iteratively adjust parameter settings while running an optimization that seeks to minimize some physiological control objective. The implementation of this method leverages two outcomes of this dissertation. First, the finding that minimization of energy expenditure is a dominant objective in the real-time control of gait makes energetic cost a logical objective for our computer-driven optimization. Second, my technique to measure instantaneous energetic cost allows this optimization to proceed using real-time measures of energy expenditure. Further development of this method may one day allow device parameters to be rapidly and optimally selected to minimize energy expenditure and improve the user experience.

The drive to continuously seek energetic optima also presents challenges and opportunities for the rehabilitation of human movement. Traditional rehabilitation of stroke-induced asymmetries, as well as other gait disorders, is often focused on restoring 'normal' symmetric limb trajectories (*26*, *131*). But the achieved symmetries are transient (*26*, *131*). Our findings perhaps suggest that the asymmetric gait is preferred because it is energetically optimal (*132*, *145*). Rehabilitation may instead take advantage of continuous cost optimization by reshaping underlying energetic landscapes with training or assistive devices to align the otherwise competing goals of symmetrical and optimal gaits. However, this hinges on the malleability of natural energetic landscapes. And, it is currently unclear how readily the energetic consequences of natural movement can be re-shaped. Future testing on both able-bodied and patient populations could explore the amount and time course of training required to permanently shift an energetic optima.

Beyond these direct applications, more fundamental questions remain such as what sensors and circuitry the body uses to perform optimization. As previously mentioned, energetic cost could be sensed either globally by known blood gas receptors (*50-52*) or locally by muscle receptors sensitive to the byproducts of metabolism (*53*, *54*). The exoskeleton paradigm used in this dissertation necessarily perturbs both and therefore does not allow us to decipher between these possible sensing mechanisms. Our lab has recently performed experiments to perturb blood gas sensors in isolation using a closed-loop gas control paradigm (*177*). Preliminary results suggest that subjects do not optimize their gait in response, suggesting that global sensors of cost are not dominant. Muscle afferents are the next logical candidate. Indeed, very recent work by Hubbuch et al. (2015) has demonstrated that disrupting proprioceptive feedback can delay adaptation toward more economical gaits (*178*). However, it still remains unclear if energy expenditure is directly sensed using group III and IV afferents sensitive to the by-products of muscle metabolism or indirectly sensed using muscle contraction characteristics, such as velocity and force, to predict metabolic demand. Experiments using nerve blocks that selectively target group III and IV afferents could provide answers (*179*, *180*). Moreover, Hubbuch et al. experiments were performed on well-learned walking tasks (*178*). Therefore, it is possible that disrupting proprioceptive feedback disrupts the rapid prediction of an optimal gait, yet not the optimization process

itself. Testing their paradigm on a task that requires optimization within a novel context would shed light on the specific role of proprioceptive feedback in the selection of optimal gaits.

Along with identifying the relevant anatomical sensors it will ultimately be important to determine where the energy optimization process occurs within the nervous system. Early experiments conducted on decerebrate cats have demonstrated that they retain the ability to adapt their gait—to step over objects, to compensate for changing treadmill speeds, and even to adapt to split belt paradigms (*181-185*). This capability points to the role of lower level brain structures in adaptation. And, lesions of one particular lower level structure, the cerebellum, disrupt adaptation in these animals (*181*, *182*). Testing on human patients with cerebellar damage exhibit similar impaired performance during adaptation tasks (*27*, *186-188*). These findings, have implied that the cerebellum plays a central role in the adaptation and learning of motor tasks, making it a plausible neuronal site of optimization. Interestingly, impairments to higher-level brain structures such as the M1 region or basal ganglia have been shown to disrupt retention and recall of adapted movements (*187*, *189-192*). This might suggest that this region plays an important role in prediction of optimal movements. To our knowledge, it has not been directly tested if particular neural deficits disrupt convergence on energetically optimal gaits. Testing on patient populations, functional imaging of the brain in those with and without neural deficits (*193-195*), and experiments on animal models, where particular neural circuitry can be disrupted or abolished, could help elucidate the anatomical origins of energy optimization and prediction during gait.

Determining if, or to what extent, subjects use a conscious or explicit strategy during adaptation to the novel cost landscapes could also provide important insight into the mechanisms of optimization. Taylor and colleagues have recently demonstrated both implicit and explicit strategies contribute to adaptation in classic visuo-motor rotation tasks for the upper arm (*196*, *197*). Moreover, Bastian and Malone have shown that during split-belt walking, giving subjects explicit instruction on how to adapt speeds adaptation yet worsens retention, while distraction tasks slow adaptation and improve retention (*198*). It is not clear in our paradigm how aware subjects are of their gait adaptations or to what extent they may explicitly direct them. Additional experiments

where subjects are given explicit instructions about the controller's function, as well as experiments where subjects are required to perform cognitive distraction tasks during adaptation could provide additional insight.

It is important that future work test the generalizability of my findings across different walking paradigms as well as other motor tasks. I expect that minimization of energy expenditure will stand as a dominant objective of the nervous system in most locomotor tasks. For example, there is already some evidence that adaptations toward symmetry during split belt walking are driven by reductions in energetic cost (*47*). However, some experiments have failed to show energy optimization. For example, our lab previously designed a paradigm where the speed-step frequency relationship was experimentally altered, creating a new energetically optimal gait (*2*). In this experiment, subjects did not adapt toward the optima but instead adapted such that they could return to a gait that lies along their natural speed-step frequency preference. This may no longer be surprising in light of my finding that most subjects will persevere at preferred and more costly gaits unless perturbed toward lower cost movements. A return to past paradigms, armed with new insight into the experienced needed to initiate optimization, will allow us to test the whether our findings represent general strategies in the control of gait. It will also be important to test whether the nervous system can leverage this capability in the control of discrete and low cost movements. Theories of motor control and learning often rely on energy optimization to explain the coordination of discrete movements like reaching, and postural tasks like standing and sitting (*127*, *128*). However, at present time, direct evidence to support this remains sparse and mixed (*48*, *49*).

To fully realize the implications of this work, it will be important to test how people optimize their gait during real-world walking. Thus far, all of my experiments have been conducted in a laboratory setting on a treadmill. One limitation of such a design is that variability in gait is reduced when walking on a level surface at fixed speed. If analogous experiments were to be conducted during over ground walking, variability could be naturally injected due to changing terrain and walking objectives. It will be interesting to determine if and how the body optimizes in this more natural context. At present it remains unclear if real-world experience or targeted laboratory experience is most

effective when adapting people to novel tasks and technology. I am also interested in understanding what energetic principles guide locomotion when people are walking not alone, but with a partner or pack. In the real-world we often walk with others and in many cases ones energetic preferences may be in conflict with those of others. Experiments designed to test how well we can predict others exertion and if we are willing or able to optimize a group objective could provide further insight into why we move the way we do in the real-world.

6.2. Summary

Throughout this dissertation, I have investigated the role of optimization in the control of human gait. I first designed an exoskeleton controller that is integrated into the user's sensorimotor loop, and is therefore adaptable to changing tasks and terrains. I next used the lower limb exoskeletons to disrupt the natural sensorimotor loop, allowing me to explore fundamental aspects of locomotor control. I made abnormal ways of walking energetically optimal and found that people discovered these gaits and opted to walk at them, even when the energetic benefits were small. This finding suggests that during gait, energy optimization is a primary objective of the human nervous system. I next tested how this optimization is carried out by the nervous system and found that optimization can be initiated by naturally high variability in gait or perturbations toward lower cost gaits. Once initiated, the body appears to use a local search strategy to gradually descend an energetic gradient and converge on novel optima. Although I found that energy use is an important objective in the real-time control of human gait, standard methods for measuring energetic cost have been restricted to steady state conditions. To allow further exploration of the role of energetic cost during locomotor adaptation and learning, I developed a technique to estimate instantaneous muscle energy use during non-steady state gait.

Collectively, this work has advanced our understanding of why people walk the way they do. Using my developed paradigm, whereby exoskeletons are used to manipulate the energetic consequences of movement, I have shown that humans coordinate their gait to optimize immediate energy expenditure. In future this paradigm, along with my technique to estimate instantaneous energy use, can be used to further

explore fundamental of aspects of human motor control. This could include determining the anatomical sensors used to measure energetic cost and the neural correlates that perform optimization. At a more applied level, my work is relevant to those seeking to rehabilitate and augment human movement. Rehabilitation programs could take advantage of continuous cost optimization by reshaping underlying energetic landscapes with training or assistive devices. Moreover, the design and control of novel wearable technology, such as exoskeletons or prosthetics, can now be informed by an understanding of the user's internal energy optimization process.

References

1. T. A. Martin, J. G. Keating, H. P. Goodkin, A. J. Bastian, W. T. Thach, Throwing while looking through prisms. II. Specificity and storage of multiple gaze-throw calibrations. *Brain*. **119 (Pt 4)**, 1199–1211 (1996).

2. M. Snaterse, R. Ton, A. D. Kuo, J. M. Donelan, Distinct fast and slow processes contribute to the selection of preferred step frequency during human walking. *J Appl Physiol*. **110**, 1682–1690 (2011).

3. S. M. O'Connor, J. M. Donelan, Fast visual prediction and slow optimization of preferred walking speed. *Journal of Neurophysiology*. **107**, 2549–2559 (2012).

4. R. Schmidt, T. Lee, *Motor Learning and Performance 5th Edition With Web Study Guide* (Human Kinetics, 2013).

5. C. S. Sherrington, *On the proprioceptive system, especially in its reflex aspect* (Brain, 1907).

6. N. A. Bernstein, *The co-ordination and regulation of movements* (1967).

7. M. C. Tresch, P. Saltiel, E. Bizzi, The construction of movement by the spinal cord. *Nat Neurosci*. **2**, 162–167 (1999).

8. M. C. Tresch, A. Jarc, The case for and against muscle synergies. *Current Opinion in Neurobiology*. **19**, 601–607 (2009).

9. L. H. Ting, J. L. McKay, Neuromechanics of muscle synergies for posture and movement. *Current Opinion in Neurobiology*. **17**, 622–628 (2007).

10. J. J. Kutch, A. D. Kuo, A. M. Bloch, W. Z. Rymer, Endpoint force fluctuations reveal flexible rather than synergistic patterns of muscle cooperation. *Journal of Neurophysiology*. **100**, 2455–2471 (2008).

11. F. J. Valero-Cuevas, M. Venkadesan, E. Todorov, Structured variability of muscle activations supports the minimal intervention principle of motor control. *Journal of Neurophysiology*. **102**, 59–68 (2009).

12. J. P. Scholz, G. Schöner, The uncontrolled manifold concept: identifying control variables for a functional task. *Exp Brain Res*. **126**, 289–306 (1999).

13. J. R. Diedrichsen, R. Shadmehr, R. B. Ivry, The coordination of movement: optimal feedback control and beyond. *Trends Cogn. Sci. (Regul. Ed.)*. **14**, 1–9

(2009).

14. E. Todorov, M. I. Jordan, Optimal feedback control as a theory of motor coordination. *Nat Neurosci*. **5**, 1226–1235 (2002).

15. D. M. Wolpert, Computational approaches to motor control. *Trends Cogn. Sci. (Regul. Ed.)*. **1**, 209–216 (1997).

16. G. M. Gauthier, J. Blouin, C. Bourdin, J.-L. Vercher, Adaptive control: a review of the ability to acquire and maintain high sensorimotor performance. *Computers in Biology and Medicine*. **37**, 989–1000 (2007).

17. J. W. Krakauer, Motor learning and consolidation: the case of visuomotor rotation. *Adv. Exp. Med. Biol.* **629**, 405–421 (2009).

18. R. Shadmehr, M. A. Smith, J. W. Krakauer, Error Correction, Sensory Prediction, and Adaptation in Motor Control. *Annu. Rev. Neurosci.* **33**, 89–108 (2010).

19. R. Held, Plasticity in sensory-motor systems. *Scientific American* (1965), doi:10.1038/scientificamerican1165-84.

20. C. S. Harris, Perceptual adaptation to inverted, reversed, and displaced vision. *Psychol Rev*. **72**, 419–444 (1965).

21. R. Shadmehr, F. A. Mussa-Ivaldi, Adaptive representation of dynamics during learning of a motor task. *Journal of Neuroscience*. **14**, 3208–3224 (1994).

22. O. Bock, Load compensation in human goal-directed arm movements. *Behav. Brain Res.* **41**, 167–177 (1990).

23. T. Lam, M. Anderschitz, V. Dietz, Contribution of feedback and feedforward strategies to locomotor adaptations. *Journal of Neurophysiology*. **95**, 766–773 (2006).

24. A. Blanchette, L. J. Bouyer, Timing-Specific Transfer of Adapted Muscle Activity After Walking in an Elastic Force Field. *Journal of Neurophysiology*. **102**, 568–577 (2009).

25. J. T. Choi, A. J. Bastian, Adaptation reveals independent control networks for human walking. *Nat Neurosci*. **10**, 1055–1062 (2007).

26. D. S. Reisman, R. Wityk, K. Silver, A. J. Bastian, Locomotor adaptation on a split-belt treadmill can improve walking symmetry post-stroke. *Brain*. **130**, 1861–1872 (2007).

27. S. M. Morton, A. J. Bastian, Cerebellar contributions to locomotor adaptations during splitbelt treadmill walking. *Journal of Neuroscience*. **26**, 9107–9116 (2006).

28. J.-F. Yang, J. P. Scholz, M. L. Latash, The role of kinematic redundancy in adaptation of reaching. *Exp Brain Res*. **176**, 54–69 (2006).

29. K. A. Thoroughman, R. Shadmehr, Learning of action through adaptive combination of motor primitives. *Nature*. **407**, 742–747 (2000).

30. C. D. Takahashi, R. A. Scheidt, D. J. Reinkensmeyer, Impedance control and internal model formation when reaching in a randomly varying dynamical environment. *Journal of Neurophysiology*. **86**, 1047–1051 (2001).

31. M. A. Smith, A. Ghazizadeh, R. Shadmehr, Interacting Adaptive Processes with Different Timescales Underlie Short-Term Motor Learning. *Plos Biol*. **4**, e179 (2006).

32. J. W. Krakauer, M. F. Ghilardi, C. Ghez, Independent learning of internal models for kinematic and dynamic control of reaching. *Nat Neurosci*. **2**, 1026–1031 (1999).

33. H. J. Ralston, Energy-speed relation and optimal speed during level walking. *Int Z Angew Physiol*. **17**, 277–283 (1958).

34. M. Y. Zarrugh, F. N. Todd, H. J. Ralston, Optimization of energy expenditure during level walking. *Eur J Appl Physiol Occup Physiol*. **33**, 293–306 (1974).

35. N. H. Molen, R. H. Rozendal, W. Boon, *Graphic representation of the relationship between oxygen-consumption and characteristics of normal gait of the human male.* (Proceedings of the Koninklijke …, 1971).

36. E. Atzler, R. Herbst, Arbeitsphysiologische Studien III. *Pflugers Arch.*, 292 (1928).

37. J. E. Bertram, A. Ruina, Multiple walking speed-frequency relations are predicted by constrained optimization. *J. Theor. Biol.* **209**, 445–453 (2001).

38. B. R. Umberger, P. E. Martin, Mechanical power and efficiency of level walking with different stride rates. *Journal of Experimental Biology*. **210**, 3255–3265 (2007).

39. J. M. Donelan, R. Kram, A. D. Kuo, Mechanical and metabolic determinants of the preferred step width in human walking. *Proceedings of the Royal Society B: Biological Sciences*. **268**, 1985–1992 (2001).

40. R. M. Alexander, *Optima for Animals* (Princeton University Press, 1996).

41. P. S. Rodman, H. M. McHenry, Bioenergetics and the origin of hominid bipedalism. *Am. J. Phys. Anthropol.* **52**, 103–106 (1980).

42. M. D. Sockol, D. A. Raichlen, H. Pontzer, Chimpanzee locomotor energetics and the origin of human bipedalism. *Proc. Natl. Acad. Sci. U.S.A.* **104**, 12265–12269 (2007).

43. R. M. Alexander, Design by numbers. *Nature*. **412**, 591–591 (2001).

44. Y. P. Ivanenko, N. Dominici, F. Lacquaniti, Development of independent walking in toddlers. *Exerc Sport Sci Rev*. **35**, 67–73 (2007).

45. R. Pagliara, M. Snaterse, J. M. Donelan, Fast and slow processes underlie the selection of both step frequency and walking speed. *Journal of Experimental Biology*. **217**, 2939–2946 (2014).

46. B. J. Whipp, S. A. Ward, N. Lamarra, J. A. Davis, K. Wasserman, Parameters of ventilatory and gas exchange dynamics during exercise. *J Appl Physiol*. **52**, 1506–1513 (1982).

47. J. M. Finley, A. J. Bastian, J. S. Gottschall, Learning to be economical: the energy cost of walking tracks motor adaptation. *The Journal of Physiology*. **591**, 1081–1095 (2013).

48. D. A. Kistemaker, J. D. Wong, P. L. Gribble, The Central Nervous System Does Not Minimize Energy Cost in Arm Movements. *Journal of Neurophysiology*. **104**, 2985–2994 (2010).

49. H. J. Huang, R. Kram, A. A. Ahmed, Reduction of Metabolic Cost during Motor Learning of Arm Reaching Dynamics. *Journal of Neuroscience*. **32**, 2182–2190 (2012).

50. J. W. Bellville *et al.*, Central and peripheral chemoreflex loop gain in normal and carotid body-resected subjects. *J Appl Physiol*. **46**, 843–853 (1979).

51. M. Fatemian *et al.*, The respiratory response to carbon dioxide in humans with unilateral and bilateral resections of the carotid bodies. *The Journal of Physiology*. **549**, 965–973 (2003).

52. M. E. F. Pedersen, M. Fatemian, P. A. Robbins, Identification of fast and slow ventilatory responses to carbon dioxide under hypoxic and hyperoxic conditions in humans. *The Journal of Physiology*. **521**, 273–287 (1999).

53. C. M. Adreani, J. M. Hill, M. P. Kaufman, Responses of group III and IV muscle afferents to dynamic exercise. *J Appl Physiol*. **82**, 1811–1817 (1997).

54. M. P. Kaufman, S. G. Hayes, The Exercise Pressor Reflex. *Clin Auton Res*. **12**, 429–439 (2002).

55. C. M. Adreani, M. P. Kaufman, Effect of arterial occlusion on responses of group III and IV afferents to dynamic exercise. *Journal of Applied Physiology* (1998).

56. B. J. Whipp, S. A. Ward, Physiological determinants of pulmonary gas exchange kinetics during exercise. *Med Sci Sports Exerc*. **22**, 62 (1990).

57. J. H. Coote, S. M. Hilton, J. F. Perez-Gonzalez, The reflex nature of the pressor response to muscular exercise. *The Journal of Physiology*. **215**, 789–804

(1971).

58. M. P. Kaufman, J. C. Longhurst, K. J. Rybicki, J. H. Wallach, J. H. Mitchell, Effects of static muscular contraction on impulse activity of groups III and IV afferents in cats. *J Appl Physiol*. **55**, 105–112 (1983).

59. D. I. McCloskey, J. H. Mitchell, Reflex cardiovascular and respiratory responses originating in exercising muscle. *The Journal of Physiology*. **224**, 173–186 (1972).

60. K. L. Snyder, M. Snaterse, J. M. Donelan, Running perturbations reveal general strategies for step frequency selection. *Journal of Applied Physiology*. **112**, 1239–1247 (2012).

61. A. M. Dollar, H. Herr, Lower Extremity Exoskeletons and Active Orthoses: Challenges and State-of-the-Art. *IEEE Trans. Robot.* **24**, 144–158 (2008).

62. B. Dellon, Y. R. A. M. I. Matsuoka, Prosthetics, exoskeletons, and rehabilitation [Grand Challenges of Robotics]. *Robotics & Automation Magazine, IEEE*. **14** (2007).

63. A. Zoss, H. Kazerooni, A. Chu, On the mechanical design of the Berkeley lower extremity exoskeleton (BLEEX), 3465–3472 (2005).

64. S. Hesse, H. Schmidt, C. Werner, A. Bardeleben, Upper and lower extremity robotic devices for rehabilitation and for studying motor control. *Curr. Opin. Neurol.* **16**, 705–710 (2003).

65. S. Lee, Y. Sankai, *Power assist control for walking aid with HAL-3 based on EMG and impedance adjustment around knee joint* (IEEE, 2002), vol. 2.

66. J. E. Pratt, B. T. Krupp, C. J. Morse, S. H. Collins, The RoboKnee: an exoskeleton for enhancing strength and endurance during walking. **3**, 2430–2435 (2004).

67. D. P. Ferris, K. E. Gordon, G. S. Sawicki, A. Peethambaran, An improved powered ankle–foot orthosis using proportional myoelectric control. *Gait & Posture*. **23**, 425–428 (2006).

68. J. F. Veneman *et al.*, Design and Evaluation of the LOPES Exoskeleton Robot for Interactive Gait Rehabilitation. *IEEE Trans. Neural Syst. Rehabil. Eng.* **15**, 379–386 (2007).

69. R. Jiménez-Fabián, O. Verlinden, Review of control algorithms for robotic ankle systems in lower-limb orthoses, prostheses, and exoskeletons. *Medical Engineering and Physics*. **34**, 397–408 (2012).

70. L. M. Mooney, E. J. Rouse, H. M. Herr, Autonomous exoskeleton reduces metabolic cost of human walking during load carriage. *J NeuroEngineering Rehabil*. **11**, 80 (2014).

71. S. H. Collins, M. B. Wiggin, G. S. Sawicki, Reducing the energy cost of human walking using an unpowered exoskeleton. *Nature*. **522**, 212–215 (2015).

72. P. Malcolm, W. Derave, S. Galle, D. De Clercq, A Simple Exoskeleton That Assists Plantarflexion Can Reduce the Metabolic Cost of Human Walking. *PLoS ONE*. **8**, e56137–7 (2013).

73. D. P. Ferris, G. S. Sawicki, M. A. Daley, A PHYSIOLOGIST'S PERSPECTIVE ON ROBOTIC EXOSKELETONS FOR HUMAN LOCOMOTION. *Int J HR*. **4**, 507–528 (2007).

74. G. S. Sawicki, D. P. Ferris, Powered ankle exoskeletons reveal the metabolic cost of plantar flexor mechanical work during walking with longer steps at constant step frequency. *Journal of Experimental Biology*. **212**, 21–31 (2008).

75. S. M. Cain, K. E. Gordon, D. P. Ferris, Locomotor adaptation to a powered ankle-foot orthosis depends on control method. *J NeuroEngineering Rehabil*. **4**, 48–14 (2007).

76. J. M. Donelan *et al.*, Biomechanical Energy Harvesting: Generating Electricity During Walking with Minimal User Effort. *Science*. **319**, 807–810 (2008).

77. Q. Li *et al.*, Biomechanical energy harvesting: Apparatus and method. *Robotics and Automation, 2008. ICRA 2008. IEEE International Conference on*, 3672–3677 (2008).

78. J. M. Donelan, R. Kram, A. D. Kuo, Mechanical work for step-to-step transitions is a major determinant of the metabolic cost of human walking. *J. Exp. Biol.* **205**, 3717–3727 (2002).

79. C. H. Soo, J. M. Donelan, Coordination of push-off and collision determine the mechanical work of step-to-step transitions when isolated from human walking. *Gait & Posture*, 1–6 (2011).

80. S. H. Collins, R. W. Jackson, (IEEE, 2013), pp. 1–6.

81. A. D. Kuo, J. M. Donelan, A. Ruina, Energetic consequences of walking like an inverted pendulum: step-to-step transitions. *Exerc Sport Sci Rev*. **33**, 88–97 (2005).

82. J. M. Donelan, R. Kram, A. D. Kuo, Simultaneous positive and negative external mechanical work in human walking. *Journal of Biomechanics*. **35**, 117–124 (2002).

83. J. S. Gottschall, R. Kram, Energy cost and muscular activity required for propulsion during walking. *J Appl Physiol*. **94**, 1766–1772 (2003).

84. Q. Li, V. Naing, M. J. Donelan, Development of a biomechanical energy harvester. *J NeuroEngineering Rehabil*. **6**, 22 (2009).

85. Z. Rubinshtein, M. M. Peretz, R. Riemer, (IEEE, 2014), pp. 3105–3109.

86. K. E. Zelik, A. D. Kuo, Human walking isn't all hard work: evidence of soft tissue contributions to energy dissipation and return. *Journal of Experimental Biology*. **213**, 4257–4264 (2010).

87. J. J. Eng, D. A. Winter, Kinetic analysis of the lower limbs during walking: what information can be gained from a three-dimensional model? *Journal of Biomechanics*. **28**, 753–758 (1995).

88. C. E. Mullins, D. L. Hepler, Methods and Apparatus for Control of Biomechanical Energy Harvesting. *US Patent 20,140,353,970* (2014).

89. A. N. Lay, C. J. Hass, R. J. Gregor, The effects of sloped surfaces on locomotion: A kinematic and kinetic analysis. *Journal of Biomechanics*. **39**, 1621–1628 (2006).

90. A. N. Lay, C. J. Hass, T. Richard Nichols, R. J. Gregor, The effects of sloped surfaces on locomotion: an electromyographic analysis. *Journal of Biomechanics*. **40**, 1276–1285 (2007).

91. D. G. Lloyd, T. F. Besier, An EMG-driven musculoskeletal model to estimate muscle forces and knee joint moments in vivo. *Journal of Biomechanics*. **93-114**, 765–776 (2003).

92. T. S. Buchanan, D. G. Lloyd, K. Manal, T. F. Besier, Neuromusculoskeletal modeling: estimation of muscle forces and joint moments and movements from measurements of neural command. *J Appl Biomech*. **20**, 367–395 (2004).

93. A. L. Hof, J. Van den Berg, EMG to force processing I: An electrical analogue of the Hill muscle model. *Journal of Biomechanics*. **14**, 747–758 (1981).

94. P. R. Cavanagh, P. V. Komi, Electromechanical delay in human skeletal muscle under concentric and eccentric contractions. *Eur J Appl Physiol Occup Physiol*. **42**, 159–163 (1979).

95. R. W. Norman, P. V. Komi, Electromechanical delay in skeletal muscle under normal movement conditions. *Acta Physiol. Scand.* **106**, 241–248 (1979).

96. A. Fougner, O. Stavdahl, P. J. Kyberd, Y. G. Losier, P. A. Parker, Control of Upper Limb Prostheses: Terminology and Proportional Myoelectric Control--A Review. *IEEE Trans. Neural Syst. Rehabil. Eng.* **20**, 663–677 (2012).

97. M. Asghari Oskoei, H. Hu, Myoelectric control systems—A survey. *Biomedical Signal Processing and Control*. **2**, 275–294 (2007).

98. P. Parker, K. Englehart, B. Hudgins, Myoelectric signal processing for control of powered limb prostheses. *Journal of Electromyography and Kinesiology*. **16**, 541–548 (2006).

99. S. K. Au, P. Bonato, H. Herr, (IEEE, 2005), pp. 375–379.

100. S. Au, M. Berniker, H. Herr, Powered ankle-foot prosthesis to assist level-ground and stair-descent gaits. *Neural Networks*. **21**, 654–666 (2008).

101. D. P. Ferris, J. M. Czerniecki, B. Hannaford, An ankle-foot orthosis powered by artificial pneumatic muscles. *J Appl Biomech*. **21**, 189–197 (2005).

102. A. L. Hof, H. Elzinga, W. Grimmius, J. P. K. Halbertsma, Speed dependence of averaged EMG profiles in walking. *Gait & Posture*. **16**, 78–86 (2002).

103. H. J. Hermens, B. Freriks, C. Disselhorst-Klug, G. Rau, Development of recommendations for SEMG sensors and sensor placement procedures. *J Electromyogr Kinesiol*. **10**, 361–374 (2000).

104. M. P. Kadaba, H. K. Ramakrishnan, M. E. Wootten, Measurement of lower extremity kinematics during level walking. *J. Orthop. Res.* **8**, 383–392 (1990).

105. R. B. Davis, S. Ounpuu, D. Tyburski, J. R. Gage, A gait analysis data collection and reduction technique. *Hum Mov Sci*. **10**, 575–587 (1991).

106. M. G. Hoy, F. E. Zajac, M. E. Gordon, A musculoskeletal model of the human lower extremity: the effect of muscle, tendon, and moment arm on the moment-angle relationship of musculotendon actuators at the hip, knee, and ankle. *Journal of Biomechanics*. **23**, 157–169 (1990).

107. S. L. Delp *et al.*, OpenSim: Open-Source Software to Create and Analyze Dynamic Simulations of Movement. *IEEE Trans. Biomed. Eng.* **54**, 1940–1950 (2007).

108. C. J. De Luca, Myoelectrical manifestations of localized muscular fatigue in humans. *Crit Rev Biomed Eng*. **11**, 251–279 (1984).

109. R. Merletti, M. Knaflitz, C. J. De Luca, *Myoelectric Manifestations of Fatigue in Voluntary and Electrically Elicited Contractions* (1990).

110. E. Park, S. G. Meek, Fatigue compensation of the electromyographic signal for prosthetic control and force estimation. *IEEE Trans. Biomed. Eng.* (1993).

111. M. Srinivasan, A. Ruina, Computer optimization of a minimal biped model discovers walking and running. *Nature*. **439**, 72–75 (2005).

112. V. A. Tucker, Energetic cost of locomotion in animals. *Comp. Biochem. Physiol.* **34**, 841–846 (1970).

113. R. M. Alexander, Optimization and gaits in the locomotion of vertebrates. *Physiol. Rev.* **69**, 1199–1227 (1989).

114. D. Sutherland, The development of mature gait. *Gait & Posture*. **6**, 163–170 (1997).

115. R. Shadmehr, S. Mussa-Ivaldi, *Biological Learning and Control* (MIT Press, 2012).

116. D. W. Franklin, D. M. Wolpert, Computational mechanisms of sensorimotor control. *Neuron*. **72**, 425–442 (2011).

117. J. L. Emken, R. Benitez, A. Sideris, J. E. Bobrow, D. J. Reinkensmeyer, Motor Adaptation as a Greedy Optimization of Error and Effort. *Journal of Neurophysiology*. **97**, 3997–4006 (2007).

118. A. E. Minetti, C. Capelli, P. Zamparo, P. E. di Prampero, F. Saibene, Effects of stride frequency on mechanical power and energy expenditure of walking. *Med Sci Sports Exerc*. **27**, 1194–1202 (1995).

119. E. C. Tumer, M. S. Brainard, Performance variability enables adaptive plasticity of “crystallized” adult birdsong. *Nature*. **450**, 1240–1244 (2007).

120. H. G. Wu, Y. R. Miyamoto, L. N. Gonzalez Castro, B. P. Ölveczky, M. A. Smith, Temporal structure of motor variability is dynamically regulated and predicts motor learning ability. *Nature Publishing Group*. **17**, 312–321 (2014).

121. P. R. Davidson, D. M. Wolpert, Widespread access to predictive models in the motor system: a short review. *J. Neural Eng.* **2**, S313–S319 (2005).

122. A. Bud Craig, Interoception: the sense of the physiological condition of the body. *Current Opinion in Neurobiology*. **13**, 500–505 (2003).

123. J. M. Marshall, Peripheral chemoreceptors and cardiovascular regulation. *Physiol. Rev.* **74**, 543–594 (1994).

124. D. S. Reisman, Interlimb Coordination During Locomotion: What Can be Adapted and Stored? *Journal of Neurophysiology*. **94**, 2403–2415 (2005).

125. K. Fortin, A. Blanchette, B. J. McFadyen, L. J. Bouyer, Effects of walking in a force field for varying durations on aftereffects and on next day performance. *Exp Brain Res*. **199**, 145–155 (2009).

126. E. Todorov, Optimality principles in sensorimotor control. *Nat Neurosci*. **7**, 907–915 (2004).

127. A. D. Kuo, An optimal control model for analyzing human postural balance. *IEEE Trans. Biomed. Eng.* **42**, 87–101 (1995).

128. E. Burdet, R. Osu, D. W. Franklin, T. E. Milner, M. Kawato, The central nervous system stabilizes unstable dynamics by learning optimal impedance. *Nature*. **414**, 446–449 (2001).

129. G. Caithness *et al.*, Failure to consolidate the consolidation theory of learning for sensorimotor adaptation tasks. *Journal of Neuroscience*. **24**, 8662–8671 (2004).

130. I. S. Howard, J. N. Ingram, D. W. Franklin, D. M. Wolpert, Gone in 0.6 seconds: the encoding of motor memories depends on recent sensorimotor states. *J. Neurosci.* **32**, 12756–12768 (2012).

131. D. S. Reisman, R. Wityk, K. Silver, A. J. Bastian, Split-Belt Treadmill Adaptation Transfers to Overground Walking in Persons Poststroke. *Neurorehabilitation and Neural Repair*. **23**, 735–744 (2009).

132. A. D. Kuo, J. M. Donelan, Dynamic principles of gait and their clinical implications. *Phys Ther*. **90**, 157–174 (2010).

133. A. d'Avella, P. Saltiel, E. Bizzi, Combinations of muscle synergies in the construction of a natural motor behavior. *Nat Neurosci*. **6**, 300–308 (2003).

134. G. J. Verkerke, A. L. Hof, W. Zijlstra, W. Ament, G. Rakhorst, Determining the centre of pressure during walking and running using an instrumented treadmill. *Journal of Biomechanics*. **38**, 1881–1885 (2005).

135. J. C. Selinger, S. M. O'Connor, J. D. Wong, J. M. Donelan, Humans Can Continuously Optimize Energetic Cost during Walking. *Current Biology*. **25**, 2452–2456 (2015).

136. J. C. Selinger, J. M. Donelan, Estimating instantaneous energetic cost during non-steady-state gait. *J Appl Physiol*. **117**, 1406–1415 (2014).

137. N. Lamarra, B. J. Whipp, S. A. Ward, K. Wasserman, Effect of interbreath fluctuations on characterizing exercise gas exchange kinetics. *Journal of Applied Physiology*. **62**, 2003–2012 (1987).

138. V. S. Huang, R. Shadmehr, Persistence of motor memories reflects statistics of the learning event. *Journal of Neurophysiology*. **102**, 931–940 (2009).

139. F. A. Kagerer, J. L. Contreras-Vidal, G. E. Stelmach, Adaptation to gradual as compared with sudden visuo-motor distortions. *Exp Brain Res*. **115**, 557–561 (1997).

140. J. Klassen, C. Tong, J. R. Flanagan, Learning and recall of incremental kinematic and dynamic sensorimotor transformations. *Exp Brain Res*. **164**, 250–259 (2005).

141. C. Michel, L. Pisella, C. Prablanc, G. Rode, Y. Rossetti, Enhancing visuomotor adaptation by reducing error signals: single-step (aware) versus multiple-step (unaware) exposure to wedge prisms. *J Cogn Neurosci*. **19**, 341–350 (2007).

142. G. A. Brooks, T. D. Fahey, T. P. White, Exercise physiology: Human bioenergetics and its applications. (1996).

143. J. M. Brockway, Derivation of formulae used to calculate energy expenditure in man. *Hum Nutr Clin Nutr*. **41**, 463–471 (1987).

144. J. A. McLean, G. Tobin, Animal and human calorimetry (1987).

145. R. L. Waters, S. Mulroy, The energy expenditure of normal and pathologic gait. *Gait & Posture*. **9**, 207–231 (1999).

146. S. V. Fisher, G. Gullickson, Energy cost of ambulation in health and disability: a literature review. *YAPMR*. **59**, 124–133 (1978).

147. M. Y. Zarrugh, C. W. Radcliffe, Predicting metabolic cost of level walking. *Eur J Appl Physiol Occup Physiol*. **38**, 215–223 (1978).

148. R. L. Waters, H. J. Hislop, J. Perry, D. Antonelli, Energetics: application to the study and management of locomotor disabilities. Energy cost of normal and pathologic gait. *Orthop. Clin. North Am.* **9**, 351–356 (1978).

149. K. G. Holt, J. Hamill, R. O. Andres, Predicting the minimal energy costs of human walking. *Med Sci Sports Exerc*. **23**, 491–498 (1991).

150. K. G. Holt, S. F. Jeng, R. Ratcliffe, J. Hamill, Energetic Cost and Stability during Human Walking at the Preferred Stride Frequency. *J Mot Behav*. **27**, 164–178 (1995).

151. A. E. Minetti, L. P. Ardigò, F. Saibene, Mechanical determinants of gradient walking energetics in man. *The Journal of Physiology*. **472**, 725–735 (1993).

152. J. M. Donelan, D. W. Shipman, R. Kram, A. D. Kuo, Mechanical and metabolic requirements for active lateral stabilization in human walking. *Journal of Biomechanics*. **37**, 827–835 (2004).

153. J. Knapik, E. Harman, K. Reynolds, Load carriage using packs: a review of physiological, biomechanical and medical aspects. *Appl Ergon*. **27**, 207–216 (1996).

154. S. J. Legg, T. Ramsey, D. J. Knowles, The metabolic cost of backpack and shoulder load carriage. *Ergonomics*. **35**, 1063–1068 (1992).

155. K. E. Zelik *et al.*, Systematic Variation of Prosthetic Foot Spring Affects Center-of-Mass Mechanics and Metabolic Cost During Walking. *IEEE Trans. Neural Syst. Rehabil. Eng.* **19**, 411–419 (2011).

156. T. Schmalz, S. Blumentritt, R. Jarasch, Energy expenditure and biomechanical characteristics of lower limb amputee gait:: The influence of prosthetic alignment and different prosthetic components. *Gait & Posture*. **16**, 255–263 (2002).

157. G. S. Sawicki, D. P. Ferris, Mechanics and energetics of level walking with powered ankle exoskeletons. *Journal of Experimental Biology*. **211**, 1402–1413 (2008).

158. J. F. Israel, D. D. Campbell, J. H. Kahn, T. G. Hornby, Metabolic Costs and Muscle Activity Patterns During Robotic- and Therapist-Assisted Treadmill

Walking in Individuals With Incomplete Spinal Cord Injury. *Phys Ther*. **86**, 1466–1478 (2006).

159. E. C. Hardin, A. J. van den Bogert, J. Hamill, Kinematic Adaptations during Running: Effects of Footwear, Surface, and Duration. *Med Sci Sports Exerc*, 838–844 (2004).

160. J. H. Van Beek, N. Westerhof, Response time of cardiac mitochondrial oxygen consumption to heart rate steps. **260**, H613–25 (1991).

161. M. C. Hogan, Fall in intracellular PO2 at the onset of contractions in Xenopus single skeletal muscle fibers. *Journal of Applied Physiology*. **90**, 1871–1876 (2001).

162. D. C. Poole, Oxygen's double-edged sword: balancing muscle O2 supply and use during exercise. *The Journal of Physiology*. **589**, 457–458 (2011).

163. P. Krustrup, A. M. Jones, D. P. Wilkerson, J. A. L. Calbet, J. Bangsbo, Muscular and pulmonary O2 uptake kinetics during moderate- and high-intensity sub-maximal knee-extensor exercise in humans. *The Journal of Physiology*. **587**, 1843–1856 (2009).

164. D. L. Turner, Cardiovascular and respiratory control mechanisms during exercise: an integrated view. *J. Exp. Biol.* **160**, 309–340 (1991).

165. J. Myers, D. Walsh, M. Sullivan, V. Froelicher, Effect of sampling on variability and plateau in oxygen uptake. *Journal of Applied Physiology*. **68**, 404–410 (1990).

166. M. S. Orendurff, How humans walk: Bout duration, steps per bout, and rest duration. *JRRD*. **45**, 1077–1090 (2008).

167. M. H. Dickinson, How Animals Move: An Integrative View. *Science*. **288**, 100–106 (2000).

168. B. J. Wall, J. Charteris, The process of habituation to treadmill walking at different velocities. *Ergonomics*. **23**, 425–435 (1980).

169. J. C. Wall, J. Charteris, A kinematic study of long-term habituation to treadmill walking. *Ergonomics*. **24**, 531–542 (1981).

170. M. Van de Putte, N. Hagemeister, N. St-Onge, G. Parent, J. A. de Guise, Habituation to treadmill walking. *Biomed Mater Eng*. **16**, 43–52 (2006).

171. B. J. Whipp, Rate constant for the kinetics of oxygen uptake during light exercise. *Journal of Applied Physiology*. **30**, 261–263 (1971).

172. T. Müller *et al.*, Estimation of Delay Times in Biological Systems. *Annals of Biomedical Engineering*. **31**, 1423–1439 (2003).

173. R. E. Kalman, A new approach to linear filtering and prediction problems. *Journal of basic Engineering*. **82**, 35–45 (1960).

174. D. Simon, Kalman filtering. *Embedded Systems Programming*. **14**, 72–79 (2001).

175. D. P. Kroese, T. Taimre, Z. I. Botev, *Handbook of Monte Carlo Methods* (2011).

176. W. Felt, J. C. Selinger, J. M. Donelan, C. D. Remy, "Body-In-The-Loop": Optimizing Device Parameters Using Measures of Instantaneous Energetic Cost. *PLoS ONE*. **10**, e0135342–21 (2015).

177. J. D. Wong, J. C. Selinger, S. M. O'Connor, J. M. Donelan, (Amsterdam, Netherlands, 2015), pp. 1–1.

178. J. E. Hubbuch, B. W. Bennett, J. C. Dean, Proprioceptive feedback contributes to the adaptation toward an economical gait pattern. *Journal of Biomechanics*. **48**, 2925–2931 (2015).

179. M. Amann, L. T. Proctor, J. J. Sebranek, D. F. Pegelow, J. A. Dempsey, Opioid-mediated muscle afferents inhibit central motor drive and limit peripheral muscle fatigue development in humans. *The Journal of Physiology*. **587**, 271–283 (2009).

180. M. Amann, Significance of Group III and IV muscle afferents for the endurance exercising human. *Clin. Exp. Pharmacol. Physiol.* **39**, 831–835 (2012).

181. D. Yanagihara, M. Udo, I. Kondo, T. Yoshida, A new learning paradigm: adaptive changes in interlimb coordination during perturbed locomotion in decerebrate cats. *Neurosci. Res.* **18**, 241–244 (1993).

182. D. Yanagihara, M. Udo, Climbing fiber responses in cerebellar vermal Purkinje cells during perturbed locomotion in decerebrate cats. *Neurosci. Res.* **19**, 245–248 (1994).

183. H. Forssberg, S. Grillner, J. Halbertsma, S. Rossignol, The locomotion of the low spinal cat. II. Interlimb coordination. *Acta Physiol. Scand.* **108**, 283–295 (1980).

184. P. J. Whelan, Control of locomotion in the decerebrate cat. *Prog. Neurobiol.* **49**, 481–515 (1996).

185. S. Rossignol, Neural control of stereotypic limb movements. *Comprehensive Physiology* (1996).

186. A. J. Bastian, Learning to predict the future: the cerebellum adapts feedforward movement control. *Current Opinion in Neurobiology*. **16**, 645–649 (2006).

187. J. M. Galea, E. Mallia, J. Rothwell, J. Diedrichsen, The dissociable effects of punishment and reward on motor learning. *Nature Publishing Group*. **18**, 597–602 (2015).

188. M. A. Smith, R. Shadmehr, Intact ability to learn internal models of arm dynamics in Huntington's disease but not cerebellar degeneration. *Journal of Neurophysiology*. **93**, 2809–2821 (2005).

189. A. Hadipour-Niktarash, C. K. Lee, J. E. Desmond, R. Shadmehr, Impairment of retention but not acquisition of a visuomotor skill through time-dependent disruption of primary motor cortex. *J. Neurosci.* **27**, 13413–13419 (2007).

190. P. Bédard, J. N. Sanes, Basal ganglia-dependent processes in recalling learned visual-motor adaptations. *Exp Brain Res*. **209**, 385–393 (2011).

191. L. Marinelli *et al.*, Learning and consolidation of visuo-motor adaptation in Parkinson's disease. *Parkinsonism & Related Disorders*. **15**, 6–11 (2009).

192. R. T. Roemmich *et al.*, Locomotor adaptation and locomotor adaptive learning in Parkinson's disease and normal aging. *Clin Neurophysiol*. **125**, 313–319 (2014).

193. M. Bakker, C. C. P. Verstappen, B. R. Bloem, I. Toni, Recent advances in functional neuroimaging of gait. *J Neural Transm*. **114**, 1323–1331 (2007).

194. J. T. Gwin, K. Gramann, S. Makeig, D. P. Ferris, Removal of Movement Artifact From High-Density EEG Recorded During Walking and Running. *Journal of Neurophysiology*. **103**, 3526–3534 (2010).

195. K. L. M. Koenraadt, E. G. J. Roelofsen, J. Duysens, N. L. W. Keijsers, Cortical control of normal gait and precision stepping: An fNIRS study. *NeuroImage*. **85**, 415–422 (2014).

196. J. A. Taylor, R. B. Ivry, Flexible Cognitive Strategies during Motor Learning. *PLoS Comput Biol*. **7**, e1001096–13 (2011).

197. J. A. Taylor, J. W. Krakauer, R. B. Ivry, Explicit and Implicit Contributions to Learning in a Sensorimotor Adaptation Task. *Journal of Neuroscience*. **34**, 3023–3032 (2014).

198. L. A. Malone, A. J. Bastian, Thinking About Walking: Effects of Conscious Correction Versus Distraction on Locomotor Adaptation. *Journal of Neurophysiology*. **103**, 1954–1962 (2010).